79-1405

RESTRICTED INVESTIGATION REPORT 1079R

CSIRO

4/74

INSTITUTE OF EARTH RESOURCES

FUEL GEOSCIENCE UNIT

RESEARCH ON TASMANITE OIL SHALE

- FINAL QUARTERLY REPORT TO ENDEAVOUR RESOURCES LIMITED

A. TELFER, N.J. RUSSELL, J.D. SAXBY,
P. BARRON AND T.D. GILBERT

P.O. BOX 136
NORTH RYDE, NSW
AUSTRALIA, 2113

NOVEMBER 1979

TABLE OF CONTENTS

LIST OF TABLES

LIST OF FIGURES

Pyrolysis

1. Tasmanite kerogen is an excellent source of liquid hydrocarbons giving yields of well over 50%. The water and gas yields are less than 20% of that for tar, and the amount of water is usually less than that of gas.
2. Total volatiles in Fischer assays (520°C) and Gray-King assays (600°C) are similar and somewhat lower than those obtained at 900°C. This is attributable to more cracking of 'fixed carbon' and oil at the higher temperature.
3. Flash pyrolysis appears to have little advantage over slower retorting methods for Tasmanite-type organic matter.

Batch Autoclave Experiments

1. The compositions of gas samples from batch autoclave studies reflect the differences between the uncatalysed experiments, which are dominated by thermal breakdown reactions (and give abundant n-alkanes), and the catalysed experiments, which are dominated by thermocatalytic reactions at lower reaction temperatures (and favour formation of isoalkanes).
2. Changes in the optical behaviour of the alginite in response to an increase in the reaction temperature suggest that tin(II) chloride inhibits the decrease in alginite fluorescence intensity, whereas zinc(ii) chloride enhances the decrease in alginite fluorescence intensity. This suggests that these catalysts promote hydrogenation via differing reaction mechanisms.
3. Irrespective of the experimental conditions, similar maximum yields of heavy hydrocarbons are generated between 425°C and 450°C. This reflects the fact that the alginite is rich in long chain precursors.
4. Ethylene, a potentially valuable monomer for petrochemicals, is only produced in significant amounts from catalysed experiments.
5. Little success was achieved in lowering the sulphur content of liquid products using various iron additives. Zinc chloride and to a lesser extent tin chloride were effective in decreasing the sulphur content by over 50% but such reagents would be too expensive for large-scale use.
6. Curie-Point pyrolysis results on extracts after pyrolysis under both nitrogen and hydrogen were similar indicating no major role for externally-added hydrogen.

SUMMARY

This is the last of four reports submitted to Endeavour Resources describing research carried out in the final quarter (July-September 1979). The main conclusions of the complete one year project are as follows:

Chemistry

1. The elemental composition of Tasmanite kerogen is C 82.3%, H 11.0%, N 0.7%, S 4.0%, O 2.0%.
2. The atomic H/C ratio of isolated tasmanite kerogen is 1.60, while the atomic O/C ratio is 0.02. High H/C values and low O/C values such as these are desirable for any process leading to liquid products.
3. The high organic sulphur content of Tasmanite kerogen ($\sim$4%) is probably due to the presence of -S- and -S-S- groups and will be a problem in any conversion process. No simple way of overcoming this adverse feature is available due to the nature and uniform distribution of these chemical groups.
4. Solid state ^{13}C NMR spectra confirm the aliphatic nature of the organic matter in Tasmanite kerogen.
5. A small concentration of unsaturated bonds (C = C) probably exists in protected positions within the organic matter of Tasmanite.
6. Environmentally hazardous trace metals do not appear to be concentrated in the Tasmanite kerogen.

Petrology

1. Tasmanite oil shale is heterogeneous in nature containing organic matter as well as quartz, muscovite, kaolinite/chlorite, dolomite, magnesium calcite, gypsum, pyrite and feldspar.
2. Most of the organic material consists of algal bodies, *Tasmanites* sp, which are very resistant to chemical and physical breakdown.
3. The macroscopic appearance (e.g. fissility) of the cores supplied varies greatly and is associated with the degree of layering of the Tasmanites.
4. The volume percentage of Tasmanites in the cores ranges up to 53% (c.f. 84% in the concentrate) and appears to be directly related to the oil or tar yield on pyrolysis.
5. Scanning electron microscope and electron microprobe analyser work shows that organic sulfur ($\sim$4%) is evenly distributed throughout each algal body.

Benefication

1. Sieving of crushed material gives an increased organic concentration in the -150 +200 mesh fraction but the beneficiation achieved is inadequate for most practical applications.
2. Repeated stages of froth flotation can produce a concentrate with a desired mineral matter content. Both an organic matter activator (such as fuel oil) and a mineral matter depressant (such as starch) to assist in the separation. Mineral contents below ∿25% will be more difficult to achieve and probably will be accompanied by low recovery rates.
3. Microscopic examination of floats and tailings shows that 'clumping' of fine organic and inorganic particles must be avoided if very high grades of concentrate are needed.

Utilization

1. The most likely uses of the present reserves of Tasmanite are as road bitumen or a source of liquid hydrocarbons. The possibility of use in the reclaim rubber industry requires further investigation. The production of petrochemicals do not appear to be attractive propositions. In the event of retorting at least some of the spent shale could be used in building materials or as a fertilizer.
2. The sulphur content of pyrolysis and hydrogenation oils is high (2-3%) but modern refineries can accommodate this at a cost. The nitrogen content of the tars (∿0.5%) is lower but may prove even more costly to overcome.

1. INTRODUCTION

This is the fourth and final report for Endeavour Resources Limited on the Tasmanite Oil Shale Project. It contains details of new work completed since the third report in July 1979 (IR 1034R) and a summary of all the work to the conclusion of the project.

The new work involved techniques, such as froth flotation and nuclear magnetic resonance spectroscopy, a continuation of pyrolytic and chemical assessment, and a follow-up to the batch autoclave experiments with and without catalysts.

Fischer and Gray King assays were carried out on the two demineralized samples mentioned in the third report (IR 1034R). These assays give product yields at temperatures of 520°C and 600°C respectively. An XRF analysis of the ash of one of these samples is also included.

Froth flotation was tested as a means of concentrating the algal bodies into an ash-free concentrate. This involved a series of tests, with a crushed sample, using a frother and one of two potentially beneficial reagents. Further testing involved the use of both reagents and frother together with repetative flotation. The products of these tests were then analysed chemically and microscopically.

Nuclear magnetic resonance (NMR) is a development that enables an estimate to be made of the fraction of aromatic, aliphatic and olefinic carbon atoms in the organic matter of Tasmanite.

Further batch autoclave experiments were carried out. By using different catalysts an attempt was made to reduce or eliminate sulphur found in the liquid products. Other investigative methods used were low temperature plasma ashing, X-ray powder diffraction of residues and electron microscopy.

The batch autoclave products were assessed for chemical compounds by the use of Curie-point pyrolysis/gas chromatography/mass spectrometry (CP/GC/MS). This technique separates and identifies the various compounds present and indicates trends in the type of compounds formed in the autoclave experiments.

An assessment of possible ways of utilizing Tasmanite oil shale is included, together with some suggestions pertaining to its use as bitumen.

Hydrogenation studies were carried out by N.J. Russell, pyrolysis-gas chromatography-mass spectrometry by T.D. Gilbert, NMR spectroscopy by P. Barron, and petrological and chemical work by A. Telfer and J.D. Saxby.

2. PYROLYSIS OF TASMANITE

2.1 Introduction

A number of different techniques are available to determine the possible oil yield on pyrolysis of a kerogen-rich shale. When oil and gas yields are low, it is difficult to compare samples and methods because the analytical precision of all techniques is correspondingly low. To overcome this, three kerogen-rich samples (a flotation concentrate and two samples demineralized by HCl and HF treatment) have been chosen for proximate, Fischer and Gray-King analyses.

2.2 Results and Discussion

Table 1 contains pyrolysis results for the three kerogen-rich samples together with comparable figures for a shale sample virtually devoid of organic matter. The volatile matter in the proximate analysis is obtained at $\sim$ 900°C under non-oxidizing conditions for 7 minutes and represents the sum of oil, gas and water. Under Fischer assay conditions the sample is heated to 520°C over 70 minutes, held at 520°C for 10 minutes and then cooled. In the Gray-King analysis the sample is heated rapidly to 300°C and then at $\sim$ 5°C/min to 600°C. After maintaining a temperature of 600°C for one hour, the sample is cooled.

Normally in the Gray-King analysis the tar and water are determined separately by distillation with toluene. In the case of 77591 this resulted in 43.6% tar and 7.3% water. However in the case of the two demineralized samples problems arose from a white solid which sublimed/distilled from the mixture and prevented a clearcut water/toluene separation. Since the problem did not arise with the flotation concentrate, the presence of volatile fluorides was suspected of being the cause. This was confirmed by emission spectroscopy which showed that the white deposit was mainly

inorganic containing sizeable percentages of Si, Mg and Ca. An attempt was made to determine water in the two problem samples by the Karl-Fischer method using apparatus kindly made available by Australian Chemical Industries (ACI). The results obtained (77591K = 56.7% tar, 21.2% water, 78694K: 46.7% tar, 1.6% water) are only approximate and in the case of 77591K the water value could well be appreciably high due to water associated with the contaminating fluorides. No tar/water separation was attempted on the Fischer assay products from the demineralized samples.

Using the moisture and ash figures of Table 1, the results of Table 2 on a dry, mineral-free basis were obtained (assuming the mineral matter is equal to the ash). The "coke" results in Table 2 were obtained by difference and should be a reasonable estimate of non-volatile material in the organic matter of Tasmanite under each set of pyrolysis conditions (i.e. comparable to fixed carbon of the proximate analysis).

Earlier work (IR 1016R) suggested there were no abnormal features in the trace element distribution in the Tasmanite shales with little in the way of economically interesting metallic components. In order to ascertain whether any metals were concentrated in the kerogen itself (as organo-metallics,etc), the ash from 78694K was analyzed by X-ray fluorescence (XRF). The following results were obtained Ba 0.00%, Pb 0.00%, Zn 0.04%, Cu 0.06%, Fe 30.21%, Mn 0.03%, Ti 3.32%, Ca 0.11%, K 17.93%, S 3.26%, P 0.06%, Si 8.22%, Al 0.48%, Mg 0.23% and Na 0.00%. Apart from the low Zn and Cu levels none of these values are particularly significant. The potassium figure may be due to illite not removed during demineralization.

The following comments can be made on the results in Table 2.

(i) The three kerogen-rich samples have all behaved similarly on pyrolysis and contrast greatly with the barren sample. As discussed in earlier reports, physical concentration of Tasmanite does not result in kerogen having different chemical or thermal decomposition properties.

(ii) In all tests well over 50% of the organic matter in Tasmanite is converted to oil with water, gas and coke formation small by comparison. Tasmanite kerogen is thus an excellent source of liquid hydrocarbons, a fact consistent with its high H/C ratio (1.60) and low O/C ratio (0.02). The low O/C values means little oxygen is available in the kerogen

structure to produce water or oxides of carbon on pyrolysis. The water and gas yields are less than 20% of the tar yield and the amount of water is usally less than that of gas.

(iii) The volatile matter obtained in the proximate analysis is higher than the total volatiles in the Fischer and Gray-King analyses. This can be attributed to greater cracking of the "fixed carbon" (to gases) at the higher temperature. The Fischer and Gray-King results are similar in most respects with only a marginal increase in volatiles resulting from the higher temperature and longer time of the Gray-King pyrolysis.

3. FROTH FLOTATION OF TASMANITE

3.1 Flotation Methods

A bulk sample of shale from the Sassafras area, representing a combination of Bore No. 27B - Interval 26'7"-31'5" (8.1-9.6 m) and Bore No. 28B - Interval 12'11"-18'4" (3.9-5.6 m), was reduced in size to -200#, and divided into three-200 gram samples. The following steps were then carried out.

(i) One 200 g sample was thoroughly mixed in a four litre flotation cell for three minutes, then three drops of methylisobutylcarbinol (MIBC) was added as frother. The floats were collected for fifteen minutes, resulting in:

200 g (LN 78813) sample + 3 drops MIBC → Floats, 23.9 g (LN 78847), 12.0%
Tailings, 170.0 g (LN 78848), 85.0%
Loss 3.0%

(ii) The second sample was also mixed in the four litre flotation cell for three minutes. Then 0.2 gram starch was added as a depressant for mineral matter. Three drops of MIBC were also added. The froth was collected for fifteen minutes.

200 g(LN 78813) + 0.2 g Starch + 3 drops MIBC → Floats, 17.2 g (LN 78849) 8.6%
Tailings, 178.8 g (LN 78850), 89.4%
Loss 2.0%

(iii) The third sample was mixed in the four litre flotation cell for three minutes. Then 0.2 ml of diesel distillate (fuel oil) was added as a collector (2 lb/ton), mixed for five minutes, and then three drops of MIBC were added to this mix. The froth was collected for fifteen minutes-

200 g (LN 78813)+ 0.2 ml Fuel Oil + 3 drops MIBC → Floats, 17.7 g (LN 78851), 8.9%
Tailings, 177.9 g (LN 78852), 89.0%
Loss 2.1%

The floats and tailings in all three samples were filtered through a Buchner funnel to avoid major losses of sample. It was concluded from the above tests that a further improvement may be achieved by using all three components together and repeating the flotation several times. The method and results can be seen in Figure 1.

3.2 Petrology of Flotation Products

The reduction in size of the sample to -200# has led to greater fragmentation of the material, especially the larger algal bodies, the smaller ones appear to have been better preserved. The framboidal pyrite also appears to have broken up into smaller separate grains. There are no signs of excessive penetration of the hard mineral grains into the soft algal bodies attributable to the crushing.

The significant feature of the flotation products is the appearance of aggregates. The latter consist of fragmented algal bodies and other mineral matter with either grain to grain contacts or a maxtrix of clay. The aggregates are variable in size, up to 350 microns in width. As well as the aggregates, there are isolated free grains and in the floating fractions these grains are usually large algal body fragments. The tailings may also contain clumps, but fewer in number, with more free dispersed grains.

The float product where a great improvement was seen in the aggregation problem was sample Float 2 (LN 79256), where there were far more free, broken *Tasmanites* sp. There was also an associated drop in the ash content, seen both microscopically (Table 3) and in the chemical analysis (Table 4).

The aggregates, which are persistent in nearly all the samples, may be a problem in any large scale flotation process. Where aggregation occurs,

ash contents approaching zero cannot be achieved, and recovery of algal bodies will also be impeded, since mixed algal-mineral aggregates are also present in the tailings.

3.3 Discussion

Our study of froth flotation confirms in general the results of the Department of Mines Laboratory, in Launceston (Ore Dressing Investigation - R.694, December 1975, for Endeavour Oil Co. N.L.). Both series of tests show that with fine crushing and the addition of an activator, depressor and frother, ash content can readily be decreased. Repeated flotation will give progressively lower ash contents. Tasmanite is unusual in that it is much more amenable to concentration by flotation than most other oil shales.

A three stage flotation test (Figure 1) carried out using starch (depressor), fuel oil (activator) and methylisobutylcarbinol (MIBC-frother), resulted in a drop from 88.5% ash in the original sample to 53.2% ash in the second float stage (Table 4).

Test "N3" carried out by the Department of Mines Laboratory using a frother, fuel oil, and calgon, plus extra crushing between stages, reduced their ash from 61.6% original sample, to 16.6% in the fourth stage.

Microscopic observation of the flotation samples has indicated that the aggregation of the mineral matter with algal bodies affects the ash content. This aggregation appears to be reduced with repeated flotation, so lowering the ash yield.

From these results it can be concluded that ash yields can be successfully reduced using a depressor, activator and frother in conjunction with fine crushing and repeated flotation when necessary.

4. NMR SPECTROSCOPY OF TASMANITE

4.1 Introduction

Recent developments in high power NMR, termed proton enhanced nuclear induction spectroscopy (Pines et al, 1973), has made it possible to record ^{13}C NMR spectra of solid materials in which the resonances due to aliphatic carbons are partly resolved from those due to aromatic and olefinic carbon atoms. This technique has been used recently by a number of groups (Bartuska et al, 1977; Resing et al, 1978; Van der Hart et al, 1976; Vitarovic et al, 1978) to characterize coals and related materials by estimating the aromatic plus olefinic proportion ($f_a = \frac{\text{Aromatic carbon}}{\text{total carbon}}$) of their carbon atoms. This technique has recently been established at North Ryde by the Fuel Geoscience Unit and applied to some petrographic concentrates from Australian coals and oil shales and has now been applied to Tasmanite (Fig. 2). Auxiliary equipment for the NMR spectrometer to further improve the resolution by the technique of "magic angle spinning" has yet to be installed on the CSIRO instrument.

The overlap of peaks and the unsymmetrical shape of the aromatic plus olefinic carbon (Van der Hart et al, 1976) apparent in Fig. 2a makes the determination of their relative areas difficult and subject to significant error (± 10% approximately). This degree of uncertainty also applies to the values of f_a which are derived from the relative areas of the two peaks. The introduction of "magic angle spinning" should remove peak overlap and thus significantly reduce the uncertainties. The effect of other instrumental parameters on the accuracy of f_a calculations has not so far been determined.

4.2 Results and Discussion

The f_a value for the vitrinite in Fig. 2a is estimated to be 0.78 ± 0.1. Fig. 2b shows the spectrum of an exinite concentrate from Glen Davis oil shale in which the aromatic plus olefinic signal is barely detectable, while in Fig. 2c there is no detectable signal in the aromatic plus olefinic region. Some caution is needed in interpreting these later two spectra in the absence of "magic angle spinning" due to the smallness of the aromatic plus olefinic signals. However the f_a are low and certainly less than 0.2 in both cases.

5. BATCH AUTOCLAVE AND LOW-TEMPERATURE PLASMA ASHING EXPERIMENTS WITH TASMANITE CONCENTRATE

5.1 Introduction

A further programme of batch autoclave experiments was undertaken using a subsample of tasmanite concentrate sample 77591. These experiments were designed to examine:

(1) The formation of ethylene (C_2H_4) at relatively low temperatures (200°C-350°C).

(2) The ability of various iron compounds to remove organic sulphur from the hexane extract (heavy (C_{10}+) hydrocarbon fraction) formed by heating the tasmanite concentrate to 425°C in nitrogen.

In addition, further data are presented in respect of the samples described in the previous report (Telfer et al., 1979).

The tasmanite concentrate, together with a vitrinite and an inertinite concentrate, was subjected to low-temperature plasma ashing (LTPA) to determine its resistance to oxidation.

The solid residues (hexane insoluble material in the case of the batch autoclave experiments) were analysed by X-ray powder diffraction (XRD) to determine the nature and relative proportions of the inorganic constituents.

Electron microscopy was used to supplement the incident light (optical) microscopic examination of selected samples.

5.2 Experimental

The autoclave equipment, experimental procedures, sampling and analysis of autoclave products and preparation and microscopic examination of polished solid residue samples have been described in the previous report (Telfer et al., 1979).

Analytical work was carried out on selected hexane extracts by the Division of Applied Organic Chemistry, Melbourne, using microanalytical

techniques. The Fuel Geoscience Unit analysed the iron compounds used in the batch autoclave experiments, using a variety of techniques including atomic emission spectrography, atomic absorption spectroscopy and X-ray fluorescence spectrometry.

5.2.1 X-Ray Powder Diffraction (XRD) Analysis

The X-ray powder diffraction (XRD) analyses were carried out on a Philips XRD camera and goniometer. These analyses were undertaken using a copper tube ($Cu_{K\alpha}$ = 1.54 Å), graphite crystal discriminator and a proportional counter. The XRD charts were prepared under the following conditions:

40 ma 60 Kv
1° (divergent) 4° (receiving) 1° (Soller)
Scan Speed 0.5°2θ/minute } (1°2θ/cm)
Chart Speed 5 mm/minute }
Time constant 4
Full scale deflection 1 x 10^3 counts/seconds.

XRD data for tin and the sulphides were taken from the Peacock Atlas (Berry & Thompson, 1962). XRD data for silicate and sulphate minerals were taken from other reference sources in the literature (Borg and Smith, 1969, Brown, 1961).

In order to estimate variations in the relative proportions of the inorganic constituents, the peak heights of constituent reflections were compared with the peak height of a quartz reflection that is free from interference by other reflections, e.g. 1.82 Å.

5.2.2 Low Temperature Plasma Ashing (LTPA) Experiments

The low-temperature plasma ashing (LTPA) was carried out on 1 gm samples of the maceral concentrate. The LTPA unit employs a radio-frequency field to produce a ring discharge in a stream of oxygen; the ashing temperature for the sample in the pyrex sample vessel probably lies between 150°C and 200°C (Gluskoter, 1965).

Subsamples (less than 0.1 gm) for petrographic examination were taken at approximately 24 hour intervals. At the same time the weight of the residue remaining in the pyrex sample vessel was recorded.

5.2.3 Atomic Emission Spectrographic and other Chemical Analyses of Iron Compounds

Atomic emission spectrographic analyses of the trace element content of iron compounds were carried out using a Hilger and Watts instrument. Two National Institute for Metallurgy (NIM) standards, the Sishen Hematite (SARM-11) and the Palabora Magnetite (SARM-12) were analysed to provide plates with similar matrices to the iron oxide samples.

Iron, calcium, magnesium, aluminium, silicon and potassium contents of the red mud catalyst were determined by X-ray fluorescence (XRF) spectrometry. The sodium content of the red mud catalyst was determined using atomic absorption spectroscopy (AAS).

5.2.4 Electron Microscopy

After vacuum coating with carbon, polished specimens of selected solid residues were examined under a Cambridge S600 (Stereoscan) scanning electron microscope (SEM) equipped with a Tracor Northern 1700 energy dispersive system (EDS). The SEM/EDS unit was operated at 24 Kv; good resolution was obtained using a spot size of 3. Electronmicrographs (secondary electrons) and element distributions were recorded photographically. Electron-micrographs (back scatter electrons), element profiles and element distributions were also recorded photographically, using a beam current of 10 nanoamps, under a Cambridge Microscan 5 electron probe microanalyser (EPMA). The latter is equipped with both EDS and wavelength dispersive X-ray fluorescence analytical systems: The EPMA/EDS is a Link Systems model 860. Some analytical data were acquired using the EPMA/EDS using a beam current of 3 nanoamps.

5.3 Results

5.3.1 Batch Autoclave Experimental Data

The catalysed batch autoclave experiments in nitrogen yield similar temperature, pressure and differential temperature ($\Delta T°C$) curves with time to those obtained for the corresponding experiments in hydrogen (Figure 3).

The batch autoclave experiments in nitrogen at 425°C using iron compounds yield similar experimental data to those obtained from the corresponding experiments run in the absence of the iron compounds (Figure 4).

5.3.2 Composition of the Autoclave Gas Samples

Data presented in the previous report (Telfer et. al., 1979) suggest that higher proportions of hydrocarbons were recorded from the autoclave gas sample collected at 20 kg/cm^2 (1.96 MPa) than that collected at 50 kg/cm^2 (4.90 MPa). Since the hydrocarbon constituents are of particular interest to this study only data for the 20 kg/cm^2 autoclave gas samples are presented in this report.

Table 5 summarizes the composition of the gas samples collected from the catalysed and uncatalysed batch autoclave experiments carried out in nitrogen and in hydrogen at temperatures of 250°C to 350°C. The proportions of carbon monoxide, carbon dioxide and hydrocarbons in these autoclave gas samples are presented in Table 6.

An unidentified component, X, having a retention time of about 3, appears between normal butane and isopentane on the DC 200 column (5' x 30% DC 200 silicone oil on 80/100 mesh chromosorb P-AW) of the Hewlett Packard 5830A gas chromatograph (GC). It is assumed that this component is a C_4 or C_5 hydrocarbon; it has been assigned a response factor of 4.9 x 10^{-8} ml. unit area for the purposes of calculation.

Table 7 summarizes the composition of the autoclave gas samples collected at 20 kg/cm^2 (1.96 MPa) from the batch autoclave experiments in nitrogen at 425°C carried out in the presence of various iron compounds. The proportions of carbon monoxide, carbon dioxide and hydrocarbons are presented in Table 8.

An unidentified component, Y, having a retention time of 2.85, appears between normal butane and isopentane on the DC 200 column. This component has a different retention time to that of the previously described unidentified component. Again it is assumed that the unidentified component is a C_4 or C_5 hydrocarbon; it has been assigned a response factor of 5 x 10^{-8} ml/unit area for the purposes of calculation.

Careful examination of the GC traces for the uncatalysed batch autoclave runs in nitrogen at 450°C and 480°C reveals the presence of trace amounts of the unidentified component with a retention time of 2.85.

The identification of the two components is difficult without analysing a complete series of C_3 to C_5 hydrocarbons. Possible compounds are reviewed and discussed, identifying some of the most likely candidates, selected on the basis of information provided by T. Gilbert. DC 200 is a methyl silicone, non-polar medium similar to squalane. The order of elution of C_4 hydrocarbons on squalane are as follows:

normal butane	C_4H_{10}
normal butene	$CH_2{:}CH.CH_2CH_3$
trans-butene 2 }	$CH_3.CH{:}CH.CH_3$
cis-butene 2 }	
1.3-butadiene	$CH_2{:}CH.CH{:}CH_2$
isopentane	$(CH_3)_2CH.CH_2CH_3$

Neopentane (2.2-dimethylpropane)($CH_3.C(CH_3)_2.CH_3$) also elutes between normal butane and isopentane with a retention time closer to that of isopentane. On the basis of their retention indices, the following hydrocarbons could elute between normal butane and isopentane.

cyclobutane	C_4H_8
1.1 dimethylcyclopropane	$C_3H_4(CH_3)_2$
isopentene	$CH{:}C(CH_3).CH_2.CH_3$

Since isobutene ($CH_2{:}C(CH_3)_2$), eluting between isobutane ($CH_3.CH(CH_3)_2$) and normal butane, has been positively identified in gas from batch autoclave experiments run with iron compounds, one of the butene isomers is a likely product, although neopentane is also likely product at high temperatures (425°C).

In the case of the tin(II) chloride and zinc(II) chloride catalysed batch autoclave experiments the choice is more difficult given the relatively low temperature of formation (250°C to 350°C) of the unidentified component.

Ethylene is present in the 20 kg/cm^2 gas samples collected from the catalysed batch autoclave experiments heated to temperatures between 300°C and 350°C, irrespective of whether a nitrogen or a hydrogen atmosphere is used. The zinc(II) chloride catalysed experiments yield gases with a higher proportion of ethylene than the tin(II) chloride catalysed experiments for a given atmosphere. The hydrogen atmosphere experiments yield a higher

proportion of ethylene than the nitrogen atmosphere experiments (Table 6). Component X is present in the gas samples from both the nitrogen and the hydrogen atmosphere, catalysed, batch autoclave experiments at 300°C. Above this temperature it is only produced in the nitrogen atmosphere experiments. Below 300°C it is only produced in the tin(II) chloride catalysed experiments. Component X does not form in the nitrogen atmosphere experiments heated to temperatures of less than 200°C. At 350°C both the nitrogen and the hydrogen atmosphere, catalysed, batch autoclave experiments yield gases in which isobutane is dominant over normal butane.

There are a number of components present in the gas produced by the batch autoclave experiments heated to 425°C under nitrogen in the presence of iron compounds that are not present in the gas produced at 425°C when the tasmanite concentrate is heated in nitrogen alone; namely ethylene, isobutene, ethane, component Y (a butene?) and isopentane. The normal C_4 and C_5 alkanes are dominant over the iso-C_4 and C_5 alkanes, which is the opposite of the case with the tin(II) chloride and zinc(II) chloride catalysed experiments.

The proportions of carbon monoxide, carbon dioxide and hydrocarbons vary with the amount of iron compound used in the batch autoclave experiments. In the case of the iron there is an increase in the proportion of carbon monoxide and a decrease in the proportion of carbon dioxide with increase in the amount of iron added. In the cases of the iron oxide and the red mud catalyst, there is a decrease in the porportion of carbon monoxide and an increase in the proportion of carbon dioxide with increase in the amounts of iron oxide or red mud catalyst added.

5.3.3 Chemical Analysis of the Hexane Extracts

Since only limited amounts of the hexane extracts were available, microanalyses were carried out on less than 100 mg of sample. Table 9 presents the ultimate analysis data for the hexane extracts produced in the catalysed and uncatalysed batch autoclave experiments heated to 425°C. Table 9 indicates that at 425°C the zinc(II) chloride catalysed experiments yield the hexane extract with the lowest contents of nitrogen, oxygen and organic sulphur and the highest carbon content.

By comparison the tin(II) chloride catalysed experiment yields the hexane extract with the highest hydrogen content and the highest atomic H/C ratio. This hexane extract is the only one that exhibits an atomic H/C ratio greater than that of the untreated tasmanite concentrate.

Table 10a presents organic sulphur data for the hexane extracts produced by the catalysed and uncatalysed batch autoclave experiments heated to temperatures between 415°C and 450°C. Table 10b presents organic sulphur data for the hexane extracts produced by the batch autoclave experiments heated to 425°C in nitrogen in the presence of various iron compounds.

There is a reduction in the organic sulphur content of the hexane extracts with increase in the reaction temperature (Table 10a). The greatest reduction in the organic sulphur content of the hexane extracts at a given temperature occurs in the zinc(II) chloride catalysed experiments. Tin(II) chloride produces an appreciable reduction in the organic sulphur content of the hexane extracts by comparison with that of the hexane extracts produced by the uncatalysed batch autoclave experiments. At 425°C the iron compounds have little influence on the organic sulphur content of the hexane extract. Iron is slightly more effective than iron oxide or the red mud catalyst in reducing the organic sulphur content of the hexane extract. The level of organic sulphur in the latter is slightly reduced by increasing the quantity of iron compound added to the tasmanite concentrate (Table 10b).

5.3.4 Low-Temperature Plasma Ashing (LTPA) Experiments

The tasmanite concentrate was subjected to low-temperature plasma ashing (LTPA), together with vitrinite and inertinite concentrates. The alginite in the tasmanite concentrate is relatively resistant to oxidation by LTPA, since it required between 1 and 2 days to halve the organic matter content of the sample and between 3 and 4 days to completely eliminate this organic matter. By comparison vitrinite was eliminated by LTPA in less than 1 day and the bulk of the inertinite was eliminated after LTPA treatment for 2 days (Table 11).

5.3.5 X-Ray Powder Diffraction (XRD) Analyses of the Solid Residues from the Batch Autoclave and Low-Temperature Plasma Ashing (LTPA) Experiments

XRD analyses were carried out on thirty samples, comprising twenty eight of the hexane insoluble residues from the catalysed and uncatalysed

batch autoclave experiments, an untreated sample of the tasmanite concentrate and a LTPA residue (210,5 hours ashing time).

The XRD data indicate that, at a given reaction temperature, the inorganic constituents are the same for the uncatalysed batch autoclave experiments carried out in nitrogen and in hydrogen, namely quartz, illite/mica (sericite/muscovite), kaolinite, gypsum, anhydrite, chlorite, pyrrhotite and pyrite. The variation in the proportions of pyrrhotite, pyrite, gypsum and anhydrite, expressed as peak height ratios measured against the 1.54 Å quartz reflection with increase in the reaction temperature, is summarized in Table 12 and illustrated in Figures 5 and 6. Above 200°C gypsum dehydrates to form anhydrite; minor amounts of the latter are present in the untreated tasmanite concentrate. Above 390°C pyrite is converted to pyrrhotite; the latter is present in the untreated tasmanite concentrate.

The XRD data permit an estimate to be made of the variation in the proportions of zinc(II) sulphide, expressed as peak height ratios measured against the 1.82 Å quartz reflection, with increase in the reaction temperature. There appears to be a steady increase in the proportion of zinc(II) sulphide formed in the zinc(II) chloride catalysed experiments between 200°C and 415°C, above the latter temperature the proportion of zinc(II) sulphide appears to remain constant. These data are summarized in Table 13 and illustrated in Figures 7 and 8.

Similarly, the variation in the proportions of tin(II) sulphide and tin, formed with increase in the reaction temperature in the tin(II) chloride catalysed experiments, can be estimated from the XRD data. Peak height ratios for tin(II) sulphide and tin reflections measured against the 1.82 Å quartz reflection are summarized in Table 14 and illustrated in Figures 8 and 9. Tin(II) sulphide appears to form between 200°C and 300°C. The amount formed appears to increase between 300°C and 425°C; above the latter temperature there may be a slight reduction in the proportion of tin(II) sulphide. Tin appears to form between 390°C and 425°C; the amount of tin formed remaining constant above 425°C.

XRD analysis of the LTPA residue indicates that pyrite has been eliminated and that gypsum has been converted to anhydrite; there appears to be a reduction in the proportions of pyrrhotite and anhydrite by comparison with the untreated tasmanite concentrate.

In the untreated tasmanite concentrate the organic matter is represented by a very broad reflection with a maximum at about 4.8 Å. The intensity of this peak is reduced with increase in the reaction temperature; it disappears from the XRD charts for the catalysed and uncatalysed batch autoclave experiments between 390°C and 415°C, except in the case of the tin(II) chloride catalysed experiments in which the 4.8 Å reflection disappears between 415°C and 425°C. The 4.8 Å organic matter reflection is not present in the XRD chart obtained from the LTPA residue. These data are illustrated in Figure 10.

XRD analyses were also carried out on hexane-insoluble residues from the batch autoclave experiments heated at 425°C in nitrogen in the presence of various iron compounds and, for reference purposes, on the powdered iron, iron oxide and red mud catalyst. The results of these XRD analyses are summarized in Table 16. The latter shows that the iron in the red mud catalyst is present as a mixture of hematite (α-Fe_2O_3), goethite (α-$Fe_2O_3.H_2O$) and traces of lepidocrocite (δ-$Fe_2O_3.H_2O$), that the iron oxide consists essentially of hematite and that the powdered iron may contain traces of hematite. The batch autoclave experiments carried out with the various iron compounds result in the formation of pyrrhotite ($Fe_{1-x}S$). In the case of the iron oxide experiment, it appears that the hematite has been converted to maghemite (δ-Fe_2O_3), presumably due to the presence of the organic matter. At first inspection the XRD chart obtained for the residue from the iron oxide experiment suggested the presence of magnetite (Fe_3O_4). However the conversion of hematite to magnetite in an inert atmosphere at a relatively low temperature, i.e. 425°C, is unlikely in view of the fact that α-Fe_2O_3 is the stable iron oxide in air at temperatures of up to about 1400°C (Deer et al., 1962). Magnetite and maghemite exhibit similar XRD patterns.

5.3.6 Chemical Analyses of the Iron Compounds used in the Batch Autoclave Experiments

Table 15 presents the XRF, AAS and atomic emission spectrographic (AES) analyses data for the iron compounds used in the batch autoclave experiments. The high level of titanium and relatively high trace levels of chromium, manganese, vanadium and zirconium in the red mud catalyst (79629) reflect the accessory mineral content, e.g. chromite, rutile (anatase), zircon, etc., of the original bauxite. The high sodium content of the red mud catalyst is not readily explained in terms of its mineralogy,

since halite, or other sodium-rich phases, have not been identified in the XRD chart (see above). The coarse-grained iron filings (S1632) prepared from electrolytic iron contains lower levels of trace elements than the fine-grained iron powder (51633). Apart from manganese and nickel, the iron oxide (S1634) contains very low levels of trace elements.

5.3.7. Petrographic Examination of the Solid Residues from the Batch Autoclave and Low-Temperature Plasma Ashing (LTPA) Experiments

In the previous report both macroscopic and incident light microscopic descriptions of the solid residues were presented. Macroscopically, the tasmanite concentrate forms a weakly agglomerated residue when heated to 390°C in nitrogen. At 415°C the residue is a coherent, pitch-like material. At temperatures of 425°C, and above, the tasmanite concentrate forms a sooty, black residue (Telfer et. al., 1979).

Incident-light microscopy reveals that at 415°C in hydrogen the alginite forms a network of partially melted *Tasmanites* sp bodies. This appears to represent the transition between the onset of softening and sticking together of the alginite observed in the residue heated to 390°C in nitrogen and the amorphous alginite matrix, which encloses inert carbonaceous material (inertinite fragments, etc) and mineral matter grains, observed in the residue heated to 415°C in nitrogen (Plate Ia-c).

At 425°C in nitrogen the bulk of the alginite has disappeared; the inert constituents are cemented together by a minimum amount of carbonaceous material (Plate Id). This corresponds with the maximum conversion of the alginite to liquid and gaseous products (Telfer, et. al., 1979). At 480°C in nitrogen the inert constituents are cemented together by small amounts of carbonized organic matter, derived in part from the original alginite and in part from the alginite-derived oil (Plate IIa).

Microscopic examination of the hexane insoluble residues from the catalysed batch autoclave experiments provides information in respect of the metal sulphides. The zinc(II) chloride catalysed experiments yield residues that contain increasing amounts of poorly-crystalline zinc(II) sulphide (ZnS ≡ sphalerite), with reddish-brown internal reflection colours, with increase in the reaction temperature above 250°C.

The tin(II) chloride catalysed experiments yield residues that contain increasing amounts of tin(II) sulphide(SnS ≡ herzenbergite) with increase in the reaction temperature above 250°C. There is a gradual increase in the maximum grain size of the tin(II) sulphide with increase in the reaction temperature, i.e. 5 μm at 250°C, 25 μm at 330°C, 50 μm at 370°C and 80 μm at 390°C; there appears to be a slight reduction in grain size above 390°C.

The tin(II) sulphide occurs as euhedral/subhedral, blade-like or acicular crystals which typically occur as stellate aggregates, i.e. a radiating state of aggregation (Plate IIb). As has been reported previously, the tin(II) sulphide crystals are often observed to coat the outside of the alginite bodies in the residues from the experiments heated to 350°C and above (Telfer et. al., 1979).

At temperatures of 450°C and above, euhedral/subhedral crystals with a tetragonal outline are present in the residues. These crystals are tentatively identified as metallic tin.

The hexane-insoluble residues produced by heating the tasmanite concentrate in nitrogen to 425°C in the presence of various iron compounds were examined by incident light microscopy. In the case of the experiments carried out with the fine-grained iron powder (51633) and the coarse-grained iron filings (51632), the iron particles are coated by a thin surface layer of iron sulphide (Plate IIc-d). Incident light microscopy does not provide any clear evidence of interaction between sulphur and the iron oxide or red mud catalyst (Plate III); electron microscopy (SEM/EDS) was required to establish that this interaction has taken place (see below, section 5.3.8).

The LTPA residues were examined by incident light microscopy. After 24 hours there is evidence of a slight increase in the alginite reflectivity and polishing relief (Plate IVa). The body colour ranges from brown to purplish brown/purple. Incident blue-light excitation produces a yellow/yellowish brown to dull brown fluorescence; the less intense, browner, fluorescence colours are associated with the purple body colours. After 48 hours of LTPA the alginite reflectivity covers a wide range of values (Plate IVb-c). The body colour is purplish brown/purple or, in the case of the higher reflectivity alginite, white. The purplish brown alginite bodies yield a weak brown fluorescence under incident blue-light excitation; the remainder of the alginite is non fluorescent.

5.3.8 Examination of Hexane-insoluble Batch Autoclave Products by Electron Microscopy

Hexane-insoluble residues from the tin(II) chloride catalysed experiments heated above 400°C were examined by SEM/EDS. The characteristic radiating state of aggregation of acicular tin(II) sulphide was observed (Plate Va). Fine-grained flakes of tin were observed intergrown with tin(II) sulphide; distributions of tin and sulphur were recorded in addition to the electron-micrograph (Plate Vb-d). Hexane-insoluble residues from the zinc(II) chloride catalysed experiments were examined on the SEM/EDS and distributions of zinc and sulphur were recorded together with the electronmicrograph (Plate VI) of the zinc(II) sulphide grains associated with the alginite.

The hexane-insoluble residues from the batch autoclave experiments heated in the presence of various iron compounds were investigated using both the SEM/EDS and EPMA. The residue from the experiment carried out with the coarse-grained iron filings contains iron particles, 50-500 μm in grain size, which are coated by a narrow rim of iron sulphide, 2-5 μm in thickness. The iron sulphide penetrates into cracks in the iron particles. Electron-micrographs and distributions of iron and sulphur were recorded on the SEM/EDS (Plate VII a-d) and an electronmicrograph, sulphur distribution and profiles for iron and sulphur were recorded on the EPMA/wavelength dispersive X-ray fluorescence analysis system (Plate VII e-h). At higher magnification (x 1000) the iron sulphide rim can be seen to consist of a network of acicular crystals with an average length of about 5 μm. Also there appears to be a gap, 1-2 μm in width, between the iron particle and the iron sulphide rim (Plate VI d). EPMA/EDS analyses of the rim yield 61.81% iron and 38.19% sulphur which correspond to a non-stoichiometric iron sulphide $Fe_{0.93}S$, i.e. pyrrhotite. The hexane-insoluble residue from the experiment carried out with the fine-grained iron powder contains iron particles, 20-100 μm in grain size; which are coated by a 2-5 μm thick rim of acicular iron sulphide (Plate VIII).

The hexane-insoluble residues from the experiments carried out with iron oxide and the red mud catalyst were examined by SEM/EDS. The iron oxide occurs as subrounded to rounded bodies, 100-250 μm in size, which consist of an aggregate of small grains with a maximum grain size of 3 μm. The iron sulphide occurs as acicular grains, up to 5 μm in length; it tends to be concentrated in the margin of the iron oxide body, although a few

iron sulphide grains are clearly visible in the interior of the body (Plate IXa); electronmicrographs and distributions of iron and sulphur were recorded on the SEM/EDS (Plate IX). Electronmicrographs and distributions of iron and sulphur were recorded on the SEM/EDS (Plate X) for the red mud catalyst. There is only a slight tendency for the sulphur to concentrate in the iron(III) oxide grains in the particles of red mud catalyst.

5.4 Discussion

Ethylene (C_2H_4) does not occur in detectable amounts in the autoclave gas samples from the uncatalysed batch autoclave experiments; ethane (C_2H_6) only occurs in gas samples from uncatalysed experiments heated at 450°C and above (Telfer et al., 1979).

In the presence of either tin(II) chloride or zinc(II) chloride ethylene is formed in either a nitrogen or a hydrogen atmosphere at low temperatures (250°C-350°C). The formation of ethylene in the absence of hydrogen suggests that the metal chlorides react directly with the alginite at low temperatures. In this respect zinc(II) chloride appears to be more reactive than tin(II) chloride. The catalysed experiments yield gases in which the isoalkanes are dominant over the normal alkanes, which indicates that thermocatalytic processes have taken place even in the absence of hydrogen.

In the presence of hydrogen ethylene, rather than ethane, is formed when alginite is heated with metal chlorides at low temperatures; at higher temperatures (350°C-370°C) ethane is formed at the expense of ethylene (Telfer et al., 1979). The formation and stability of ethylene in the presence of hydrogen is of interest since it may reflect the presence of broken organosulphur bonds that lead to the formation of hydrogen sulphide thus inhibiting the hydrogenation of ethylene to ethane. At higher temperatures, the hydrogen sulphide probably reacts with the catalyst to form metal sulphides; although the catalyst may react directly with the organic sulphur in the alginite.

The metal chloride catalysed experiments in hydrogen yield hexane extracts with a relatively low organic sulphur content ($\geq$ 1%), due to scavenging of sulphur by tin and zinc. Clearly this is not a practical way to remove sulphur from the hexane extract ($\equiv$ oil). For this reason

batch autoclave experiments were carried out with various iron compounds in nitrogen, heating the autoclave to 425°C, the temperature at which the alginite is completely melted. Although there was some slight reduction in the organic sulphur content of the hexane extract with fine-grained iron powder and coarse-grained iron filings, iron oxide and red mud catalyst did not noticeably reduce the organic sulphur content of the hexane extract.

The failure of iron to reduce the organic sulphur content of the hexane extract is not due to the lack of reaction between the iron and the organic sulphur. Optical and electron microscopical studies indicate that the iron particles are rimmed by iron sulphide (pyrrhotite). The reaction between the iron and the sulphur probably ceases once the iron particles are completely coated. For this reason the fine-grained iron powder, with its greater surface area, should be more effective than the coarse-grained iron filings. However, there is not much difference between organic sulphur contents of the hexane extracts from the experiments carried out with fine-grained iron powder and those from the experiments carried out with coarse-grained iron filings, even when 20% by weight of iron is added to the alginite.

The iron oxide and red mud catalyst produced virtually no reduction in the organic sulphur content of the hexane extract by comparison with the organic sulphur content of the hexane extract produced by heating alginite to 425°C in nitrogen only. Electron microscopy reveals the marginal reaction between iron oxide grains and sulphur to form acicular iron sulphide (pyrrhotite).

The autoclave gas analyses for the iron compound batch autoclave experiments show a dominance of normal alkane over isoalkanes, which indicates that thermal, rather than thermocatalytic, processes have taken place. The absence of thermocatalytic reactions may be the reason for the inability of the iron compounds to influence the organic sulphur content of the hexane extracts. It is possible that, in the case of the metal chloride experiments, the catalyst reacts directly with the organic sulphur on the surface of, and within, the alginite bodies; whereas the iron compounds only react with organic sulphur liberated as hydrogen sulphide.

Although thermocatalytic processes do not appear to have taken place in the case of the iron compound experiments, the formation of isobutene ($CH_2{:}CH.CH_2CH_3$) probably represents a specific reaction between iron and

alginite. The appearance of alkenes at low to moderately high temperatures, i.e. >425°C, may reflect the unsaturated nature of some of the carbon-carbon bonds in the original alginite structure.

5.5 Curie-Point Pyrolysis Gas Chromatographic-Mass Spectrometric Analysis of Tasmanite Autoclave Products

5.5.1 Introduction

The tasmanite autoclave experiments yield products of great complexity. These mixtures cover a wide molecular weight range and a range of chemical classes. To fractionate these mixtures and identify individual components requires lengthy analytical procedures. A technique which is gaining wide acceptance for characterizing such complex materials is Curie point pyrolysis (CP). CP combined with either gas chromatography (GC) or gas chromatography-mass spectrometry (GC/MS) provides an analytical tool for the analysis of both the extracts and insoluble residues.

This technique has been previously used in many studies to characterize samples of geochemical interest (Jones and Cramer, 1977). It has the advantage that only small quantities of samples are required, the pyrolysis is rapid, reproducible and forms only primary products. In this study the extracts and residues have been typified using pyrolysis high resolution gas chromatography-mass spectrometry.

5.5.2 Experimental Method

Analytical pyrolysis-gas chromatography was carried out on a Pye pyrolyser using Ni/Fe wires with a curie point of 610°C. The products were directly introduced into a Hewlett Packard 5710 GC fitted with a SCOT (50 m x 0.5 mm I.D.) capillary column coated with OV101. The pyrolysis GC/MS data was obtained utilizing the Pye pyrolyser coupled to a Finnigan 4023 GC/MS system fitted with a (30 m x 0.25 mm) SP 2100 WCOT capillary column. The mass spectra was obtained using a scan time of 0.95 seconds, an electron energy voltage of 70 eV, over the scan range from 50 to 650 m/e in EI ionization mode.

5.5.3 Results and Discussion

Processing of the CP/GC/MS data has involved chemical class correlations, individual mass spectral molecular structure determinations and cross matching with the National Bureau of Standards - Environmental Protection Agency (NBS-EPA) mass spectral library.

(i) Extracts

The yield of hexane-soluble material from the untreated Tasmanite oil shale is extremely small. Hence the pyrogram from the hexane soluble products of the 200°C reaction will be used as a base-line point for comparative purposes. The pyrograms of the extracts at 250°, 330°, 350° and 370°C were almost identical to that at 200°C.

The pyrograms consist basically of a large unresolved envelope of alicyclic and aromatic constituents with a number of prominant components including n-alkanes (C_{13}-C_{26}), max. C_{15} and C_{17}, branched chain alkanes, isoprenoids C_{16}-C_{20}, alkyl cyclohexanes and substituted di- and tri-aromatics (Figure 11).

Although much of the extract has not been resolved by the high resolution capillary column, the GC/MS analysis yields valuable compositional information concerning this unresolved envelope.

In order to correlate pyrolysis products to the original material it is necessary to characterize or identify the majority of compounds present. This characterization has been achieved by the use of specific ion monitoring which has been carried out on a number of chemical classes and a number of homologous series have been detected. The ions chosen are characteristic of the compound class and are intense within that compound mass spectra. This allows detection of trace quantities of these materials.

The use of specific-ion monitoring for aliphatics (m/e 71) and dialkyl benzenes (m/e 105) for the extracts from the hydrogenation experiments at various temperatures are presented in Figure 12.

The dialkyl benzenes (3 isomers) start to become apparent at around 370°C. The relative amounts of dialkyl benzenes, methyl, di-, tri and tetramethyl-naphthalenes increase considerably at 415°C; n-hydrocarbons in the range C_{12}-C_{22} were dominant products of the pyrograms.

The dialkyl benzenes were still present at 480°C, but in lower relative abundance than at 415°C. The 480°C extract is dominated by n-alkanes and a noticeable absence of branched chain and isoprenoids is apparent compared to the 200°C extract.

There are four major components which have been labelled A, B, C and D in Figure 11. At this stage the structures of A, B and C have not been deduced, but compound D has been tentatively identified as 3, 3, 4, 4-tetramethyl dibenzyl. The pyrogram of the autoclave products from the 390°C reaction shows marked differences compared to that from 200°C. In particular the abundance of the compounds giving rise to peaks A and B relative to those responsible for C and D had also decreased. At 415°C a further reduction in the quantities of A and B relative to C and D had occurred along with a further decrease in the abundance of C relative to D. No evidence for the compounds producing the peaks labelled could be found at 480°C.

The results obtained from the experiments under nitrogen gave almost identical results. This suggests that the Tasmanite itself was a sufficiently rich source of hydrogen to permit identical reactions to occur, as though in the presence of an external source of hydrogen.

(ii) Residues

Pyrolysis of the hexane insoluble residues again showed that at all temperatures there were insignificant differences between the results obtained under hydrogen or nitrogen atmospheres (Figure 13).

The pyrograms of products obtained from autoclave temperatures up to 390°C contained the characteristic alkene/alkane doublets present in the original tasmanite and maximizing in the range C_7-C_{11}. At temperatures greater than 390°C a decrease in the relative intensity of the doublets was observed along with an increase in intensity of a complex "hump" of unresolved aromatic compounds. The pyrograms from the products of the 480°C reaction were dominated by this complex unresolved envelope, although traces of alkene/alkane doublets could still be observed. This might suggest that, even under these reaction conditions, small amounts of the original alginite remain unreacted, but petrographic evidence reveals the absence of any alginite. However minor amounts of vitrinite and inertinite observed could be responsible for these doublets.

6. UTILIZATION OF TASMANITE

6.1 General Comments

Most of the possible uses of Tasmanite require upgrading of the shale to decrease the mineral matter content. As described in an earlier report chemical demineralization is a very effective way of concentrating kerogen but this is not at all practical on a large scale. Fortunately Tasmanite, unlike most other oil shales, is amenable to relatively simple methods of physical upgrading. Techniques based on density differences, although not tested in the present research, would almost certainly be effective. However, probably froth flotation will prove to be the most satisfactory. Earlier work and this report show that mineral matter contents of 50% and much lower can be achieved without great difficulty.

The possibility of blending Tasmanite with a suitable coal may have attractions from the point of view of decreasing both ash and organic sulphur contents. Coals from the Mersey River area or eastern Tasmania would be the most suitable geographically but the very low ash, low sulphur coals of the Latrobe valley could also be a possibility. The value of blending depends of course on the use being considered. Some processes may benefit from the properties of a blend i.e. lower volatile content, lower ash, lower organic sulphur, more aromatics on pyrolysis, increased char (fixed carbon) potential etc.

The following are some of the uses that have been suggested or could be considered for Tasmanite:

(a) Liquid Hydrocarbons. Retorting of Tasmanite leads to a liquid product which, although obtained in good yield, still requires further upgrading (hydrogenation etc). Catalytic (or non-catalytic) hydrogenation leads to a better liquid product but, from the results of the present work, further treatment is needed before the product would be suitable as a refinery feed-stock. High sulphur contents present a problem but this can be overcome at a cost. The nitrogen content of the oil, although not high, may prove to be a more difficult refining problem.

(b) Specific Petrochemicals. The hope has often been expressed that, because of its unusual genesis and occurrence, tasmanite could be a source of particular, economically-important petrochemicals. Unfortunately, in all of our extraction and hydrogenation work the products are all multicomponent systems with no one compound dominating. It thus seems

unlikely that particular chemicals can be separated from Tasmanite or its decomposition products in any economically viable manner.

(c) Petroleum Coke. All naturally-occurring organic materials lead to some form of coke or char on pyrolysis and in some cases resemblances to petroleum coke are seen. Tasmanite is unlikely to be a good source of such coke on an economic basis for several reasons such as the high volatile and high sulphur content of the kerogen, the lack of dominant aromatic structures in the kerogen and the high ash content of any pyrolysis residue.

(d) Road Bitumen. Tasmanite has been tested and used as road bitumen and this appears to be its most obvious use. The high sulphur content is likely to be an advantage in assisting cross-linking of the bitumen into a resistant surface. The use of Tasmanite bitumen as a thin surface layer (in the same way as gilsonite is used) is an attractive proposition. Further details on road bitumens are given in the next section.

(e) Spent Shale as Cement of Fertiliser. Much oil shale research has centred on possible uses for spent shale after retorting. Some use could probably be made of spent Tasmanite shale in cement, road building or as a fertiliser. However, this shale doesn't appear to have any outstanding benefits in this regard and such uses would always be very much subsidiary to the oil or related product.

(f) Reclaim Rubber. The chemical structures of Tasmanite kerogen and rubber have some similarities. Thus lateral thinking suggests there may be a possibility of blending a Tasmanite concentrate with rubber (e.g. tyres) in the reclaiming process (Paul, 1979). Sulphur and 'filler' minerals are often added in this process and a Tasmanite concentrate would provide these as well as cross-linked kerogen which would 'depolymerize' in the same way as vulcanized rubber. The price of tyre reclaim is at present about 20 cents/lb making the addition of even a few percent Tasmanite to a reclaim mixture an interesting proposition.

6.2 Road Bitumens

The following are some of the most commonly used bitumen surfaces (Broome, 1973):

(a) Hot rolled asphalt - a mixture of fine aggregate (sand), filler and bitumen is used as a mortar for coarser-grained aggregate (rock, gravel or slag). It is mixed, laid and compacted hot giving a dense surface.

(b) Asphaltic concrete - a similar mixture to (a) except that the mineral aggregate is continuously graded from fine to coarse and bonded with a softer grade bitumen.

(c) Mastic asphalt - basically a graded limestone powder closely mixed with bitumen, possibly with gravel, grit or rock chippings. It is laid hot, and when finished provides a completely dense impervious surface.

(d) Bitumen macadam - prepared at a lower temperature with graded aggregate coated with a softer bitumen such as cut-back which is a bitumen that has had its viscosity reduced by the addition of a suitable volatile solvent. This surface has a more open texture.

(e) Fine cold asphalt - this consists of fine graded aggregate, coated warm with soft bitumen or cut-back, and can be stored before laying at atmospheric temperatures.

(f) Bitumen surfacing - bitumen sprayed on the road surface and embedded with a continuous cover of aggregate (Sherrard, 1958).

(g) Bitumen emulsions - this is a bitumen in a water emulsion which can be applied at ambient temperatures rather than being heated first as is usually the case (Broome and Wadelin, 1973).

All these road surfacings have their own set of specifications. Hence any new bitumen (such as that from Tasmanite) will be suitable for particular applications as determined by its specifications. The following tests are included in any specification (Broome and Wadelin, 1973):

(a) Penetration - this test is related to the hardness or consistency of the material.

(b) Softening Point - the measure of the change in consistency at a certain temperature, where the penetration of the bitumen has reached a certain point.

(c) Viscosity - this measurement is required to find the viscosity of the bitumen at the temperatures it is likely to be applied to a surface.

(d) Brittleness - a measure of the flexibility of the bitumen in withstanding temperature changes. The point at which it becomes brittle and breaks is the breaking point.

(e) Volatility - this is required as a test, to make sure that excessive volatile loss does not lead to over hardening of the bitumen causing cracks to form.

(f) Flash Point - the point at which the bitumen becomes flammable. For working purposes the correct viscosity must be achieved before the flash point is reached.

(g) Solubility - determines insoluble and soluble percentages of the bituminous material.

(h) Ash

(i) Relative Density (or specific gravity)

(j) Ductibility - a test for bitumen flexibility

(k) Acidity - a test useful in the production of mastic asphalts and anionic emulsions.

All the above are standard tests founded by the American Society for Testing Materials (ASTM) and the Institute of Petroleum (IP British). The majority of the tests require specialised equipment and are outside the scope of analyses and research currently being undertaken by the CSIRO Fuel Geoscience Unit.

7. ACKNOWLEDGEMENTS

Many members of the CSIRO Institute of Earth Resources at North Ryde have contributed to the research described in this report. We particularly acknowledge the contributions of N.C. Morgan, S. Goadby, J. Hadley and D. Rutherford (inorganic analyses), E. Murray and G. Hansen (sample preparation), A. Findlay and K.A. Maxwell (autoclave experiments), A.R. Horne (XRD), N. Watson (organic analyses), Dr. R.P. Philp (GC-MS), P. Ferry and R. Cosstick (low temperature ashing), L.F. Brunckhorst (electron microscopy) and J.F. Stephens (NMR). The cooperation of the Tasmanian Department of Mines and the support of Endeavour Resources Limited are also appreciated.

8. REFERENCES

Bartuska, V.J., G.E. Marciel, J. Schaefer, and E.O. Stejskal, (1977), Prospects for carbon-13 nuclear magnetic resonance analysis of solid fossil-fuel materials, *Fuel*, 56, 354.

Berry, L.G., and Thompson, R.M. (1962). X-ray powder data for ore minerals: the Peacock Atlas. Geological Society of America, Memoir 85.

Borg, I.Y., and Smith, D.K. (1969). Calculated X-ray powder patterns for silicate minerals. Geological Society of America, Memoir 122.

Broome, D.C. (1973). Bitumen. In "Modern Petroleum Technology" (ed. G.D. Hobson and W. Pohl). 4th Edition Applied Science Publishers Ltd. 804-815.

Broome, D.C. and Wadelin, F.A. (1973). Bitumen (Asphalt). In "Criteria for Quality of Petroleum Products". (ed. J.P. Allinson). Applied Science Publishers Ltd. 226-241.

Brown, G. (Editor) (1961). The X-ray identification and crystal structures of clay minerals. Mineralogical Society (Clay Minerals Group), Monograph 2.

Deer, W.A., Howie, R.A. and Zussman, J. (1962). Rock forming minerals, 5. Non-silicates. Longmans, Green and Co. Ltd., London, U.K.

Jones, G.E.R., and Cramer, C.A. (1977) Analytical Pyrolysis, Proc. 3rd Intern. Symp. Anal. Pyrolysis, Amsterdam, Elsevier.

Gluskoter, H.J. (1965). Electronic low temperature ashing of bituminous coal. *Fuel*, 44(4), 285-290.

Paul, J.P., (1979). Reclaiming Rubber, Chemtech, February, 104-108.

Pines, A., M.G. Gibby and J.S. Waugh, (1973), Proton-enhanced NMR of dilute spins in solids. *J. Chem. Phys.*, 59, 569.

Resing, H.A., A.N. Garroway, and R.N. Hazlett, (1978), Determination of aromatic hydrocarbon fraction in oil shale by ^{13}Cn.m.r. with magic-angle spinning, *Fuel*, 57, 450.

Sherrard, H.M. (1958). Bitumen Surface Treatment, and Gravel-Bitumen and Bituminous Macadam Surface Coarses. In "Australian Road Practice - An Introduction to Highway Engineering". Melbourne University Press, 220-236.

Telfer, A., Russell, N.J., Philp, R.P. and Saxby, J.D. (1979). Research on Tasmanite oil shale - third quarterly report to Endeavour Resources Limited. C.S.I.R.O. Restricted Investigation Report 1034R (unpublished).

Van der Hart, D.L., and H.L. Retcofsky, (1976). Estimation of coal aromaticities by proton-decoupled carbon-13 magnetic resonance spectra of whole coals.

Vitarovic, D., D. Vucelic, M.J. Gasic, N. Juranic, and S. Marcura, (1978) Analysis of the organic matter of oil shales by nuclear magnetic resonance. *Org. Geochem.*, 1, 89.

TABLE 1. PROXIMATE ANALYSES, FISCHER ASSAYS AND GRAY-KING ANALYSES ON TASMANITE

(all results as percentages, air-dried basis)

Lab No. Sample	77591 flotation concentrate	77591K demineralized flotation concentrate	78694K demineralized China Flat shale	78814 barren shale
Proximate analysis				
moisture	3.5	4.6	1.0	2.0
ash	32.6	7.0	24.7	93.3
volatile matter	60.2	82.4	67.4	3.7
fixed carbon	3.7	6.0	6.9	1.0
Fischer assay				
'coke'	43.9	19.7	40.1	96.4
tar	40.1	) 70.9	) 47.1	0.3
water	7.5	)	)	3.0
gas	8.3	9.3	12.8	0.3
Gray-King analysis				
'coke'	41.9	14.1	39.4	
tar & water	50.9	77.9	48.3	
gas	7.2	8.0	12.3	

TABLE 2. COMPARISON OF PROXIMATE ANALYSES, FISCHER ASSAYS AND GRAY-KING ASSAYS ON TASMANITE

(all results as percentages; dry, mineral-free basis)

Lab No. Sample	77591 flotation concentrate	77591K demineralized flotation concentrate	78694K demineralized China Flat shale
Proximate analysis			
volatile matter	94.3	93.2	90.7
fixed carbon	5.7	6.8	9.3
Fischer assay			
coke	17.9	14.4	20.6
tar	62.8	75.0	62.1
water	6.3		
gas	13.0	10.6	17.3
Gray-King analysis			
coke	14.5	8.0	19.8
tar & water	74.2	82.9	63.6
gas	11.3	9.1	16.6

TABLE 3. PETROGRAPHIC ANALYSES OF FLOTATION PRODUCTS

(Results given as percentages by volume)

mple	Lab. No.	Tasmanites	Fragmented† material	Other organic material	Clay	Carb-onate	Pyrite	Quartz	Sphalerite	Mica	Total No. of counts
Original sample om Sassafras ea +	78813	23	-	-	41	5	2	27	1	1	458
MIBC* loat	78847	24	23	tr	47	1	1	3	1	-	425
IBC ailing	78848	9	14	tr	42	4	2	28	1	tr	831
*+MIBC loat	78849	21	15	1	57	1	1	4	tr	-	730
+MIBC iling	78850	7	17	-	29	5	2	38	1	1	992
FO*+MIBC oat	78851	31	18	1	46	tr	1	3	-	-	485
O +MIBC ailing	78852	5	19	-	11	6	1	56	2	tr	604
Float 2	79256	36	50	tr	11	-	1	2	tr	tr	899
Tailing 2	79257	10	24	1	48	1	2	14	-	-	367
Float 3	79258	2	32	tr	35	2	5	23	1	-	1126
Tailing 3	79259	1	12	tr	23	5	3	55	1	tr	491
rren udstone ϕ	78814	-	-	-	57	-	2	41	-	-	61

† Fragmented material - fragments under 5 μ in size and not identifiable

ϕ From Bore No.8, 13'1"-22'1" (error large due to small number of counts)

MIBC - Methylisobutylcarbinol, ST - starch, FO - Fuel oil

* Original sample from the Sassafras area is a combination of Bore No.27B - Interval 26'7" - 31'5" (8.1-9.6 m) and Bore No. 28B - Interval 12'11"-18'4" (3.9-5.6 m)

tr Trace

TABLE 4. PROXIMATE ANALYSES OF FLOTATION PRODUCTS

(Results given as percentages by weight)

SAMPLE	LAB NO.	AIR-DRIED BASIS				DRY, ASH-FREE BASIS	
		Moisture	Ash	Volatile Matter	Fixed Carbon	Volatile Matter	Fixed Carbon
MIBC+ Float	78847	1.7	77.7	19.0	1.6	92.5	7.5
MIBC Tailing	78848	1.4	88.7	9.8	0.1	98.6	1.4
ST+ + MIBC Float	78849	1.6	74.1	22.0	2.3	*	*
ST. + MIBC Tailing	78850	0.7	90.8	8.2	0.3	97.6	2.4
F.O.+ + MIBC Float	78851	1.9	70.6	24.8	2.7	90.2	9.8
F.O. + MIBC Tailing	78852	0.8	91.4	7.6	0.2	97.2	2.8
FO+ST+MIBC Float 2	79256	1.5	53.2	42.3	3.0	93.3	6.7
FO+ST+MIBC Tailing 2	79257	1.6	86.4	11.2	0.8	93.3	6.7
FO+ST+MIBC Float 3	79258	1.3	89.0	9.1	0.6	94.3	5.7
FO+ST+MIBC Tailing 3	79259	1.0	92.8	6.2	0.0	99.8	0.2
Original Sample from Sassafras area‡	78813	1.2	88.5	10.6	*	*	*

* - Fixed carbon is estimated by difference. Since the calculated value is negative for this sample, the actual fixed carbon must be very small, or volatile matter is greater than 100%.

+ - ST - Starch, + FO - Fuel Oil, MIBC - Methylisobutylcarbinol

‡ - Original sample from the Sassafrass area is a combination of Bore No. 27B - Interval 26'7"-31'5" (8.1-9.6m) and Bore No. 28B - Interval 12'11"-18'4" (3.9-5.6m)

TABLE 5: GAS CHROMATOGRAPHIC ANALYSIS (VOLUME %) OF AUTOCLAVE GAS SAMPLES COLLECTED AT 20 KG/CM^2 FROM METAL HALIDE EXPERIMENTS

Experiment Number	Reaction Temperature (°C)	Catalyst	Cylinder Gas	Carbon Monoxide	Carbon Dioxide	Hydrocarbons					Cylinder Gas
						Alkanes		C_6+ Compounds	Ethylene	*Unidentified Compound	
						Methane + Ethane	C_3-C_5				
TC-83	250	$SnCl_2$	N_2	-	0.13	-	-	-	-	0.02	99.85
TC-84	250	$ZnCl_2$	N_2	-	0.13	-	-	-	-	-	99.87
TC-54	250	$SnCl_2$	H_2	+	0.13	-	-	-	-	0.02	99.85
TC-52	250	$ZnCl_2$	H_2	-	0.14	-	-	-	-	-	99.86
TC-79	280	$SnCl_2$	N_2	-	0.23	-	-	-	-	tr	99.77
TC-81	280	$ZnCl_2$	N_2	-	0.20	-	-	-	-	-	99.80
TC-55	280	$SnCl_2$	H_2	-	0.22	-	0.01	-	-	0.01	99.76
TC-56	280	$ZnCl_2$	H_2	-	0.21	-	-	-	tr	-	99.79
TC-32	300	-	N_2	-	0.21	-	-	-	-	-	99.79
TC-58	300	$SnCl_2$	N_2	tr	0.29	tr	0.01	-	tr	tr	99.70
TC-51	300	$ZnCl_2$	N_2	-	0.30	-	0.01	-	0.06	tr	99.61
TC-24	300	-	H_2	-	0.25	-	-	-	-	-	99.75
TC-22	300	$SnCl_2$	H_2	tr	0.31	-	tr	-	tr	tr	99.69
TC-23	300	$ZnCl_2$	H_2	tr	0.33	-	-	-	0.07	tr	99.60
TC-31	330	-	N_2	tr	0.29	tr	-	-	-	-	99.71
TC-57	330	$SnCl_2$	N_2	tr	0.37	tr	0.04	0.25	tr	tr	99.34
TC-50	330	$ZnCl_2$	N_2	-	0.39	-	tr	tr	0.06	tr	99.55
TC-34	330	-	H_2	tr	0.33	tr	-	-	-	-	99.67
TC-18	330	$SnCl_2$	H_2	tr	0.39	-	0.01	tr	0.04	-	99.56
TC-21	330	$ZnCl_2$	H_2	tr	0.41	-	0.01	-	0.09	-	99.49
TC-27	350	-	N_2	tr	0.36	tr	-	-	-	-	99.64
TC-80	350	$SnCl_2$	N_2	tr	0.39	tr	0.05	tr	tr	tr	99.56
TC-82	350	$ZnCl_2$	N_2	tr	0.39	tr	0.06	tr	tr	-	99.55
TC-33	350	-	H_2	tr	0.33	tr	-	-	-	-	99.67
TC-16	350	$SnCl_2$	H_2	tr	0.42	tr	0.04	tr	0.05	-	99.49
TC-17	350	$ZnCl_2$	H_2	tr	0.35	-	0.05	tr	0.08	-	99.52

* Unidentified compound has a retention time of about 3.0; it appears between n-butane and i-pentane. It has been assigned a response factor of 4.9×10^{-8} ml/unit area

TABLE 6. PROPORTIONS OF CARBON MONOXIDE, CARBON DIOXIDE AND HYDROCARBONS BY VOLUME IN AUTOCLAVE GAS SAMPLES COLLECTED AT 20KG/CM^2 FROM METAL HALIDE EXPERIMENTS

Experiment number	Reaction temperature (°C)	Catalyst	Cylinder Gas	Carbon Monoxide	Carbon Dioxide	Alkanes					C_6 + Compounds	Ethylene	*Unidentified Compound
						Methane	Ethane	Propane	Iso-butane	Normal Butane			
TC-83	250	$SnCl_2$	N_2	-	83.7	-	-	-	-	-	-	-	16.3
TC-84	250	$ZnCl_2$	N_2	-	100	-	-	-	-	-	-	-	-
TC-54	250	$SnCl_2$	H_2	-	88.4	-	-	-	-	-	-	-	11.6
TC-52	250	$ZnCl_2$	H_2	-	100	-	-	-	-	-	-	-	-
TC-79	280	$SnCl_2$	N_2	-	100	-	-	-	-	-	-	-	tr
TC-81	280	$ZnCl_2$	N_2	-	100	-	-	-	-	-	-	-	-
TC-55	280	$SnCl_2$	H_2	-	93.6	-	-	3.3	-	-	-	-	3.1
TC-56	280	$ZnCl_2$	H_2	-	100	-	-	-	-	-	-	tr	-
TC-32	300	-	N_2	-	100	-	-	-	-	-	-	-	-
TC-58	300	$SnCl_2$	N_2	tr	98.2	tr	tr	1.8	-	-	-	tr	tr
TC-51	300	$ZnCl_2$	N_2	-	76.9	-	-	8.8	-	-	-	14.3	tr
TC-24	300	-	H_2	-	100	-	-	-	-	-	-	-	-
TC-22	300	$SnCl_2$	H_2	tr	100	-	-	-	-	-	-	tr	tr
TC-23	300	$ZnCl_2$	H_2	tr	82.9	-	-	-	-	-	-	17.1	tr
TC-31	330	-	N_2	tr	100	tr	-	-	-	-	-	-	-
TC-57	330	$SnCl_2$	N_2	tr	56.1	tr	tr	5.6	tr	-	38.3	tr	tr
TC-50	330	$ZnCl_2$	N_2	-	87.0	-	-	-	tr	-	tr	13.0	tr
TC-34	330	-	H_2	tr	100	tr	-	-	-	-	-	-	-
TC-18	330	$SnCl_2$	H_2	tr	88.7	-	-	2.0	-	-	tr	9.3	-
TC-21	330	$ZnCl_2$	H_2	tr	79.8	-	-	1.8	tr	-	-	18.4	-
TC-27	350	-	N_2	tr	100	tr	-	-	-	-	-	-	-
TC-80	350	$SnCl_2$	N_2	tr	88.6	tr	tr	11.4	tr	-	tr	tr	tr
TC-82	350	$ZnCl_2$	N_2	tr	86.4	tr	tr	11.5	2.1	tr	tr	tr	-
TC-33	350	-	H_2	tr	100	tr	-	-	-	-	-	-	-
TC-16	350	$SnCl_2$	H_2	tr	82.4	tr	-	8.0	tr	-	tr	9.6	-
TC-17	350	$ZnCl_2$	H_2	tr	74.0	-	-	8.1	1.8	tr	tr	16.1	-

* Unidentified compound has a retention time of about 3.0; it appears between n-butane and i-pentane. It has been assigned a response factor of 4.9×10^{-8}ml/unit area.

TABLE 7. GAS CHROMATOGRAPHIC ANALYSIS (VOLUME %) OF AUTOCLAVE GAS SAMPLES COLLECTED AT 20KG/CM^2 FROM BATCH AUTOCLAVE EXPERIMENTS RUN AT 425°C USING A NITROGEN ATMOSPHERE AND IRON COMPOUNDS

Experiment Number	Iron Compound	Weight of Tasmanite Concentrate	Weight of Iron Compound	Carbon Monoxide	Alkanes						C_6+ Compounds	Alkenes	Nitrogen (Cylinder gas)
					Carbon Dioxide	Methane	Ethane	Propane	Butanes	Pentanes			
TC-8	-	-	-	0.08	0.89	0.42	-	0.18	0.08	0.01	-	-	98.34
TC-61	Fine-grained	4.75	0.25	0.15	0.68	0.34	0.11	0.16	0.05	0.01	-	a 0.01	98.49
TC-76	Iron powder	4.75	0.25	0.18	0.69	0.37	0.14	0.19	0.07	0.01	tr	a,b tr	98.35
TC-62	Reduced by	4.50	0.50	0.20	0.56	0.27	0.09	0.13	0.05	-	-	a 0.01	98.69
TC-71	Hydrogen	4.50	0.50	0.19	0.49	0.23	0.06	0.17	0.03	tr	tr	a,b 0.01	98.83
TC-69*	(51633)	4.00	1.00	0.17	0.48	0.21	0.07	0.18	0.03	tr	tr	a,b 0.01	98.85
TC-70*		4.00	1.00	0.14	0.40	0.14	tr	0.10	0.01	tr	tr	a 0.01	99.20
TC-68*	Coarse-grained	4.50	0.50	0.02	0.80	0.33	0.10	0.11	0.06	-	tr	a,b 0.01	98.56
TC-65*	Iron filings	4.00	1.00	0.10	0.69	0.31	0.10	0.16	0.05	tr	tr	a,b 0.01	98.59
TC-77*	From Electrolytic iron (51632)	4.00	1.00	0.10	0.65	0.31	0.12	0.15	0.07	0.01	tr	a,b tr	98.60
TC-63	Iron Oxide	4.50	0.50	0.15	0.69	0.32	0.11	0.16	0.05	-	-	a 0.01	98.51
TC-74	(Fe_2O_3=99.9%)	4.50	0.50	0.15	0.74	0.38	0.15	0.21	0.07	0.01	tr	a,b tr	98.29
TC-67*	(51634)	4.00	1.00	0.17	1.23	0.49	0.17	0.22	0.07	0.01	tr	a,b 0.02	97.63
TC-66*	Nippon light	4.50	0.50	0.07	0.71	0.29	0.10	0.17	0.04	tr	tr	a,b 0.01	98.61
TC-73*	Metal industry	4.50	0.50	tr	1.04	0.41	0.17	0.22	0.09	0.02	tr	a,b tr	98.06
TC-64	Red mud	4.00	1.00	tr	0.97	0.29	0.10	0.14	0.05	-	-	a 0.01	98.44
TC-72*	Catalyst (79629)	4.00	1.00	tr	0.99	0.32	0.13	0.17	0.06	0.01	tr	a,b 0.01	98.31

a = i-butene (C_4H_8) b = ethylene (C_2H_4)

* Trace amounts (<0.01%) of an unidentified compound with a retention time of 2.86, i.e. a retention time between that of n-butane and i-pentane

TABLE 8. PROPORTIONS OF CARBON MONOXIDE, CARBON DIOXIDE AND HYDROCARBONS BY VOLUME IN AUTOCLAVE GAS SAMPLES COLLECTED AT 20KG/CM^2 FROM IRON COMPOUND EXPERIMENTS

Experiment number	Iron compound	Weight of Tasmanite concentrate	Weight of iron compound	Carbon Monoxide	Carbon Dioxide	Alkanes							C_6^+ Compounds	Alkenes		*Unidentified compound
						Methane	Ethane	Propane	Iso-butane	Normal butane	Iso-pentane	Normal pentane		Ethylene	Iso-butene	
TC-8	-	-	-	4.6	53.4	25.3	-	11.0	0.5	4.4	-	0.8	-	-	-	-
TC-61	Fine-grained iron powder (51633)	4.75	0.25	10.2	45.0	22.4	7.5	10.6	0.4	3.0	-	0.2	-	-	0.7	-
TC-76		4.75	0.25	10.7	41.6	22.7	8.6	11.7	0.5	3.9	tr	0.3	tr	tr	tr	-
TC-62		4.50	0.50	15.5	42.7	20.9	6.9	9.9	0.4	2.9	-	-	-	-	0.8	-
TC-71		4.50	0.50	15.9	42.0	19.7	5.1	14.2	0.3	2.1	-	tr	tr	tr	0.7	-
TC-69		4.00	1.00	15.1	41.4	18.6	6.1	15.4	0.3	2.4	-	tr	tr	tr	0.7	tr
TC-70		4.00	1.00	18.1	50.6	17.2	tr	12.0	tr	1.4	-	tr	tr	-	0.7	tr
TC-68	Coarse-grained iron fillings (51632)	4.50	0.50	1.1	51.9	21.6	6.6	14.6	0.3	2.9	tr	0.3	tr	tr	0.7	tr
TC-65		4.00	1.00	7.0	48.3	21.8	7.3	11.1	0.4	3.1	tr	0.3	tr	tr	0.7	tr
TC-77		4.00	1.00	7.1	46.0	22.7	8.3	10.5	0.5	4.3	tr	0.6	tr	tr	tr	tr
TC-63	Iron Oxide (51634)	4.50	0.50	10.2	46.2	21.7	7.5	10.4	0.4	2.9	-	-	-	-	0.8	-
TC-74		4.50	0.50	8.5	43.2	22.3	9.0	12.4	0.4	3.9	tr	0.3	tr	tr	tr	-
TC-67		4.00	1.00	7.3	51.7	20.5	7.1	9.2	0.3	2.6	tr	0.2	tr	tr	0.9	0.2
TC-66	Red Mud catalyst (79629)	4.50	0.50	4.9	51.4	21.0	6.9	12.6	0.3	2.3	tr	tr	tr	tr	0.6	tr
TC-73		4.50	0.50	tr	53.5	20.9	8.8	11.2	0.4	4.1	tr	1.0	tr	tr	tr	0.1
TC-64		4.00	1.00	tr	61.9	18.8	6.5	9.0	0.3	2.7	-	-	-	-	0.8	-
TC-72		4.00	1.00	tr	58.5	19.1	7.7	10.2	0.4	3.0	tr	0.4	tr	tr	0.7	tr

* Unidentified compound has a retention time of 2.86; it appears between n-butane and i-pentane. It has been assigned a response factor of 5 x 10^{-8}ml/unit area.

TABLE 9. ULTIMATE ANALYSES (DRY ASH FREE BASIS) FOR UNTREATED TASMANITE CONCENTRATE AND THE HEXANE EXTRACTS OBTAINED FROM BATCH AUTOCLAVE EXPERIMENTS AT 425°C

SAMPLE		ULTIMATE ANALYSIS					ATOMIC RATIOS	
		C%	H%	N%	ORGANIC S%	O% (by difference)	H/C	O/C
UNTREATED TASMANITE CONCENTRATE		75.5	10.1	0.8	2.9	10.7	1.61	0.11
BATCH AUTOCLAVE EXPERIMENTS	N_2	85.1	9.8	0.8	2.1	2.2	1.38	0.02
	H_2	82.7	10.4	0.7	2.7	3.5	1.51	0.03
	H_2 + $SnCl_2$	85.4	11.7	0.5	1.2	1.8	1.64	0.02
	H_2 + $ZnCl_2$	87.1	10.7	0.3	1.0	0.9	1.47	0.01

TABLE 10. ORGANIC SULPHUR CONTENT (WEIGHT%) OF HEXANE EXTRACTS (HEAVY HYDROCARBONS) OBTAINED FROM BATCH AUTOCLAVE EXPERIMENTS

a: METAL HALIDE EXPERIMENTS:

REACTION TEMPERATURE	UNCATALYSED BATCH AUTOCLAVE EXPERIMENTS		CATALYSED BATCH AUTOCLAVE EXPERIMENTS	
			TIN(II) CHLORIDE	ZINC(II) CHLORIDE
	NITROGEN	HYDROGEN	HYDROGEN	HYDROGEN
415	2.5	2.8	2.1	1.3
425	2.1	2.7	1.2	1.0
450	2.0	1.6	1.2	0.9

b: EXPERIMENTS RUN AT 425°C IN NITROGEN WITH IRON COMPOUNDS:

WEIGHT OF TASMANITE CONCENTRATE (gms)	WEIGHT OF IRON COMPOUNDS (gms)	IRON POWDER REDUCED BY HYDROGEN (51633)	COARSE IRON FILINGS FROM ELECTROLYTIC IRON (51632)	IRON OXIDE (51634)	NIPPON LIGHT METAL INDUSTRY RED MUD CATALYST (79629)
4.75	0.25	1.8	-	-	-
4.50	0.50	1.7	1.9	2.0	2.1
4.00	1.00	1.7	1.8	1.9	2.0

TABLE 11. A COMPARISON BETWEEN THE LOW-TEMPERATURE PLASMA ASHING BEHAVIOUR OF THE TASMANITE CONCENTRATE AND THAT OF OTHER MACERAL CONCENTRATES

Sample	Duration of LPTA experiment (hours)			
	24	48	72	96
	Weight % of residue remaining			
Tasmanite concentrate (32.3% ash)	62.0	45.3	38.1	32.3
A vitrinite concentrate (0.8% ash)	0.8	0.6	0.6	0.4
An inertinite concentrate (16.2% ash)	36.0	20.1	15.3	12.6

TABLE 12. VARIATION IN THE PROPORTIONS OF PYRRHOTITE, PYRITE, GYPSUM AND ANHYDRITE WITH INCREASE IN REACTION TEMPERATURE IN TERMS OF XRD PEAK HEIGHT RATIOS MEASURED AGAINST THE 1.54Å QUARTZ REFLECTION

Sample		XRD peak height ratios			
		$\frac{Po_{3.00Å}}{(Qz_{1.54Å}+Po_{3.00Å})}$	$\frac{Py_{3.12Å}}{(Qz_{1.54Å}+Py_{3.12Å})}$	$\frac{Gy_{3.06Å}}{(Qz_{1.54Å}+Gy_{3.06Å})}$	$\frac{An_{3.50Å}}{(Qz_{1.54Å}+An_{3.50Å})}$
Untreated Tasmanite concentrate		0.28	0.51	0.56	0.23
Batch autoclave experiments (hydrogen atmosphere - no catalyst)	200°C	0.29	0.38	0.41	0.30
	300°C	0.28	0.33	-	0.48
	390°C	0.34	0.22	-	0.49
	425°C	0.38	0.04	-	0.49
	480°C	0.36	0.04	-	0.53
Low-temperature plasma ash (210.5 hours)		0.21	-	-	0.12

Po = Pyrrhotite ($Fe_{1-x}S$)

Py = Pyrite (FeS)

Gy = Gypsum ($CaSO_4.2H_2O$)

An = Anhydrite ($CaSO_4$)

Qz = Quartz (SiO_2)

TABLE 13. VARIATION IN THE PROPORTIONS OF ZINC(II) SULPHIDE WITH INCREASE IN THE REACTION TEMPERATURE IN THE ZINC(II) CHLORIDE CATALYSED BATCH AUTOCLAVE EXPERIMENTS

Batch autoclave experiment temperature (°C)	XRD peak height ratios			
	$\frac{ZnS/FeS_2\ 3.12Å}{Qz\ 1.82Å+ZnS/FeS_2\ 3.12Å}$	$\frac{ZnS\ 1.91Å}{Qz\ 1.91Å+ZnS\ 1.91Å}$	$\frac{ZnS/FeS_2\ 1.63Å}{Qz\ 1.82Å+ZnS/FeS_2\ 1.63Å}$	$\frac{ZnS\ 1.54Å+Qz\ 1.54Å}{Qz\ 1.54Å+ZnS\ 1.54Å/1.82Å}$
200	0.24	0.0	0.05	0.38
300	0.36	0.12	0.10	0.45
330	0.37	0.19	0.11	0.37
350	0.37	0.25	0.15	0.37
390	0.50	0.33	0.18	0.37
415	0.48	0.40	0.23	0.42
425	0.47	0.38	0.24	0.38
450	0.51	0.41	0.25	0.38
480	0.51	0.43	0.24	0.38

ZnS = Sphalerite (Zinc(II) Sulphide) (ZnS)

Qz = Quartz

TABLE 14. VARIATION IN THE PROPORTIONS OF TIN(II) SULPHIDE AND TIN WITH INCREASE IN THE REACTION TEMPERATURE IN THE TIN(II) CHLORIDE CATALYSED BATCH AUTOCLAVE EXPERIMENTS

	XRD Peak Height ratios	Batch autoclave reaction temperature (°C)								
		200	300	330	350	390	415	425	450	480
Tin reflections	$\frac{Sn_{3.04Å}}{Qz_{1.82Å}+Sn_{3.04Å}}$	0.0	0.06	0.06	0.09	0.09	0.23	0.26	0.17	0.21
	$\frac{Sn_{2.77Å}}{Qz_{1.82Å}+Sn_{2.77Å}}$	0.14	0.26	0.24	0.34	0.48	0.56	0.68	0.61	0.61
	$\frac{Sn_{2.01Å}}{Qz_{1.82Å}+Sn_{2.01Å}}$	0.08	0.11	0.12	0.14	0.34	0.32	0.28	0.31	0.34
Tin(II) sulphide reflections	$\frac{SnS_{4.04Å}}{Qz_{1.82Å}+SnS_{4.04Å}}$	0.0	0.18	0.15	0.19	0.32	0.40	0.30	0.24	0.25
	$\frac{SnS_{3.41Å}}{Qz_{1.82Å}+SnS_{3.41Å}}$	0.25	0.30	0.32	0.25	0.41	0.49	0.33	0.34	0.44
	$\frac{Sn_{3.24Å}}{Qz_{1.82Å}+SnS_{3.24Å}}$	0.0	0.20	0.26	0.29	0.57	0.42	0.38	0.46	0.57
	$\frac{SnS_{2.93Å}}{Qz_{1.82Å}+SnS_{2.93Å}}$	0.0	0.23	0.32	0.20	0.44	0.49	0.38	0.41	0.38
	$\frac{SnS_{2.31Å}}{Qz_{1.82Å}+SnS_{2.31Å}}$	0.0	0.13	0.18	0.21	0.41	0.41	0.33	0.40	0.35
	$\frac{SnS_{1.88Å}}{Qz_{1.82Å}+SnS_{1.88Å}}$	0.0	0.11	0.19	0.17	0.31	0.39	0.44	0.26	0.25
	$\frac{SnS_{1.78Å}}{Qz_{1.82Å}+SnS_{1.78Å}}$	0.0	0.11	0.12	0.14	0.23	0.36	0.42	0.31	0.30
	$\frac{SnS_{1.63Å}}{Qz_{1.82Å}+SnS_{1.63Å}}$	0.08	0.14	0.15	0.10	0.26	0.25	0.33	0.17	0.23

Sn = α-tin

SnS = Herzenbergite (Tin(II)sulphide) (SnS)

Qz = Quartz

TABLE 15. ANALYTICAL DATA FOR THE IRON COMPOUNDS USED IN THE BATCH AUTOCLAVE EXPERIMENTS

(values in p.p.m. unless otherwise indicated)

Element	Fine-grained iron powder (51633)	Coarse-grained iron filings (51632)	Iron oxide (51634)	Red mud catalyst (79629)
Ag	-	-	-	<0.1
† Al	-	-	-	9.86%
As	-	-	-	200
B	-	(<4)	<4	40
† Ca	-	-	++	1.34
Co	80	80	-	-
Cr	20	-	20	200
Cu	8	15	4	5
† Fe	+++	+++	+++	28.03%
Ga	(<8)	(<3)	0.3	8
Ge	-	-	-	1
† K	-	-	-	0.09%
† Mg	-	-	+	0.04%
Mn	-	-	400	300
Mo	(<1)	(1)	2	6
* Na	-	-	+	5.52%
Ni	150	40	100	(4)
P	-	-	-	0.08%
Pb	3	15	15	50
S	-	-	-	0.16%
Si	-	-	+	6.02%
Sn	-	20	1	25
Ti	600	-	(2)	3.58%
V	250	-	(15)	200
W	-	-	-	<8
Y	-	-	-	(30)
Zn	(80)	(150)	<30	40
Zr	-	-	-	1500

+++ major constituent

++ minor to moderately abundant constituent

+ minor constituent

values in parenthesis are tentative

† XRF analysis * AAS analysis

TABLE 16. XRD DATA FOR IRON COMPOUND BATCH AUTOCLAVE EXPERIMENTS

Sample	Non iron-bearing compounds	Iron-bearing compounds
Untreated Tasmanite concentrate	Quartz, gypsum, anhydrite, illite/mica, kaolinite and chlorite	Pyrite and pyrrhotite
Powdered iron (51633)	-	Iron; traces of hematite
Iron oxide (51634)	-	Hematite
Red mud catalyst (79629)	Quartz, anatase, (TiO_2) boehmite (δ-$Al_2O_3.H_2O$)	Hematite, goethite and traces of lepidocrocite
TC-64 Tasmanite concentrate + red mud catalyst	Quartz, anhydrite, illite mica and boehmite(?)	Hematite and pyrrhotite (lepidocrocite)
TC-67 Tasmanite concentrate + iron oxide	Quartz, anhydrite and illite/mica	Maghemite (Magnetite?) pyrrhotite and traces of hematite
TC-69 Tasmanite concentrate + powdered iron	Quartz, anhydrite and illite/mica	Iron, pyrrhotite and traces of hematite.

Figure 1 Froth Flotation test - outline and results

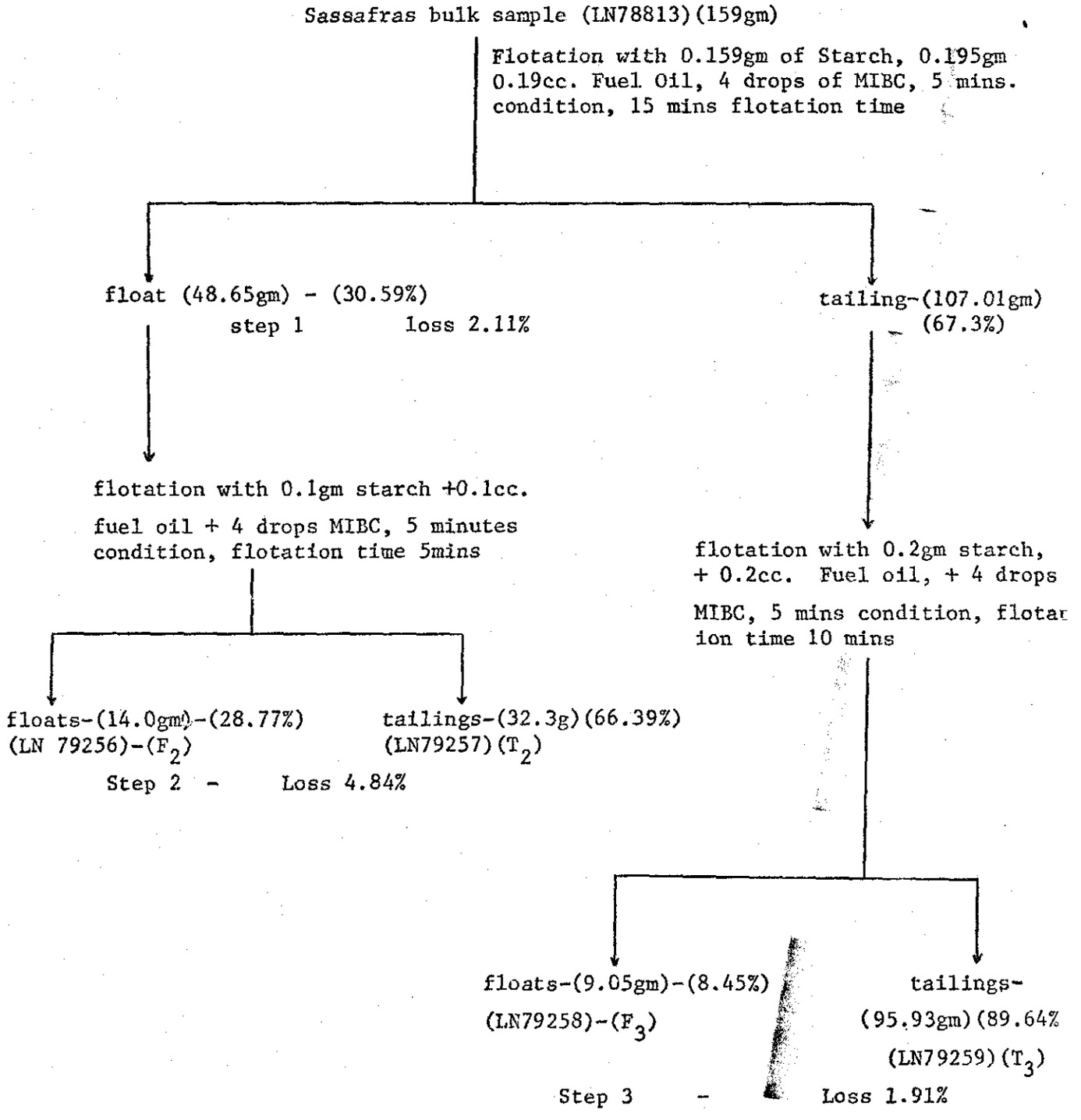

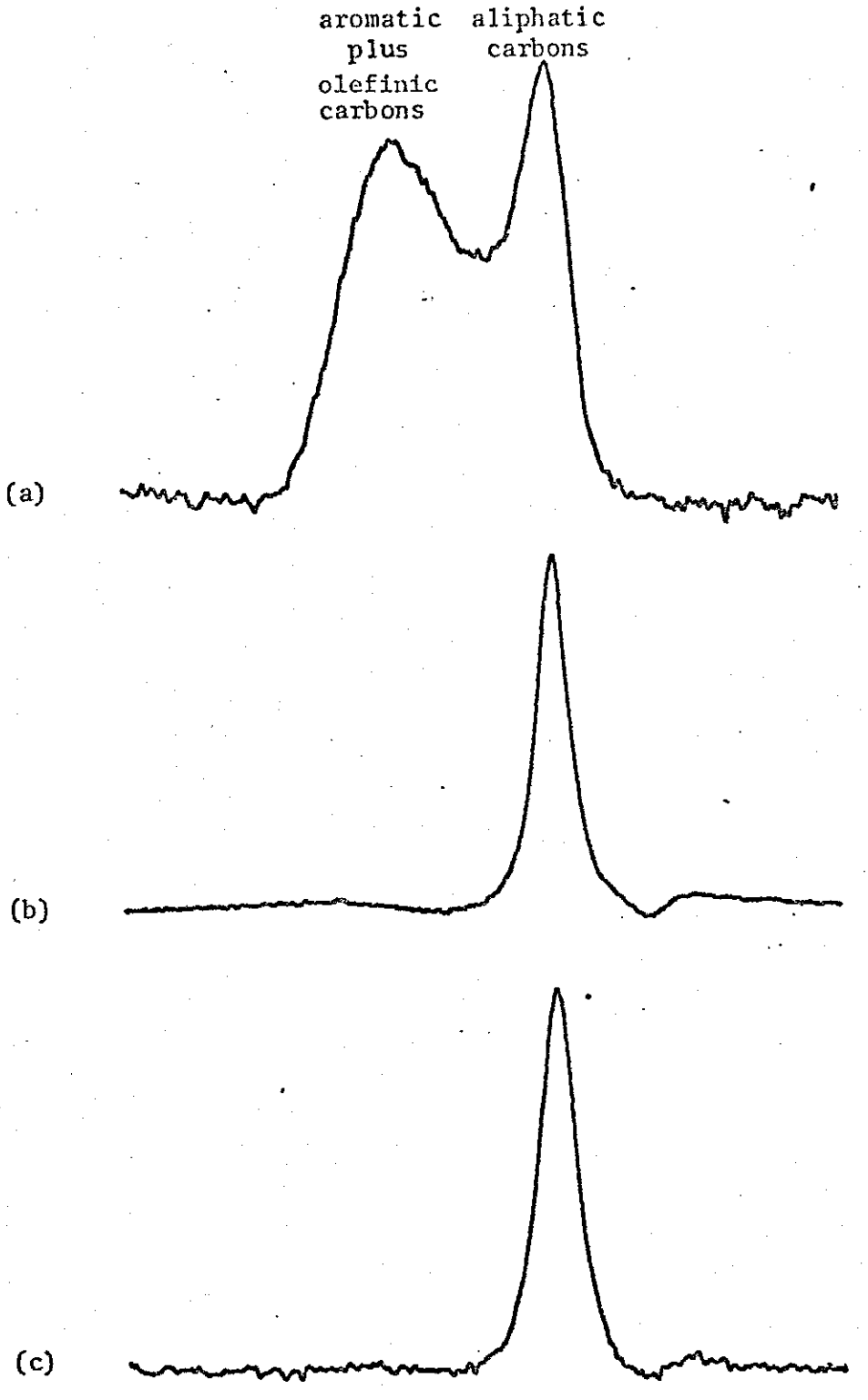

Fig. 2. Proton enhanced 22.63 MHz ^{13}C spectra of some petrographic concentrates from Australian coals and oil shales

(a) vitrinite concentrate

(b) exinite concentrate from Glen Davis oil shale

(c) Tasmanite concentrate

053

FIGURE 3 : Pressure (P) Temperature (T) and Differential Thermal Analysis (DTA) Curves (versus time) for uncatalysed and catalysed batch autoclave experiments heated to 350°C

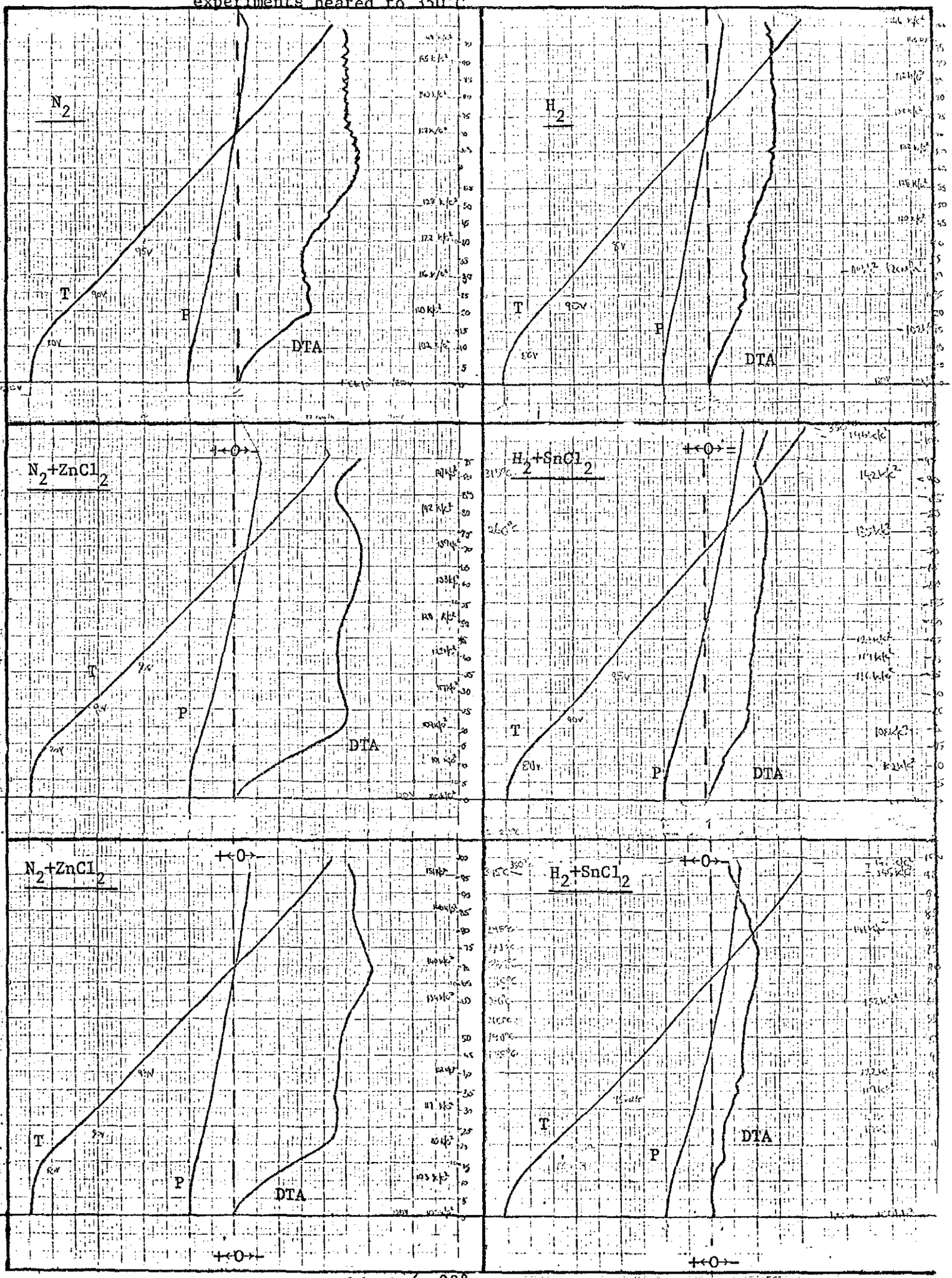

Initial temperature ambient (c.23°C)
Initial pressure 100 kg/cm^2 (9.8 Mpa)

116059

FIGURE 4: Pressure (P) Temperature (T) and Differential Thermal Analysis (DTA) Curves (versus time) for batch autoclave experiments heated in nitrogen to 425°C in the presence of iron compounds

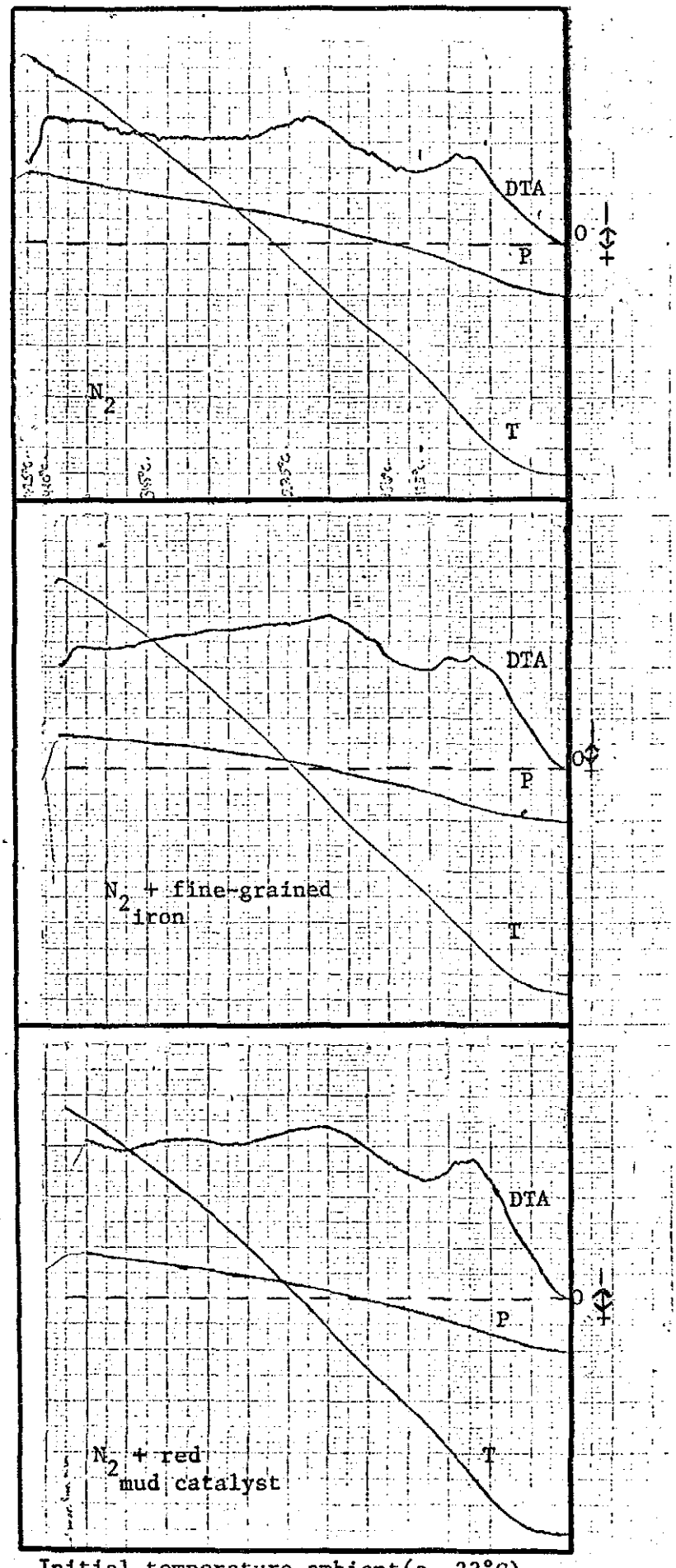

Initial temperature ambient (c. 23°C)
Initial pressure 100 kg/cm^2 (9.8MPa)
Final pressure 160 kg/cm^2 (15.7 MPa)

FIGURE 5: Variation in the XRD reflections of Gypsum, Anhydrite, Pyrrhotite and Pyrite with increase in the reaction temperature in uncatalysed batch autoclave residues

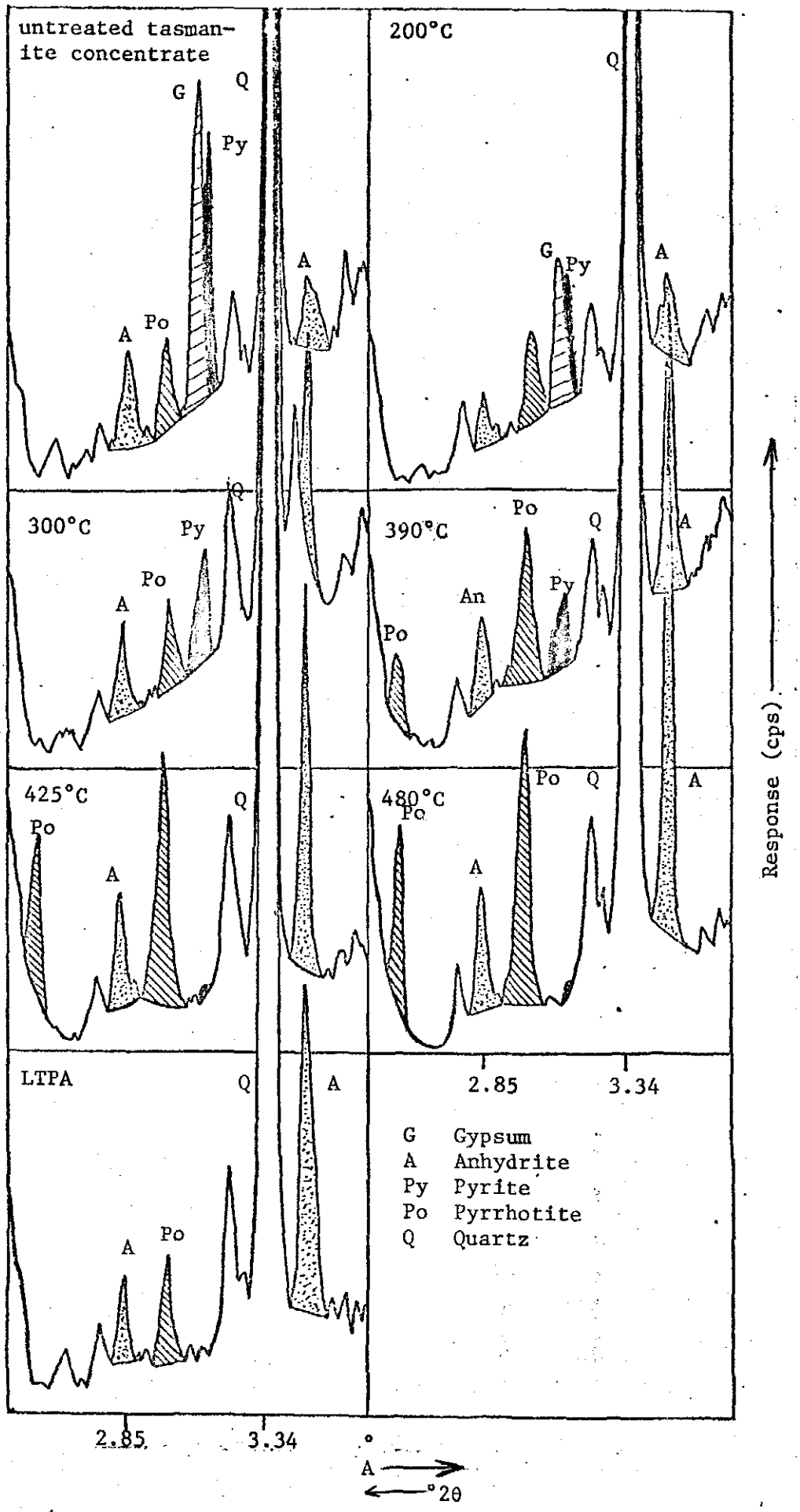

FIGURE 6: Variation in peak height ratios for sulphide and sulphate minerals with increase in reaction temperature (uncatalysed batch autoclave experiments) (peak height ratios measured against the quartz 1.54 Å reflection)

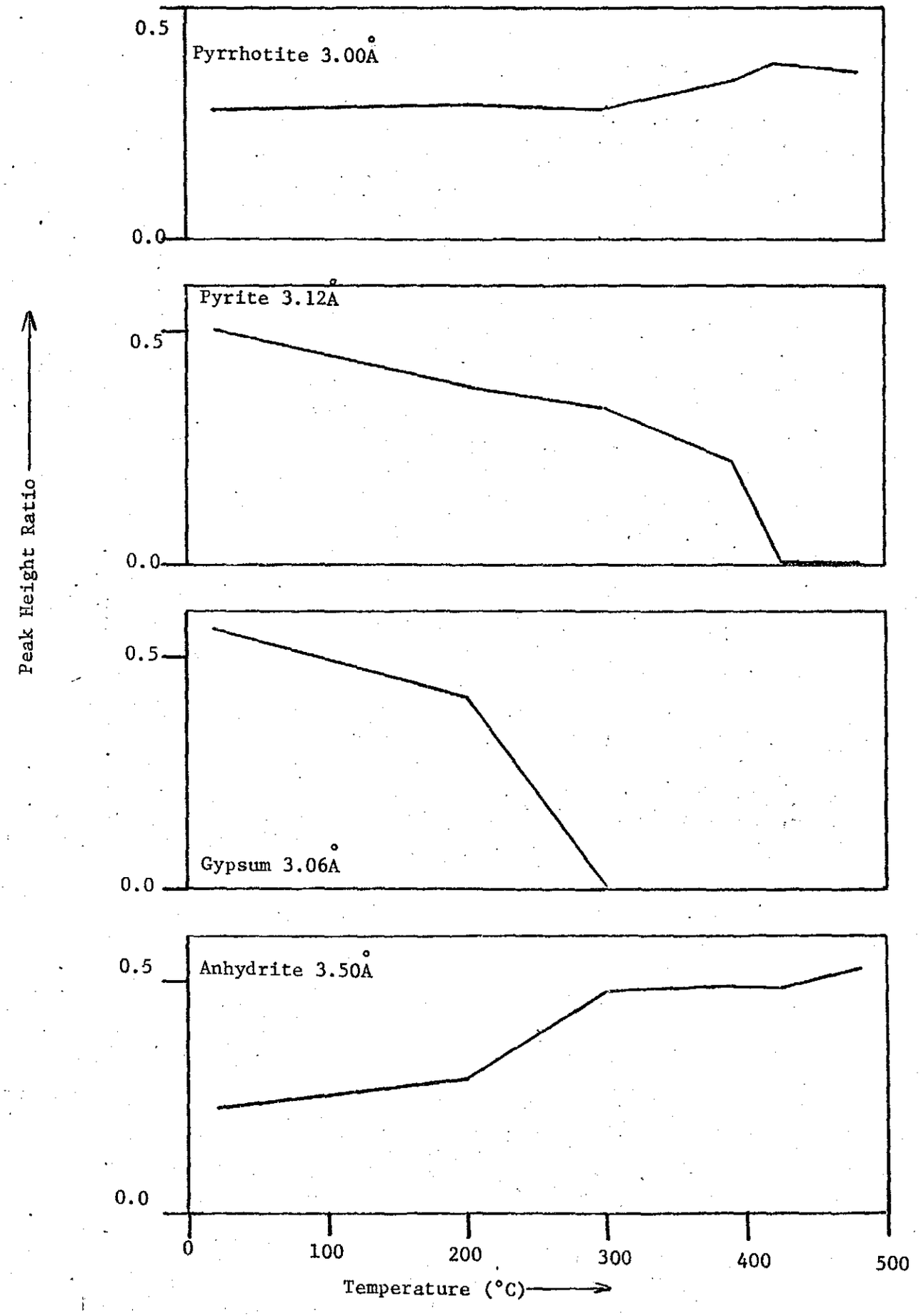

FIGURE 7: Variation in the XRD reflections of zinc (II) sulphide with increase in the reaction temperature in the zinc (II) chloride catalysed experiments (zinc (II) sulphide reflections are shaded)

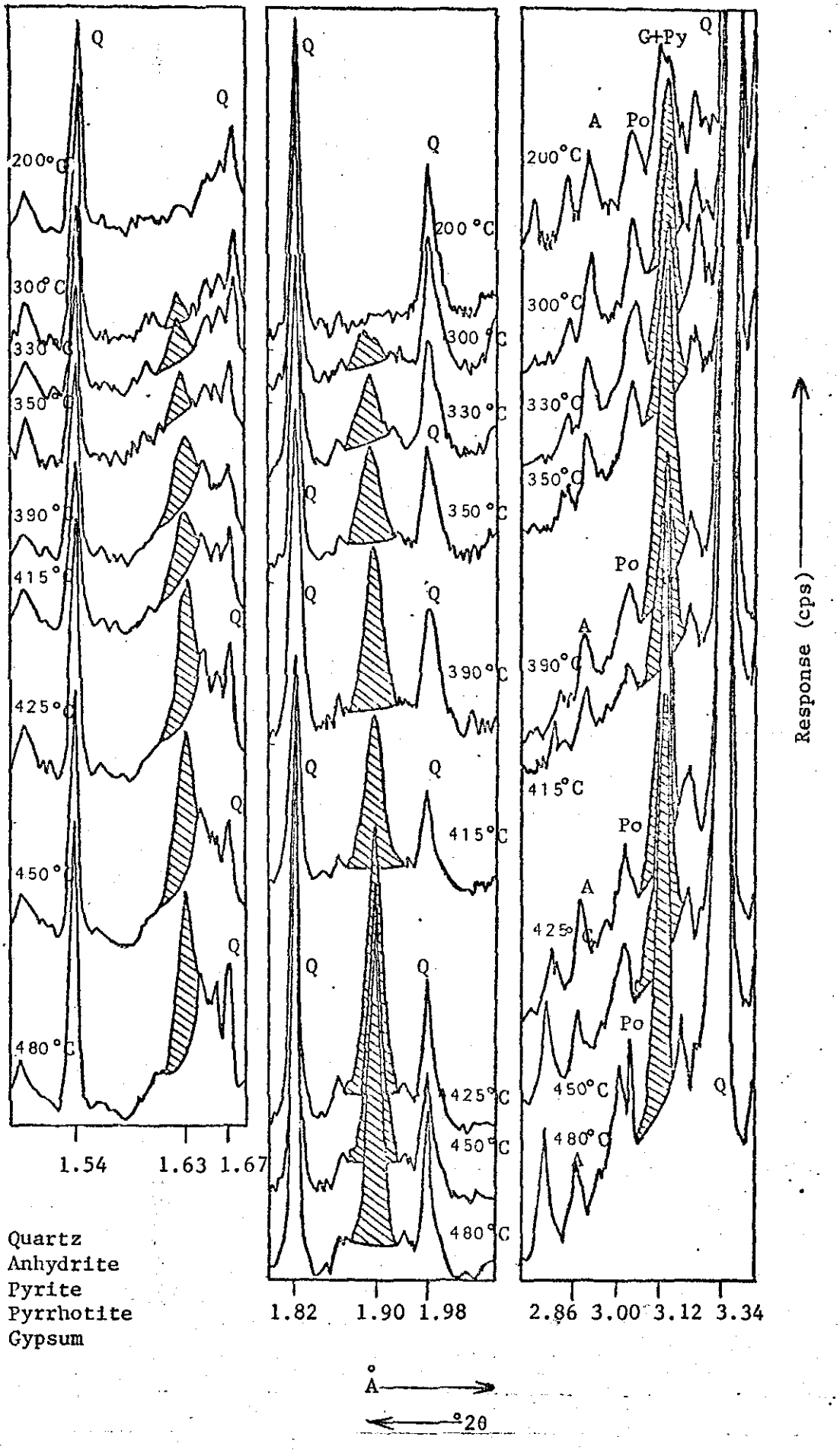

Q Quartz
A Anhydrite
Py Pyrite
Po Pyrrhotite
G Gypsum

FIGURE 8 Variation in peak height ratios for metal halide derivatives with increase in the reaction temperature (catalysed batch autoclave experiments) (peak height ratios measured against the quartz 1.82A reflection):

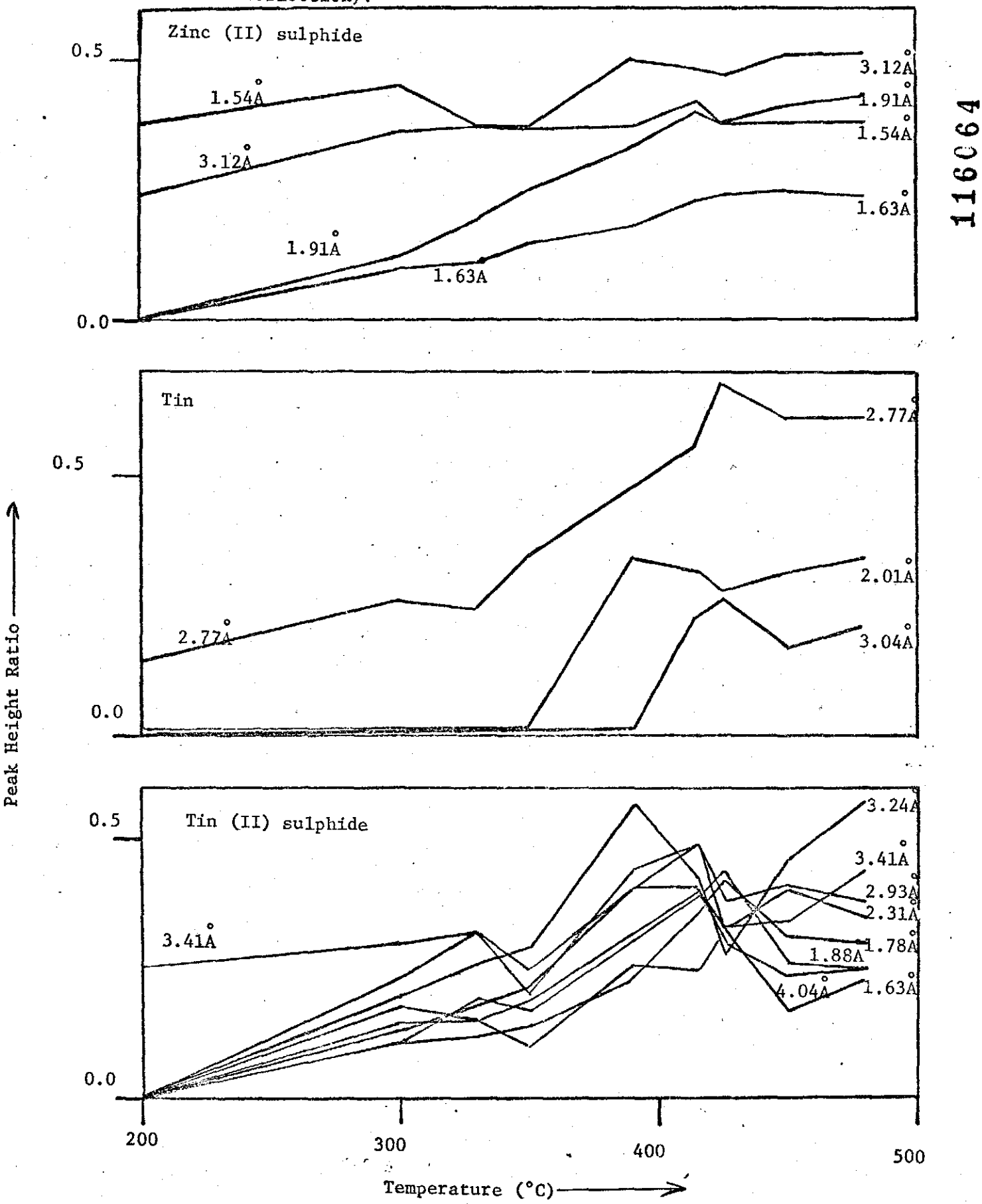

116064

FIGURE 9: Variation in the XRD reflections of tin and tin (II) sulphide with increase in the reaction temperature in the zinc (II) chloride catalysed experiments

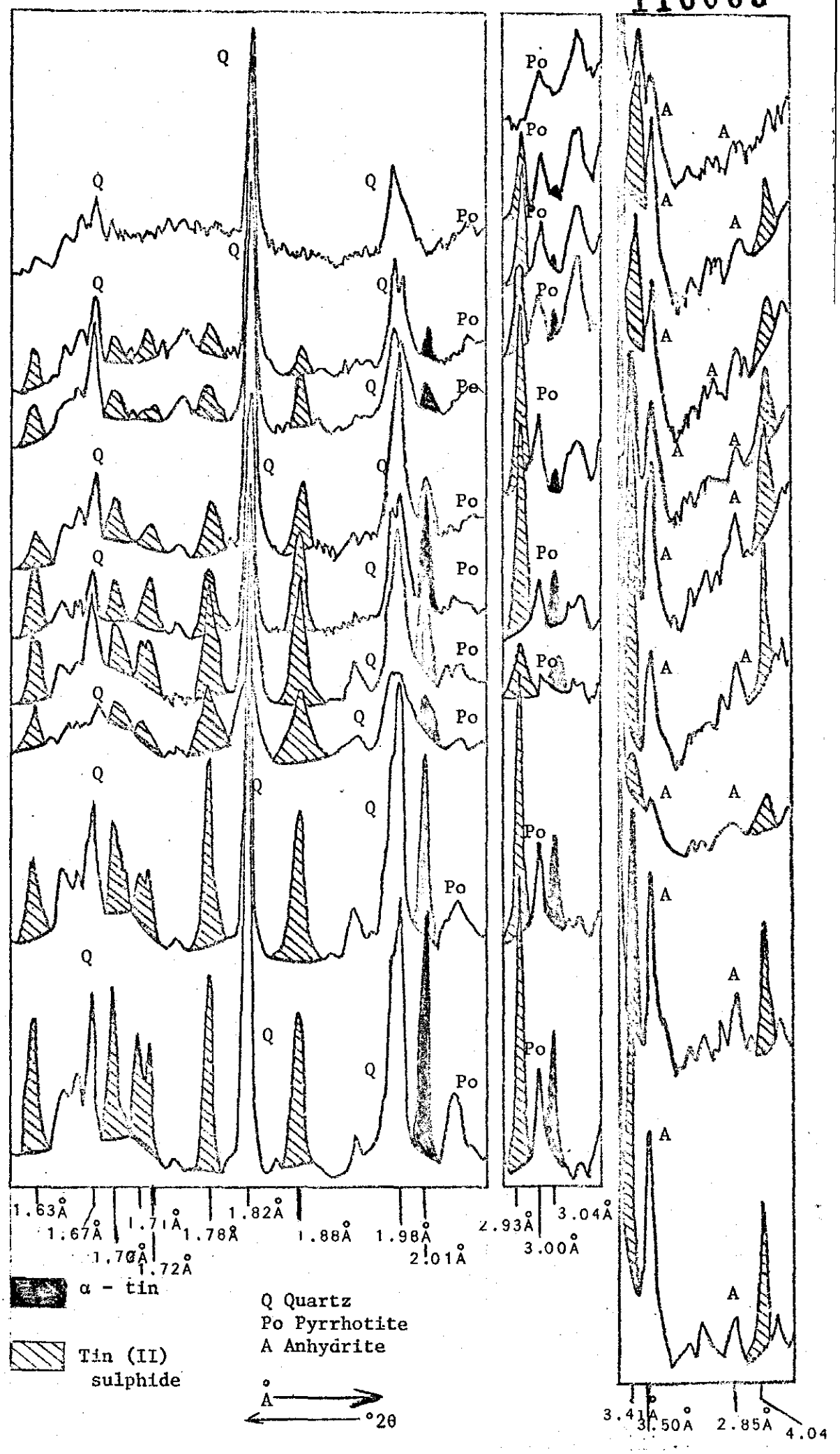

FIGURE 10 Reduction of broad reflection ascribed to organic matter at 4.8Å with increase in the reaction temperature in the uncatalysed batch autoclave residues

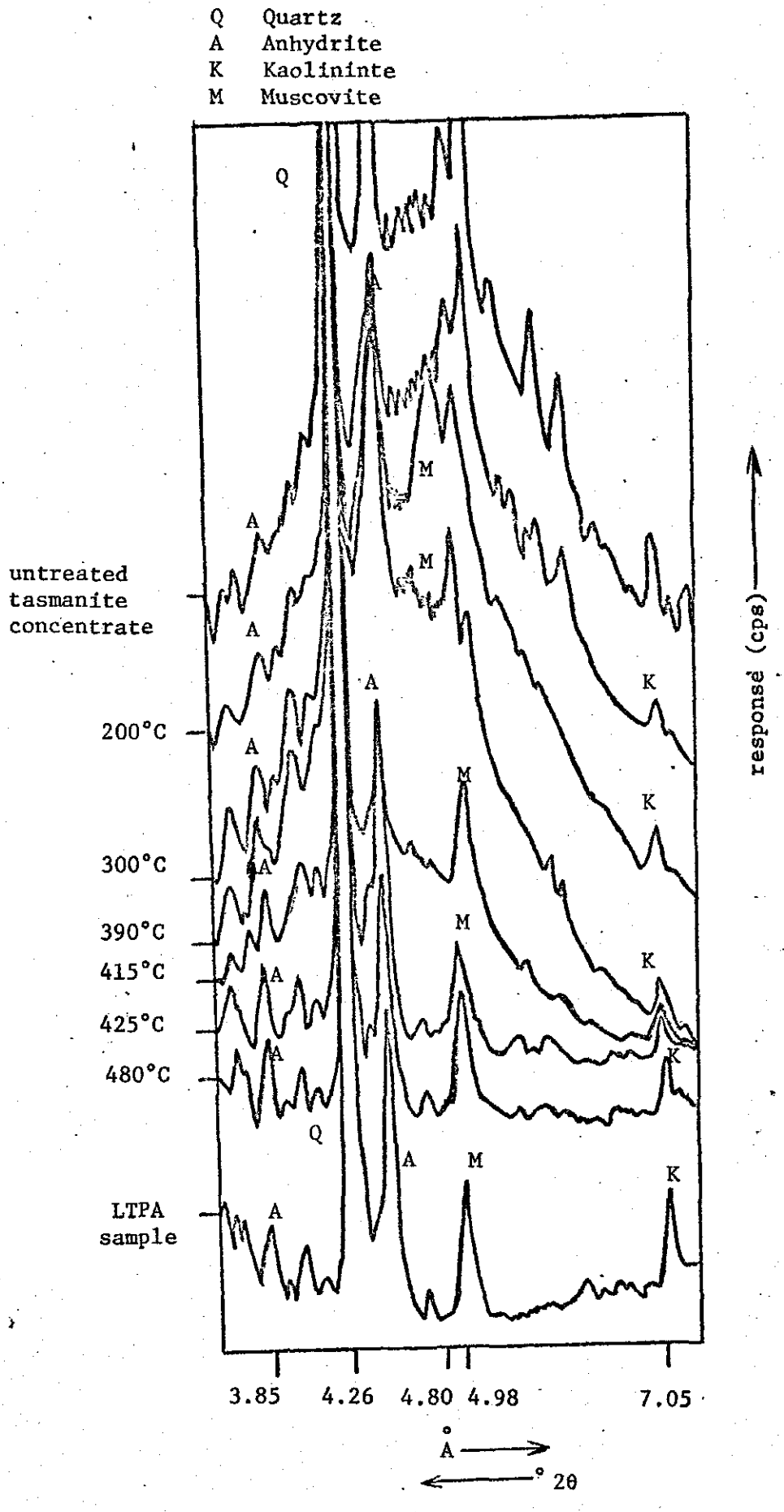

FIGURE 11 Curie Point Pyrolysis - GC/MS Reconstructed Ion Chromatograms (RIC) for Hexane Extracts

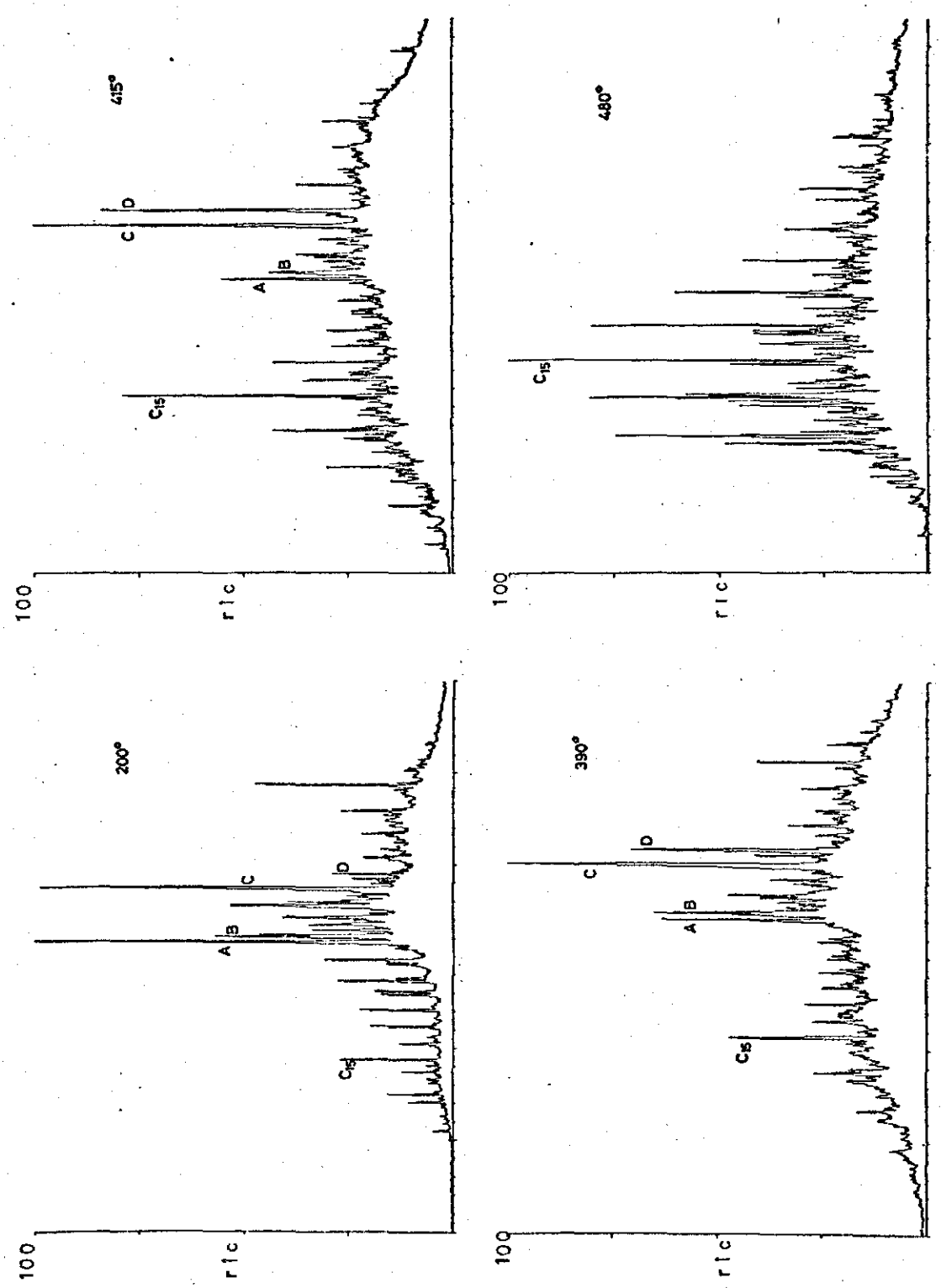

FIGURE 12 Specific Ion Monitoring of GC/MS Traces to Demonstrate Variation in amounts of Aliphatics (m/e 71) and Dialkyl Benzenes (m/e 105) at Various Autoclave Temperatures

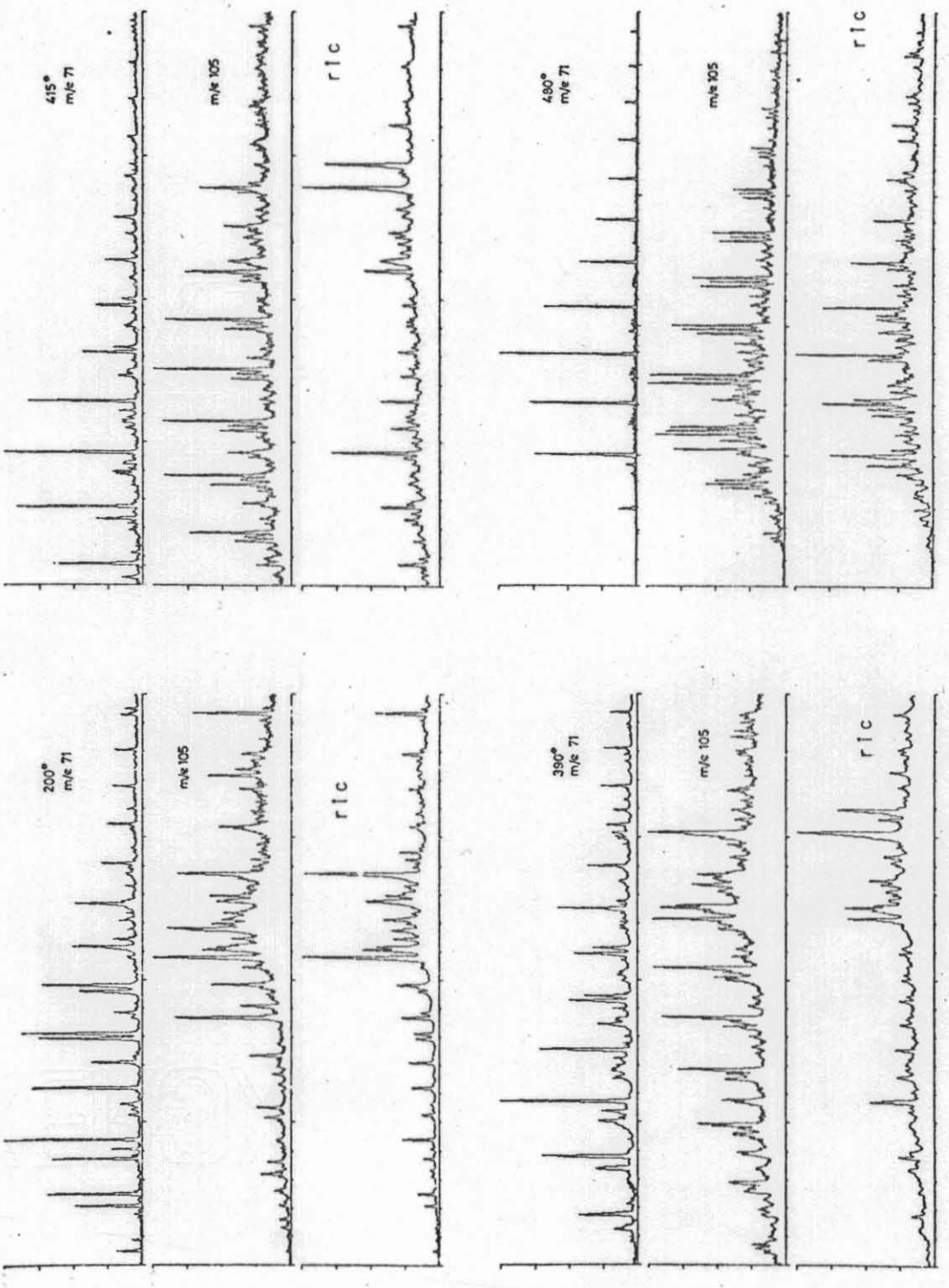

FIGURE 13 Curie Point Pyrolysis - GC Traces for Hexane-Insoluble Residues

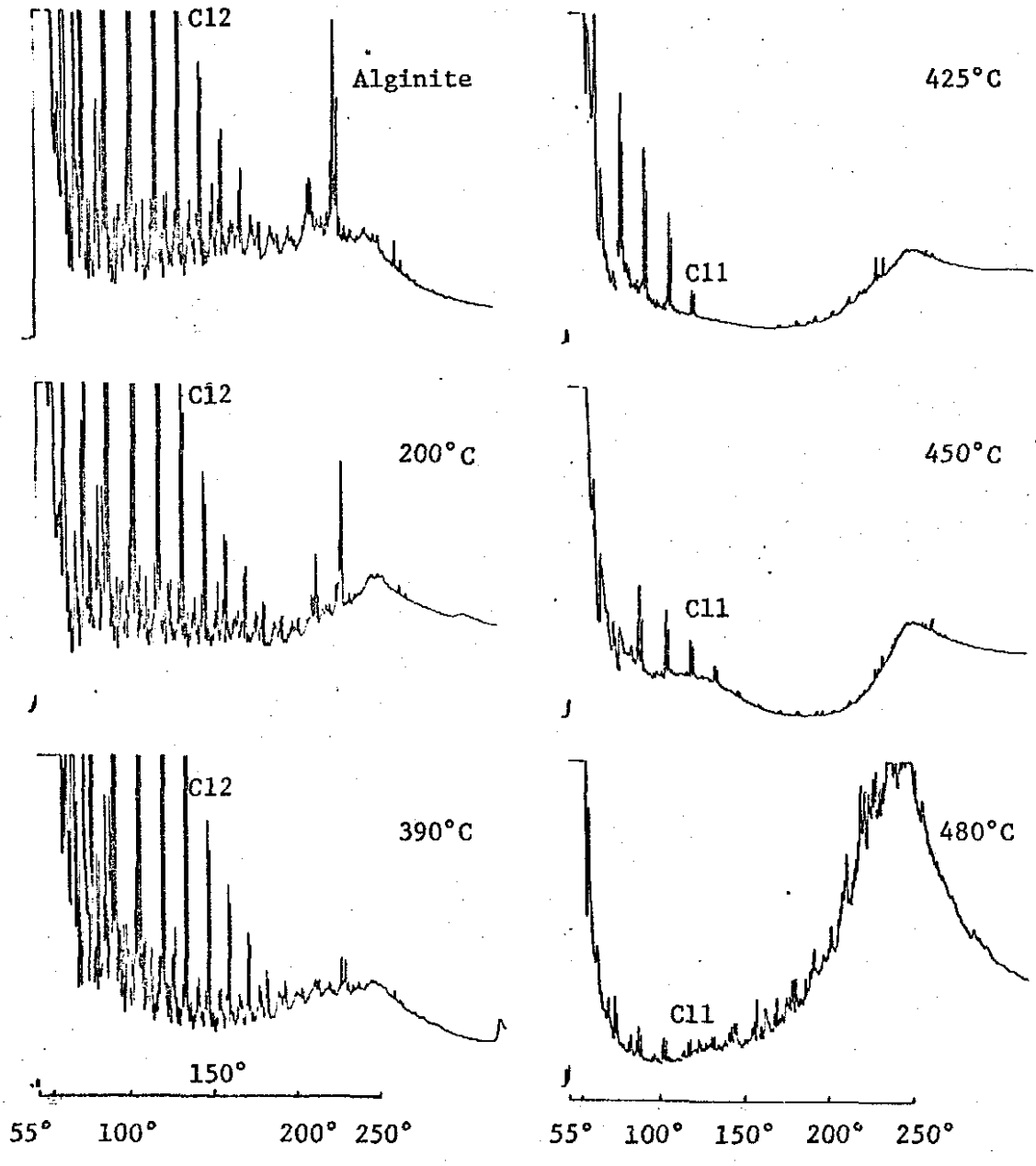

PLATES

PLATE I:

Ia Alginite melted and flowed together (H_2, 415°C)
(incident white light, X 170)

Ib Detail of melted alginite which contains grains of quartz (grey, high relief) and angular grains of unaltered inertinite (white, high relief) (H_2, 415°C)
(incident white light, X 400)

Ic Softening and agglomerating of alginite bodies (N_2, 415°C)
(incident white light, X 400)

Id Carbonized alginite bodies, quartz and other inert material bonded by a skeletal residue (N_2, 425°C)
(incident white light, X 170)

PLATE I

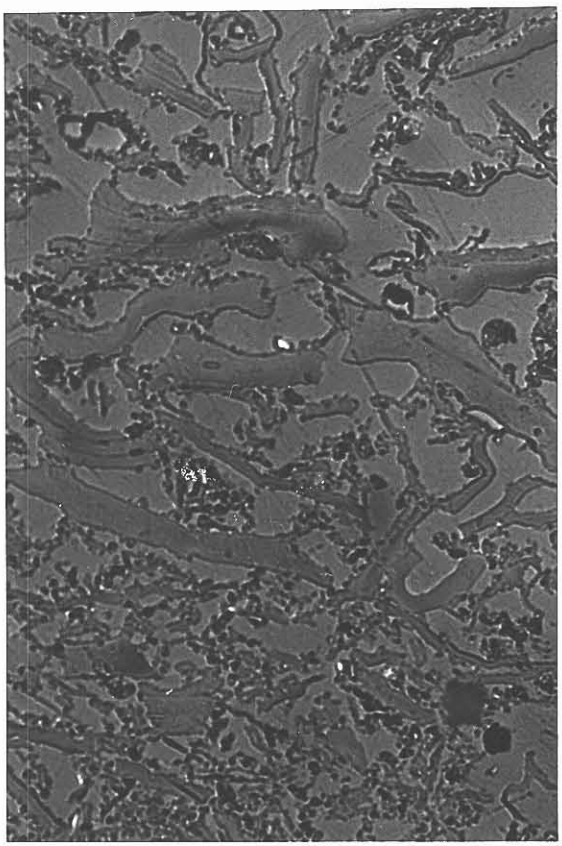

Ic

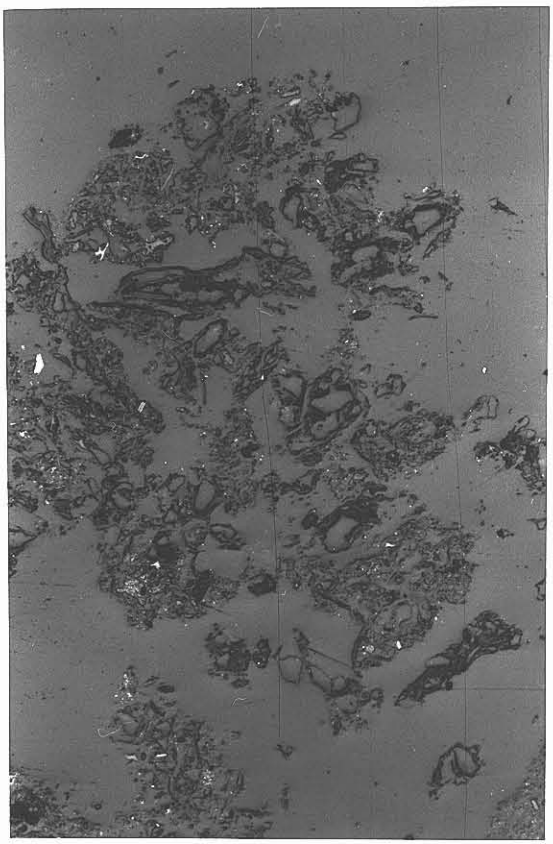

Id

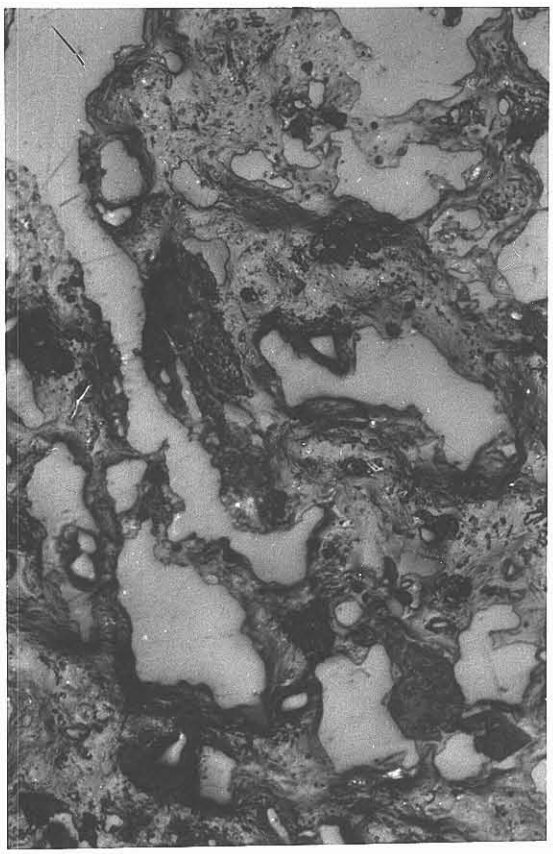

Ia

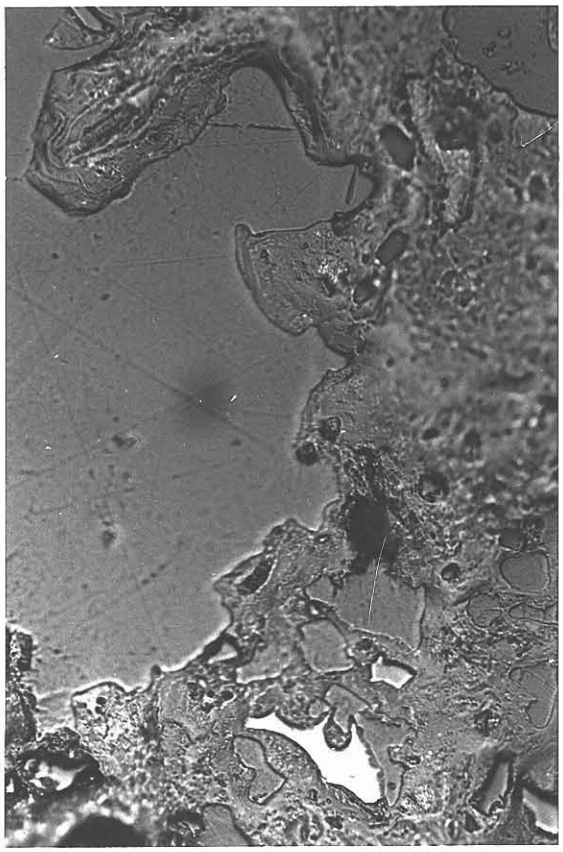

Ib

PLATE II:

IIa Skeletal, carbonized residue derived from alginite (N_2, 480°C)
(incident white light, X 170)

IIb Euhedral/subhedral tin (II) sulphide exhibiting a radiating state of aggregation (H_2 + $SnCl_2$, 480°C)
(incident white light, partially crossed polarizers, X 400)

IIc Coarse-grained iron filing particle partially rimmed by very fine-grained anisotropic, iron sulphide (N_2 + iron filings, 425°C)
(incident white, light partially crossed polarizers, X 170)

IId Fine-grained iron particles rimmed by very fine-grained, anisotropic, iron sulphide (N_2 + iron powder, 425°C)
(incident white light, partially crossed polarizers, X 400)

PLATE II

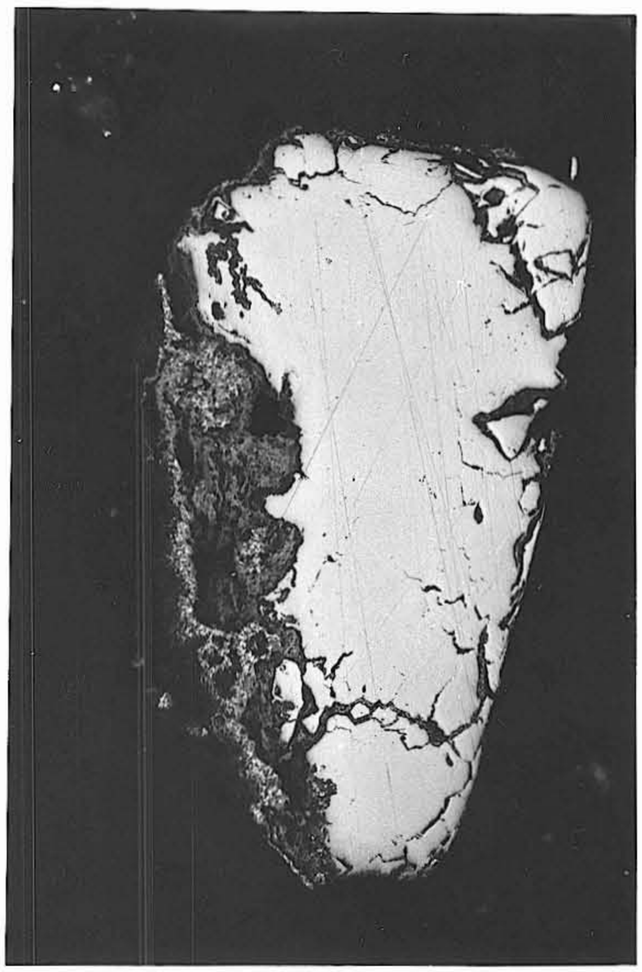

IIc

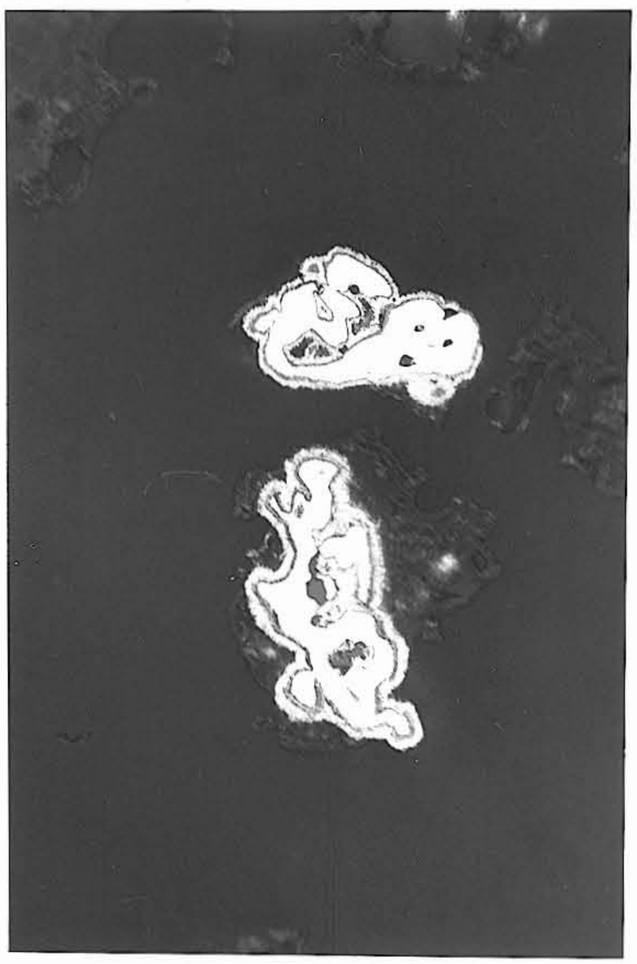

IId

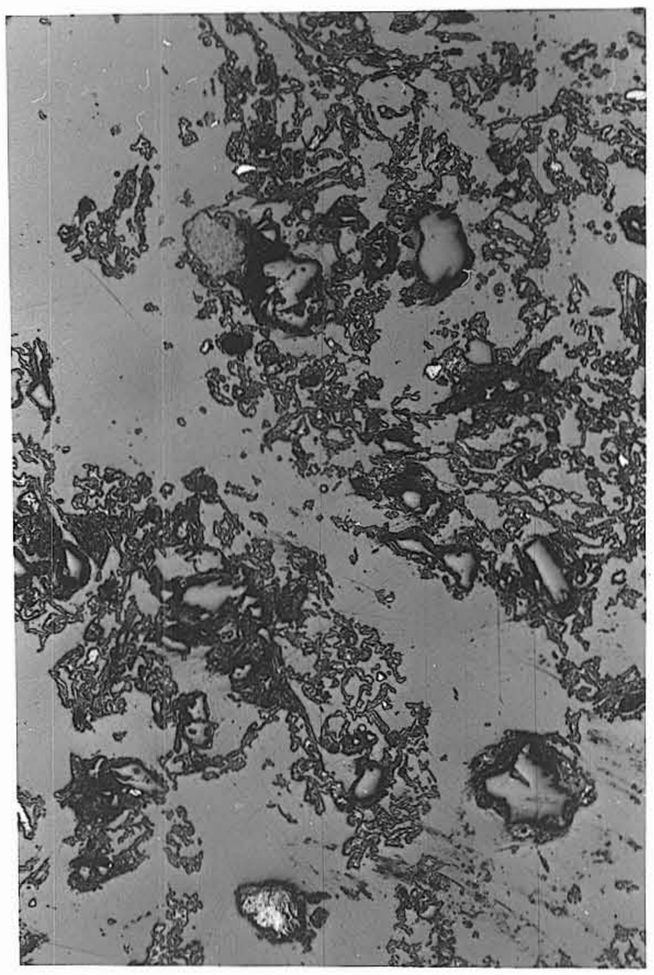

IIa

IIb

PLATE III:

IIIa General view of red mud catalyst particles and carbonized alginite residue (N_2 + red mud catalyst, 425°C)
(incident white light, X 40)

IIIb Detail of red mud catalyst particle showing its heterogenous texture (N_2 + red mud catalyst, 25°C)
(incident white light, oil immersion, X 170)

IIIc General view of iron oxide particles and carbonized, skeletal, alginite residue containing angular quartz grains (N_2 + iron (III) oxide, 425°C)
(incident white light, X 40)

IIId Detail of iron oxide particles (N_2 + iron oxide, 425°C)
(incident white light, oil immersion, X 170)

PLATE III

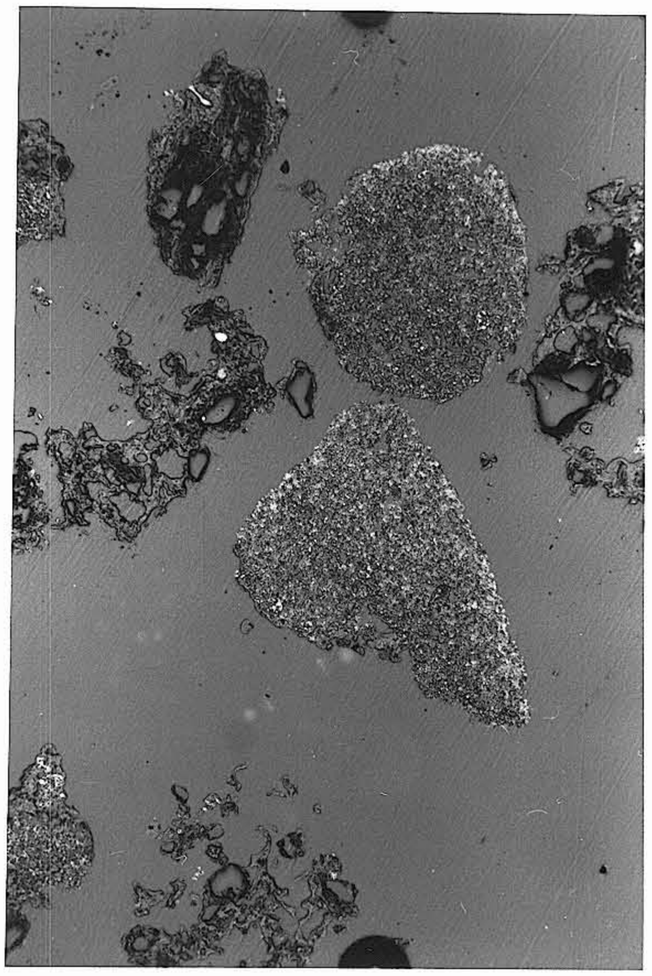

IIIc

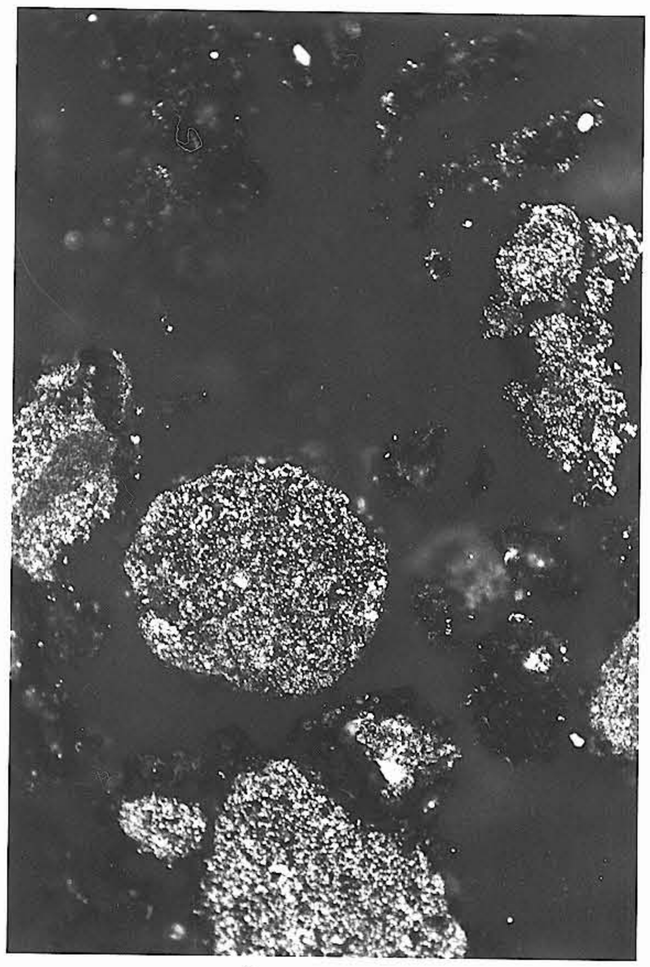

IIId

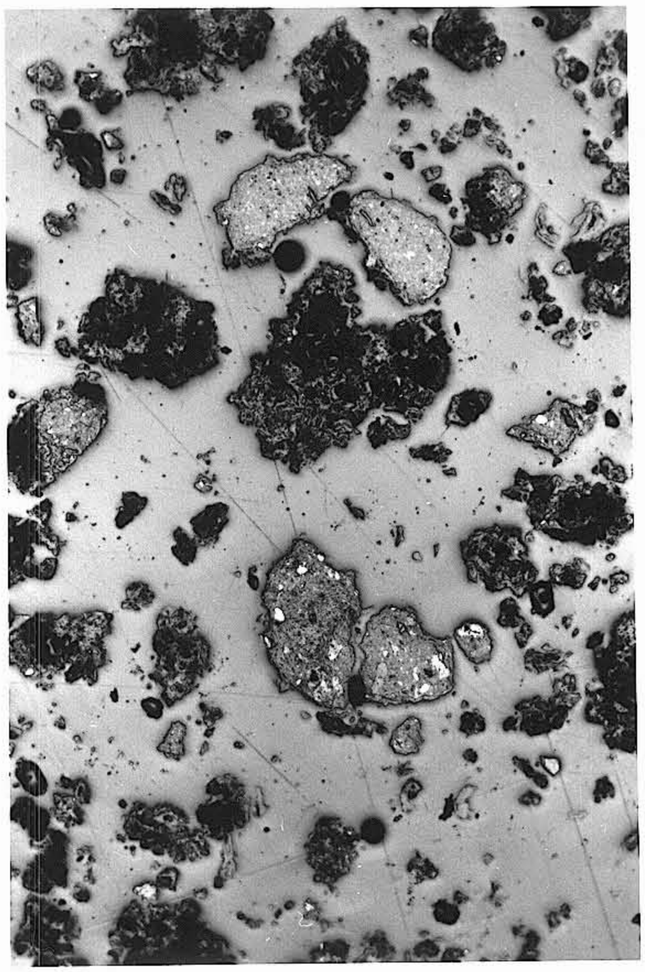

IIIa

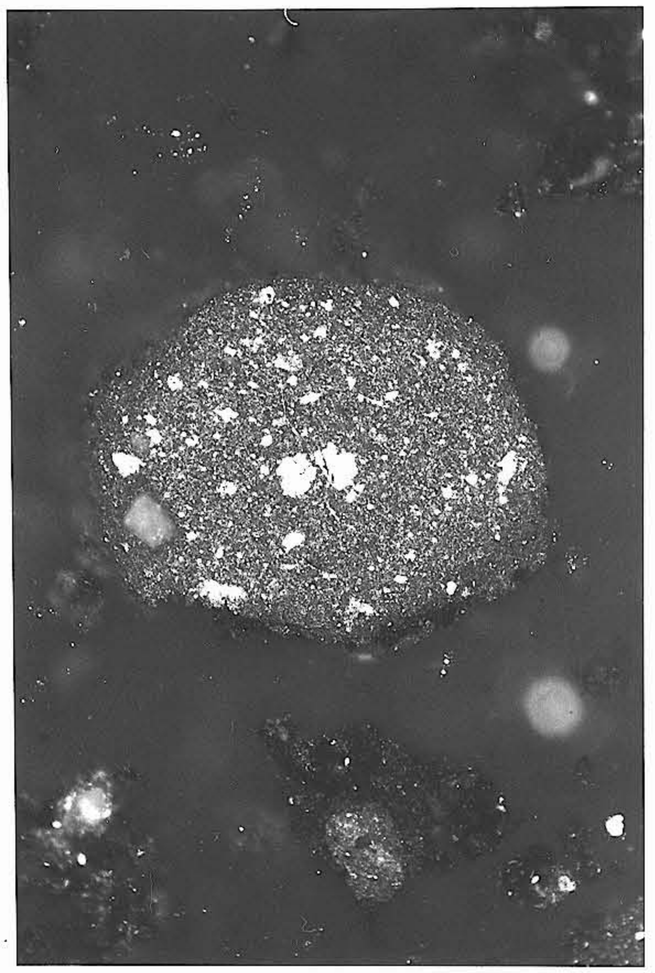

IIIb

PLATE IV:

IVa Relatively unaltered alginite bodies in LTPA residue after ashing for 24 hours
(incident white light, X 170)

IVb Variation in the reflectivity and polishing relief of alginite bodies in LTPA residue after ashing for 48 hours
(incident white light, X 170)

IVc Variation in the reflectivity and polishing relief of alginite bodies in LTPA residue after ashing for 48 hours. Plates IVb and IVc reveal a complete range of properties from low reflectivity, low polishing relief alginite to high reflectivity (white), high polishing relief alginite
(incident white light, X 170)

116077

PLATE IV

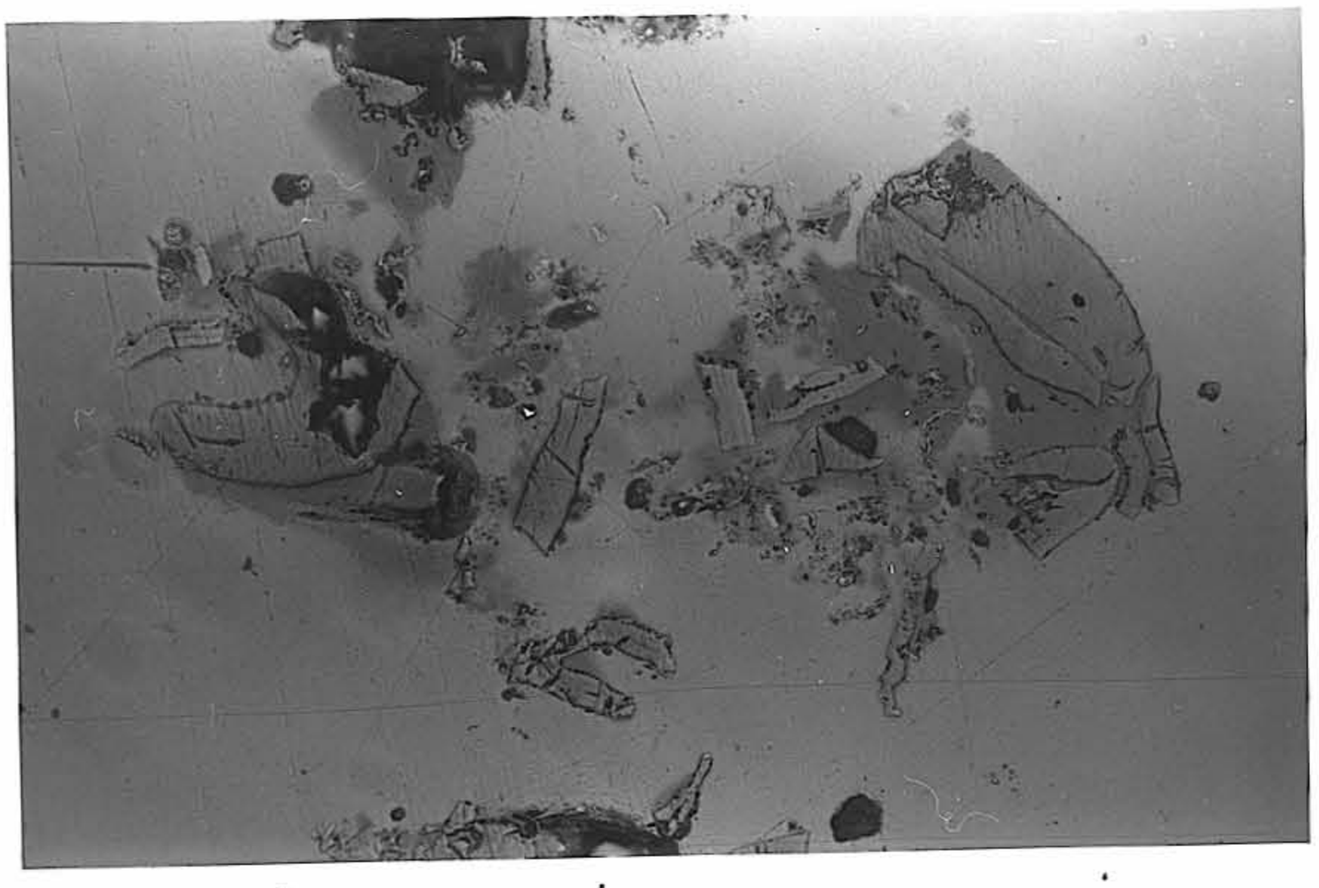

IVa

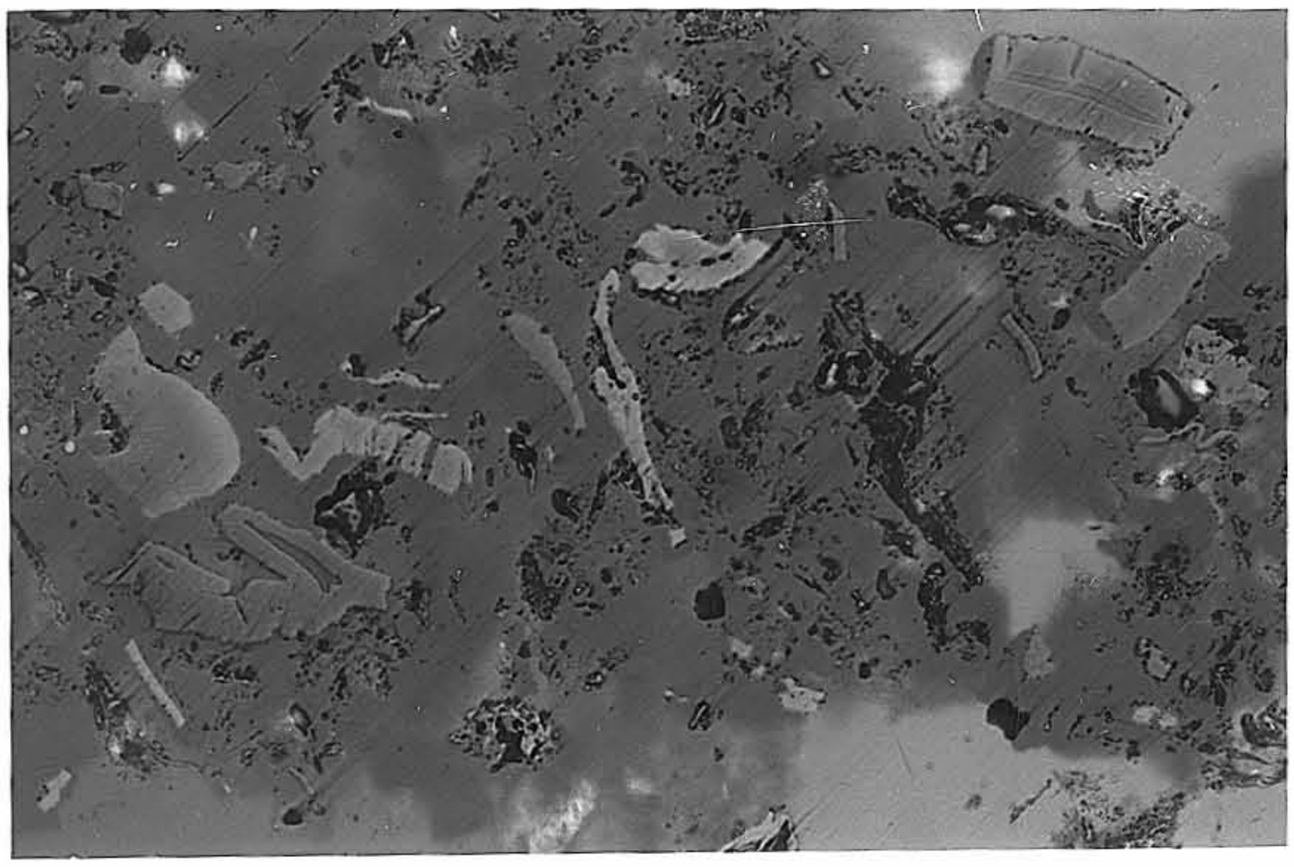

IVb

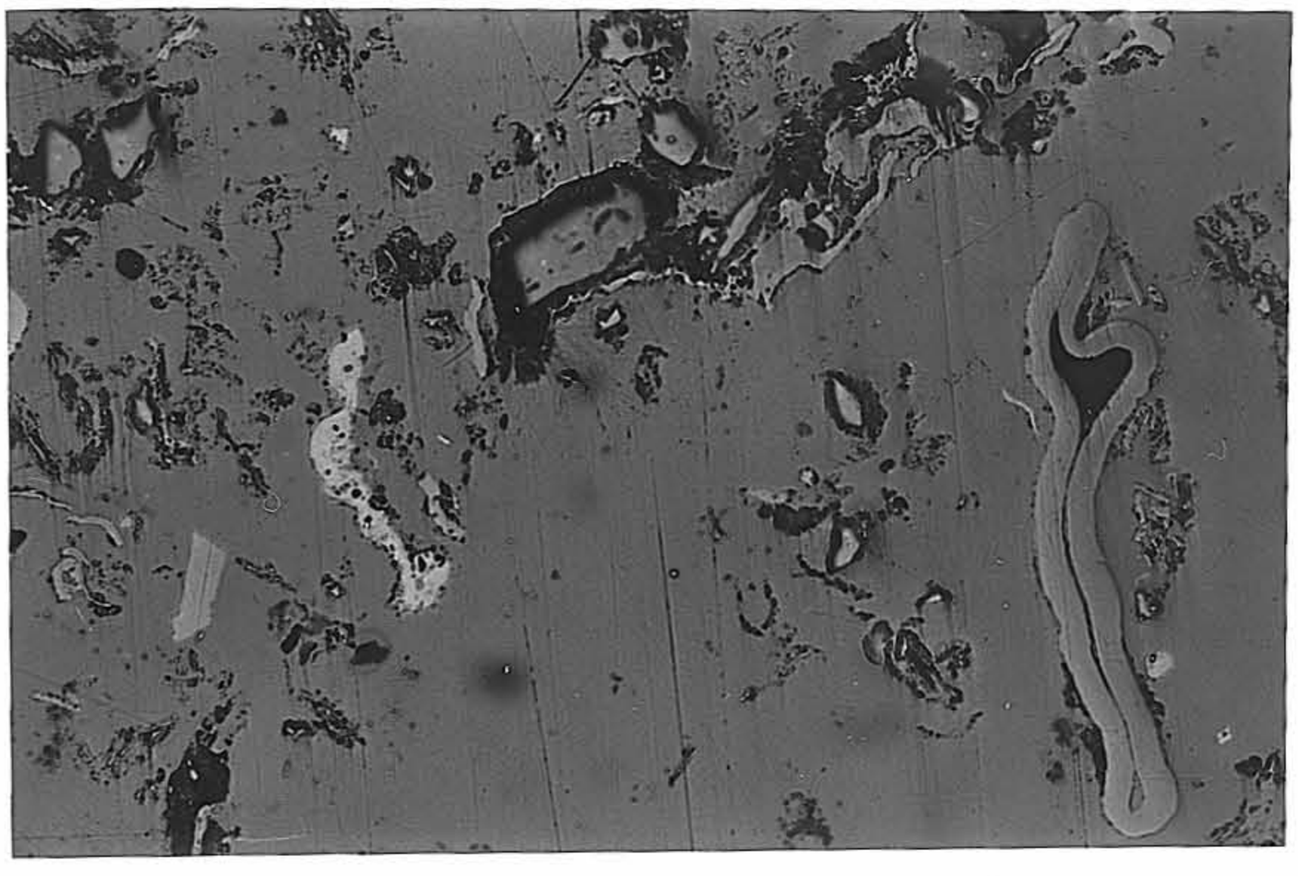

IVc

PLATE V:

Va Electronmicrograph of tin (II) sulphide crystals (H_2 + $SnCl_2$, 480°C) (25Kv, SEM secondary electrons, X 500)

Vb Detail of intergrowth between tin and tin (II) sulphide in Figure Va (X 2500)

Vc Distribution of $Sn_{L\alpha}$ in Figure Vb (SEM/EDS)

Vd Distribution of $S_{K\alpha}$ in Figure Vb (SEM/EDS)

PLATE V

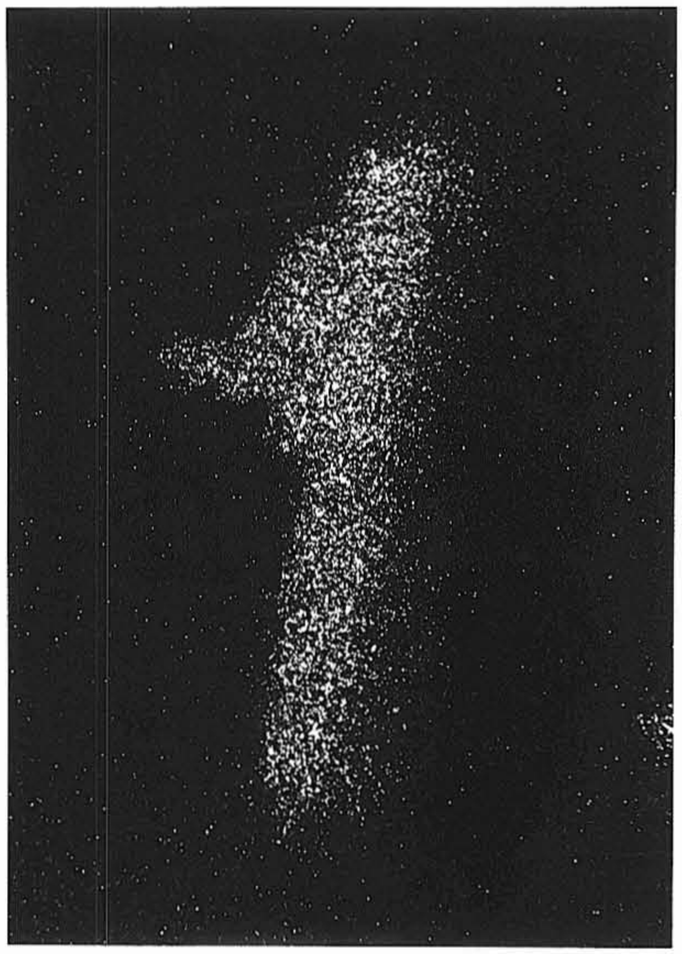

Vc

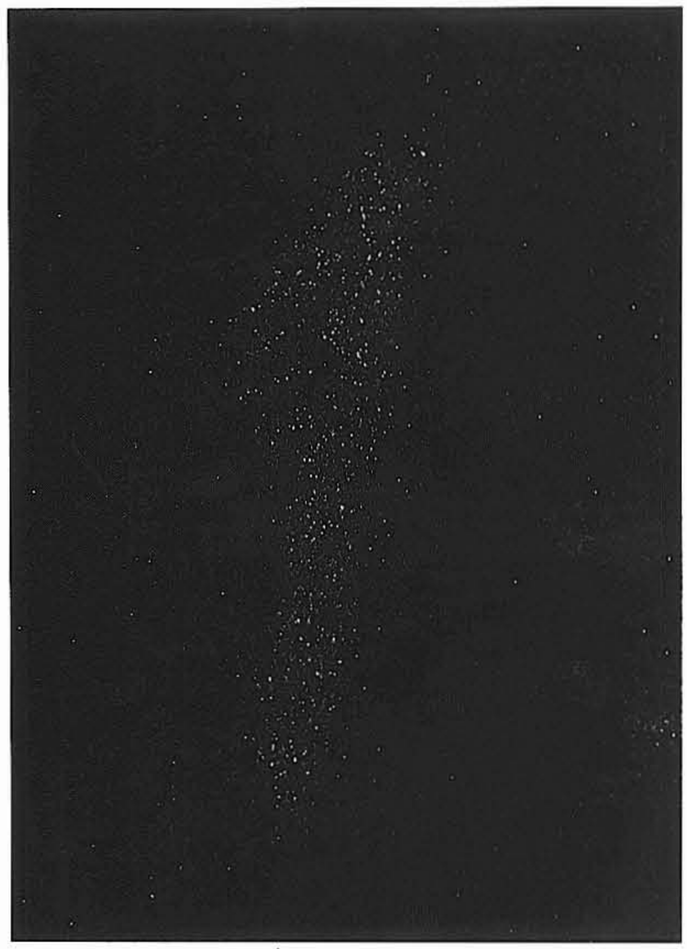

PA

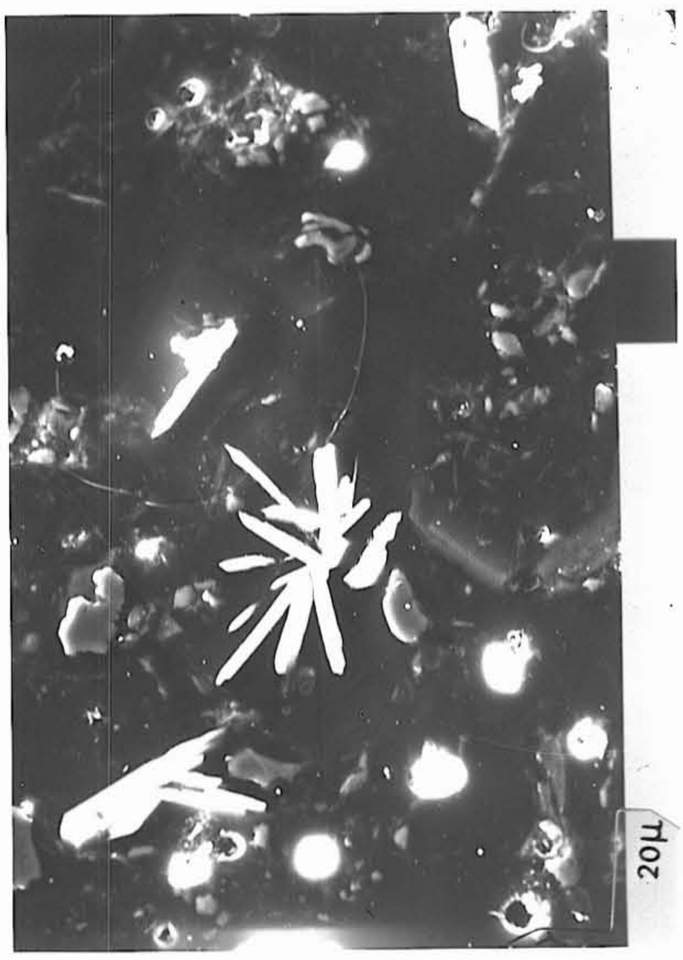

Va

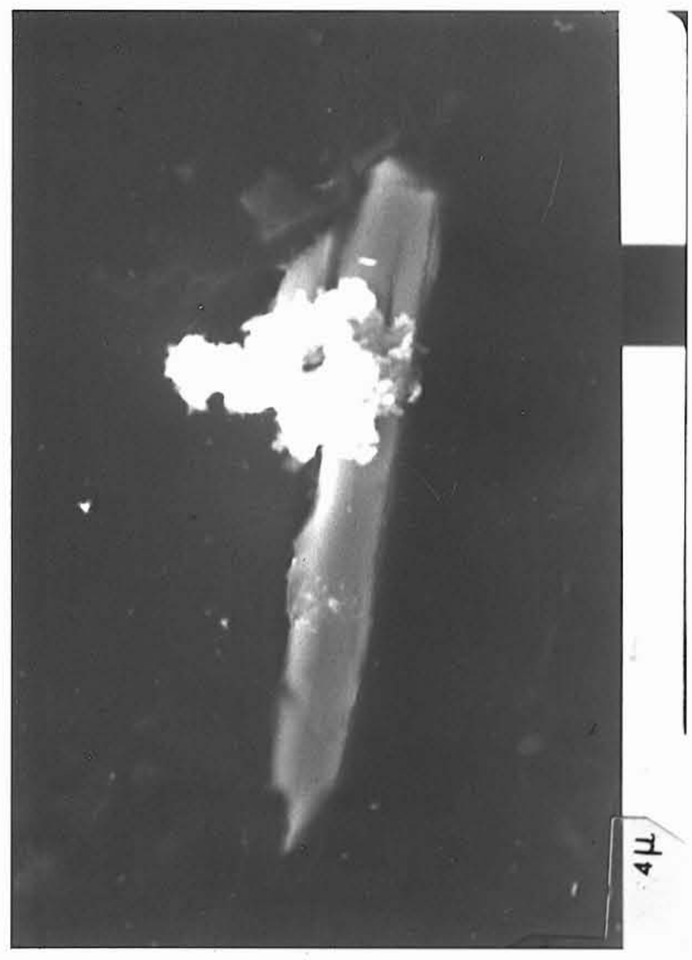

Vb

PLATE VI:

VIa Electronmicrograph of alginite body (H_2 + $ZnCl_2$, 390°C) (25Kv, SEM secondary electrons, X 100)

VIb Detail from Figure VIa showing zinc (II) sulphide crystals concentrated in the axial zone and along the margins of the alginite body (X 500)

VIc Distribution of $Zn_{K\alpha}$ in Figure VIb coinciding with the occurrence of zinc (II) sulphide in VIb (SEM/EDS)

VId Distribution of $S_{K\alpha}$ in Figure VIb. Sulphur is concentrated in association with zinc in zinc (II) sulphide grains. It is also slightly concentrated in the alginite body (unreacted organic sulphur?) (SEM/EDS)

116081

PLATE VI

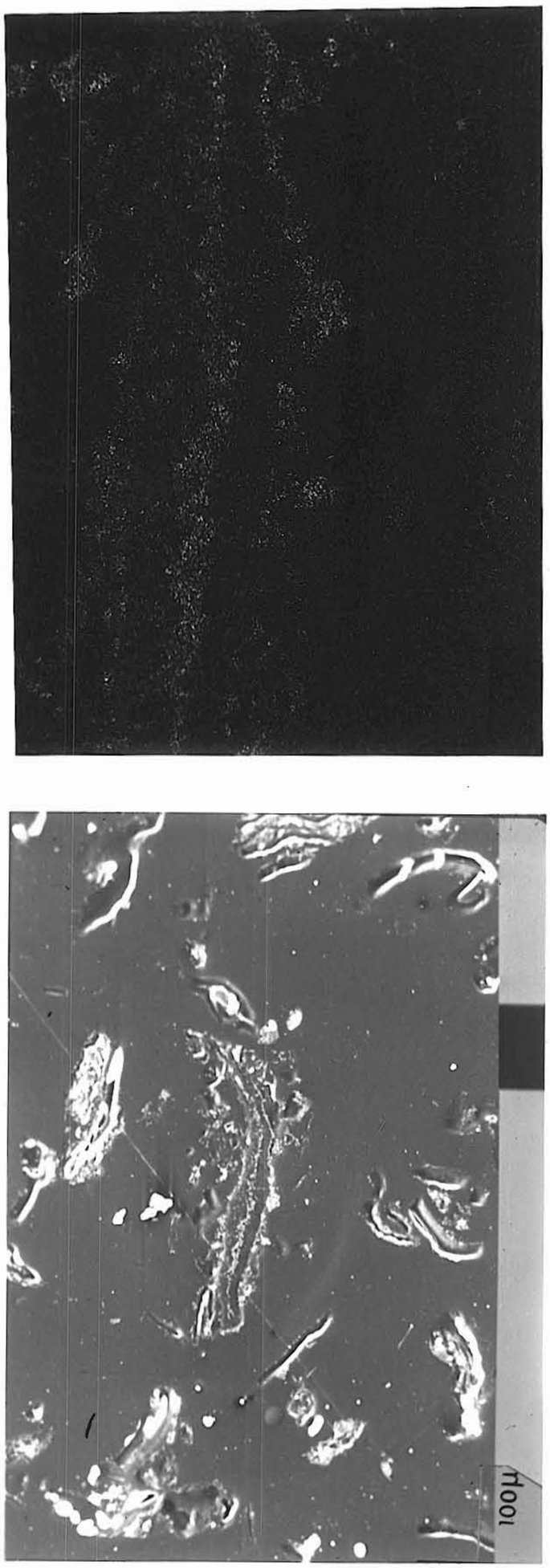

VIa

VIc

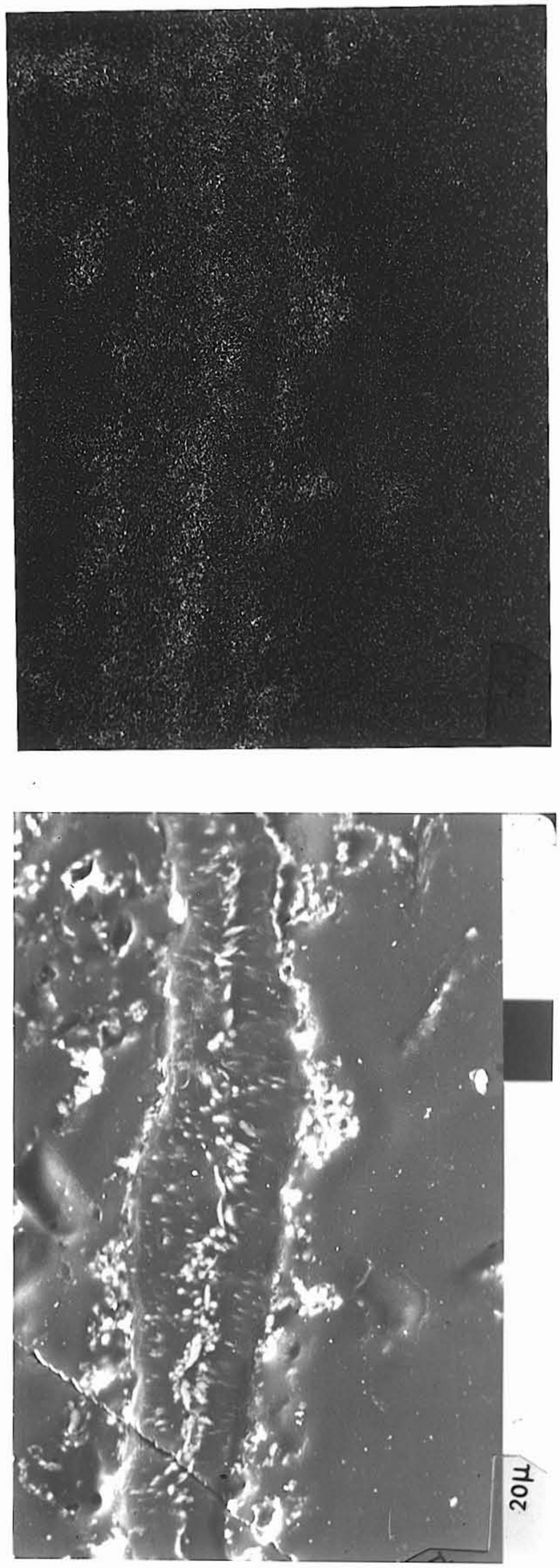

VIb

VId

PLATE VII:

VIIa Coarse-grained iron particle with rim of iron sulphide (N_2 + coarse iron filings, 425°C) (25Kv, SEM secondary electrons, X 250)

VIIb Distribution of $Fe_{K\alpha}$ in Figure VIIa. Note the lower content of iron in the margins. (SEM/EDS)

VIIc Distribution of $S_{K\alpha}$ in Figure VIIa. Note the concentration of sulphur in the margin. (SEM/EDS)

VIId Detail from Figure VIIa showing acicular nature of iron sulphide rim (X 1000)

VIIe Electronmicrograph and horizontal profile line for margin of coarse-grained iron particle (EPMA/wavelength dispersive system back scatter electrons, X 200)

VIIf Distribution of $S_{K\alpha}$ in Figure VIIe shows concentration of sulphur in the margin (PET, 4900 counts)

VIIg Profile for $Fe_{K\alpha}$ along horizontal line in Figure VIIe showing drop in iron concentration in the margin (LiF2, flow counter, FSD $3x10^3$ cps)

VIIh Profile for $S_{K\alpha}$ along horizontal line in Figure VIIe showing concentration of sulphur in the margin (PET, FSD $3x10^3$ cps)

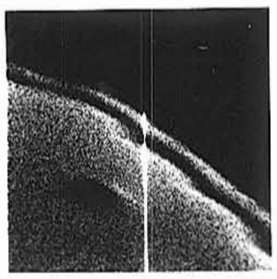

VIIe

VIIf

VIIg

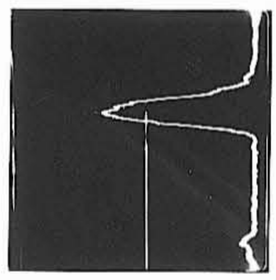

VIIh

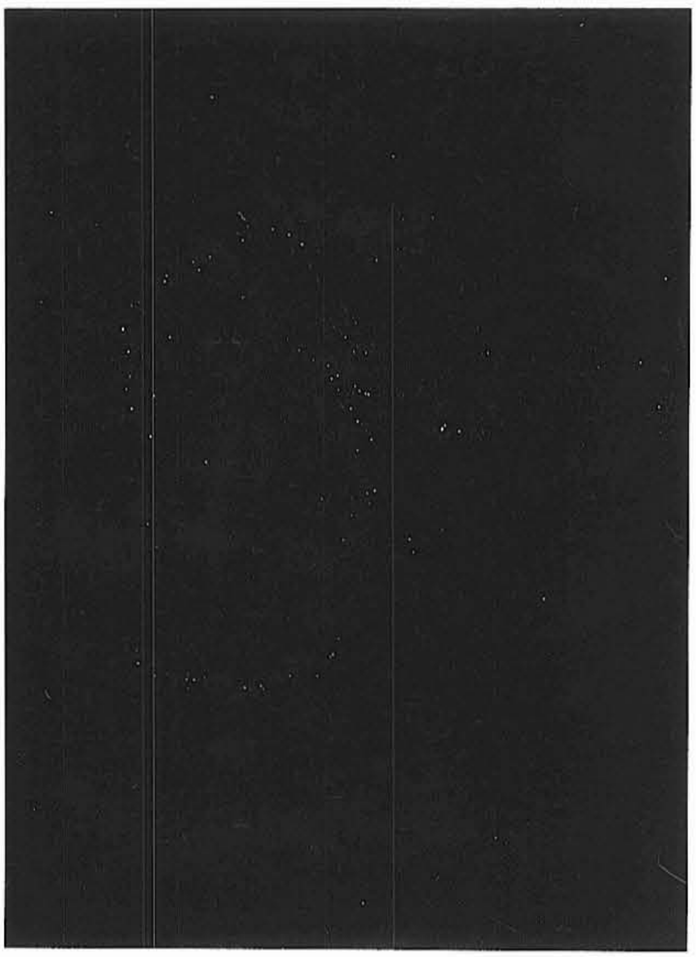

VIIc

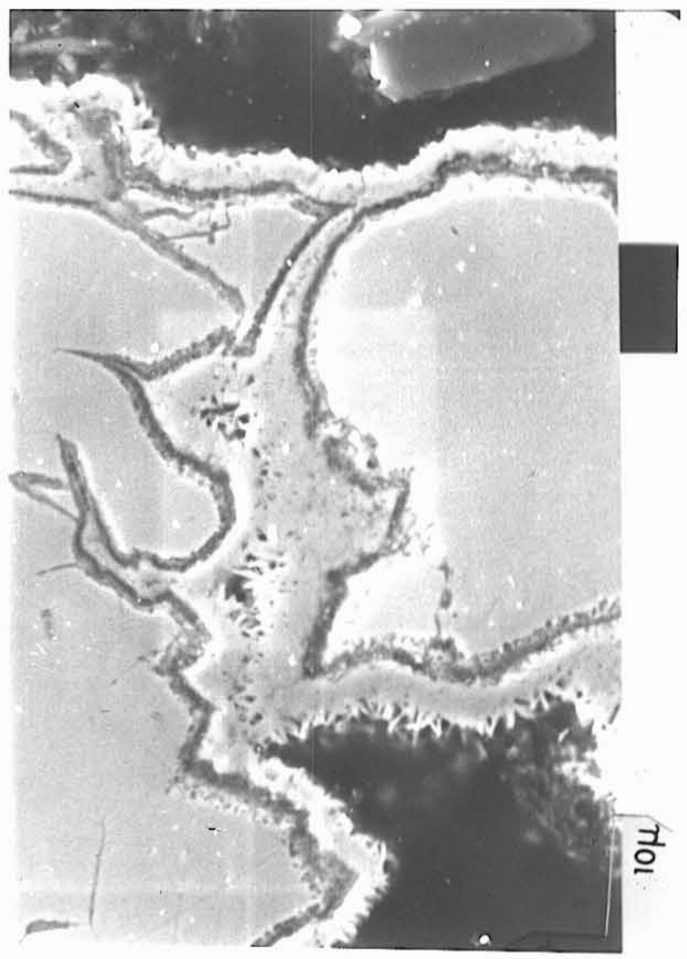

VIId

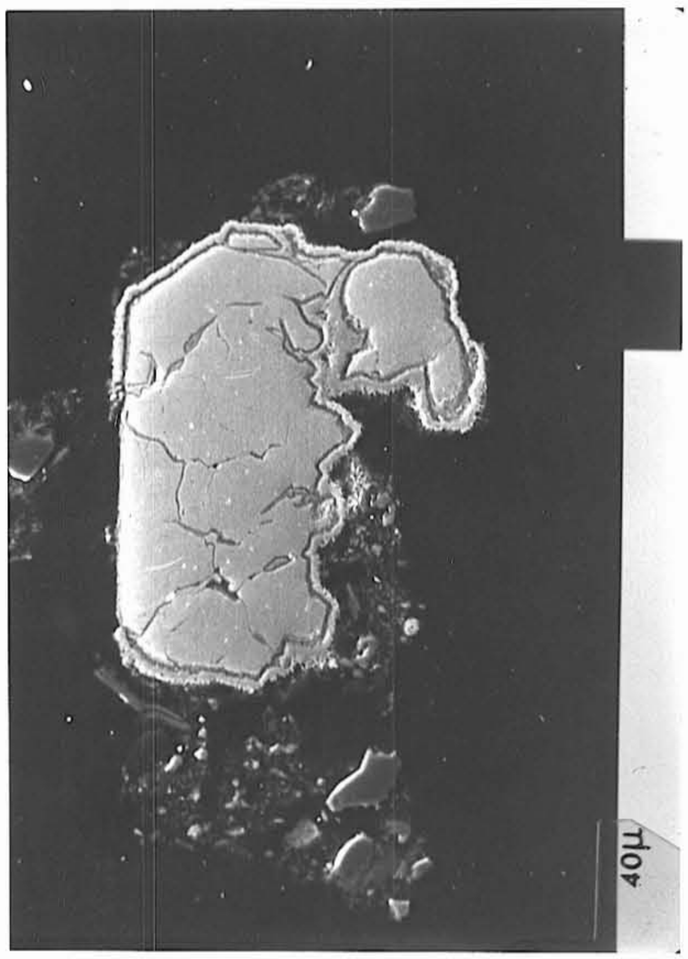

VIIa

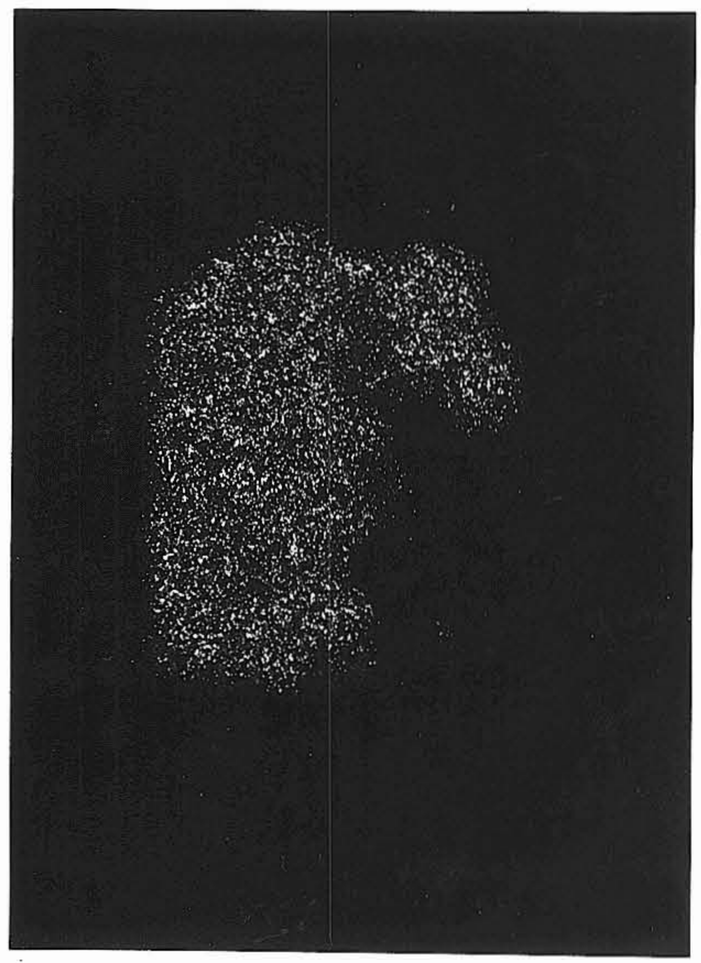

VIIb

PLATE VIII:

VIIIa Electronmicrograph of fine-grained iron particles rimmed by iron sulphide; note the gap between the iron and the iron sulphide margin (N_2 + fine-grained iron powder, 425°C) (25Kv, SEM secondary electrons, X 1000)

VIIIb Similar view to Figure VIIIa. In this instance the acicular nature of the iron sulphide rim is more clearly visible (X 1000)

VIIIc Distribution of $Fe_{K\alpha}$ in Figure VIIIb. Note the lower content of iron in the margins (SEM/EDS)

VIIId Distribution of $S_{K\alpha}$ in Figure VIIIb. Note the concentration of sulphur in the margins (SEM/EDS)

PLATE VIII

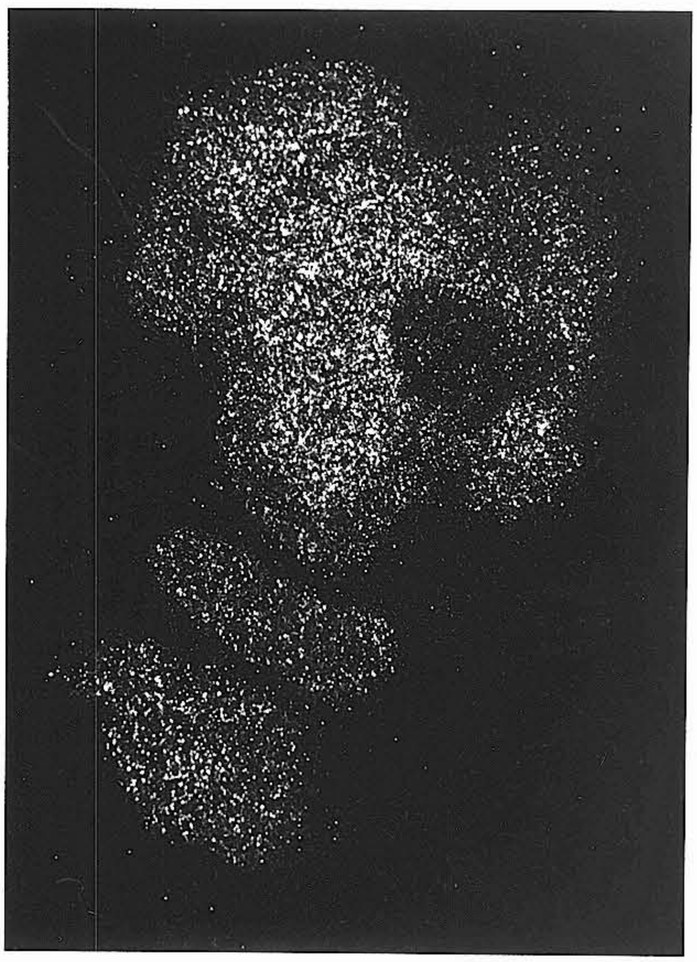

VIIIc

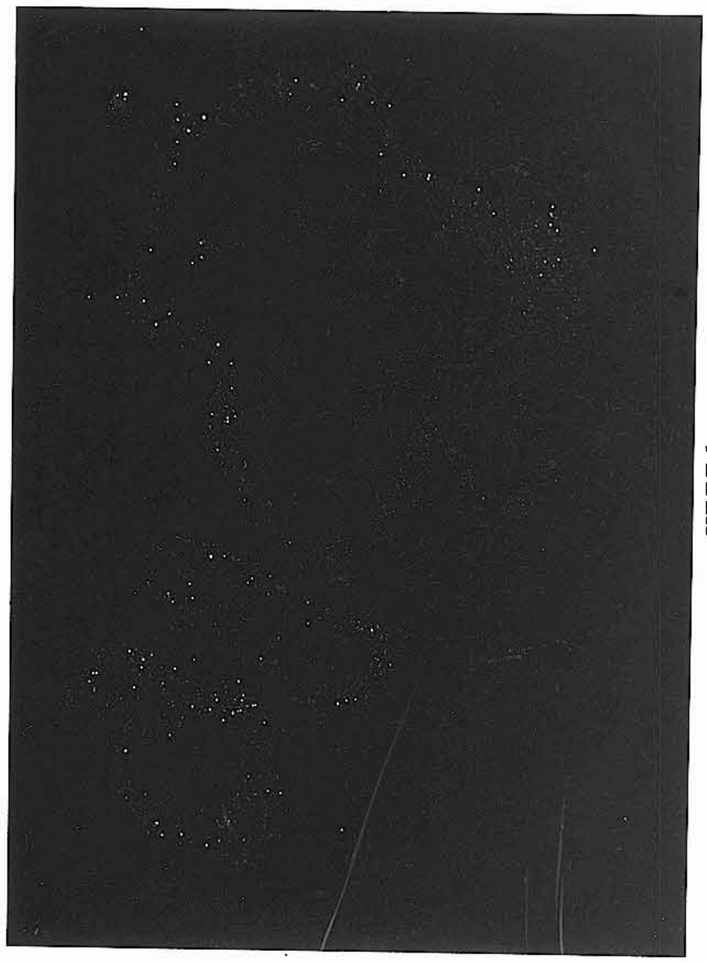

VIIId

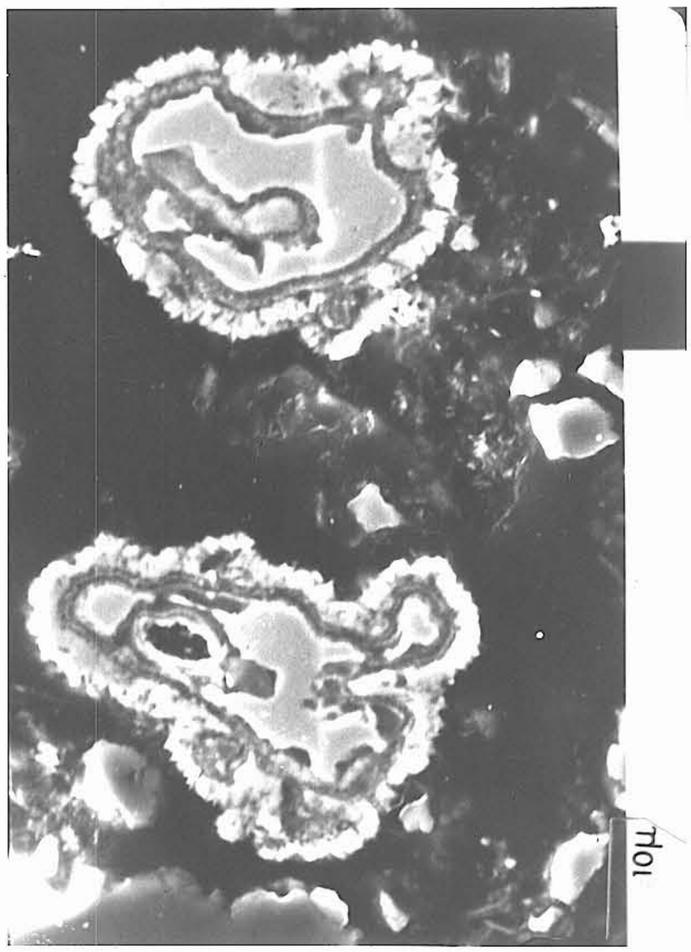

VIIIa

VIIIb

PLATE IX:

IXa Electronmicrograph of iron oxide particle consisting of spherical iron oxide grains and acicular iron sulphide grains; the latter are concentrated in the margin of the iron oxide particle (N_2 + iron oxide, 425°C)
(25Kv, secondary electrons, X 1000)

IXb Electronmicrograph of iron (III) oxide particle (X 250)

IXc Distribution of $Fe_{K\alpha}$ in Figure IXb (SEM/EDS)

IXd Distribution of $S_{K\alpha}$ in Figure IXb. Note the slight concentration of sulphur in the margin of the particle (SEM/EDS)

PLATE IX

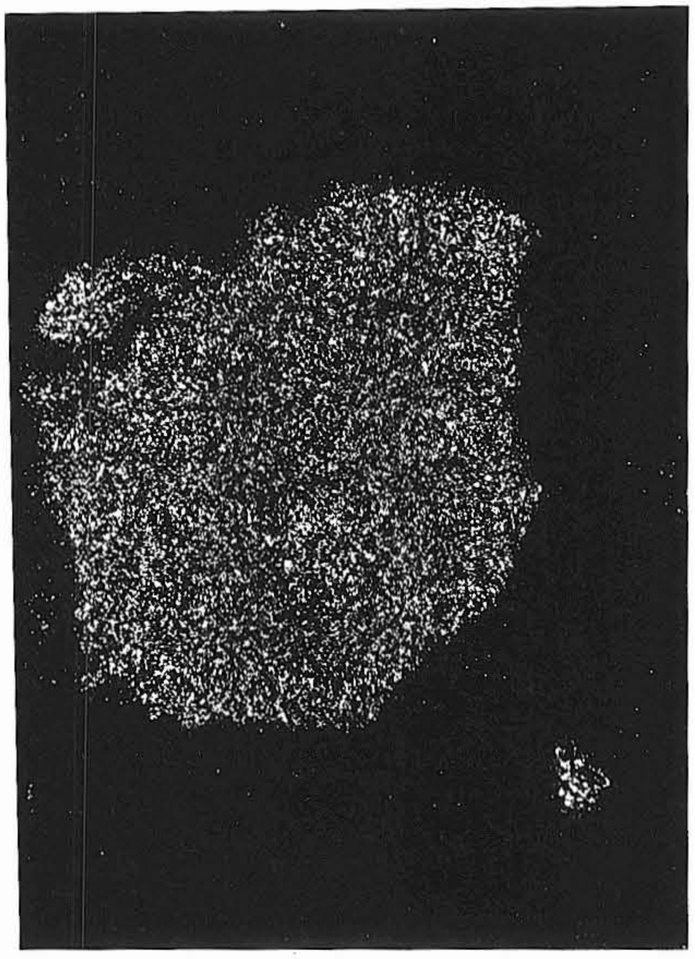

IXc

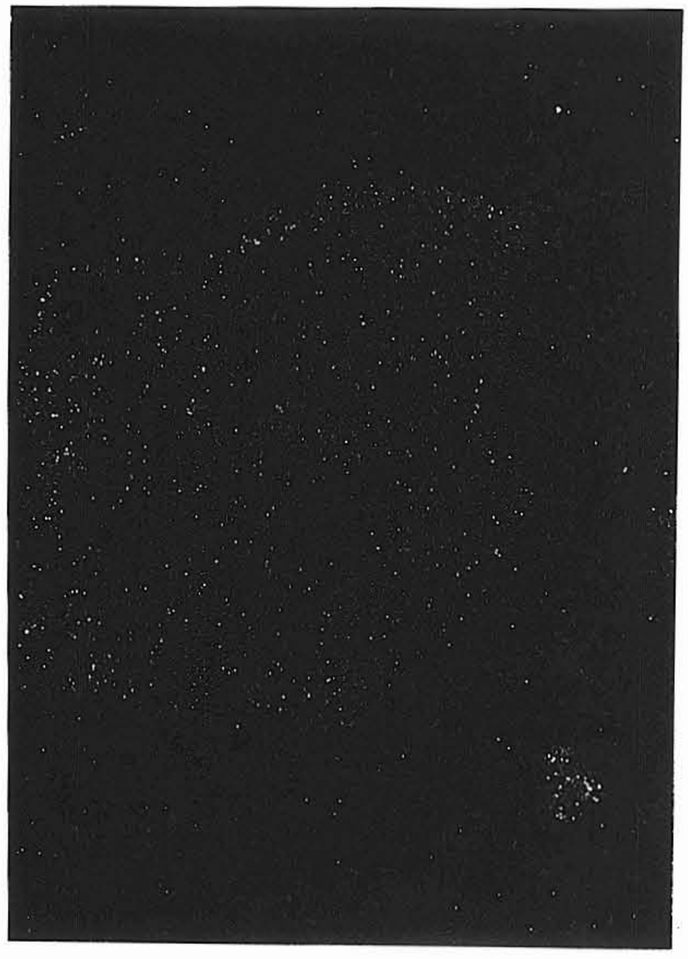

IXd

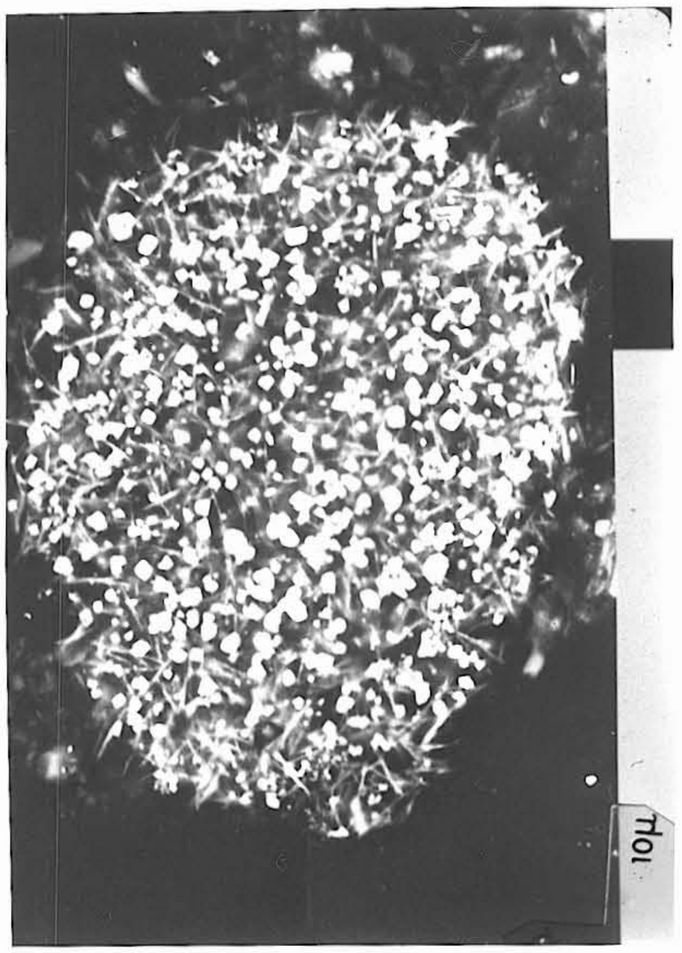

IXa

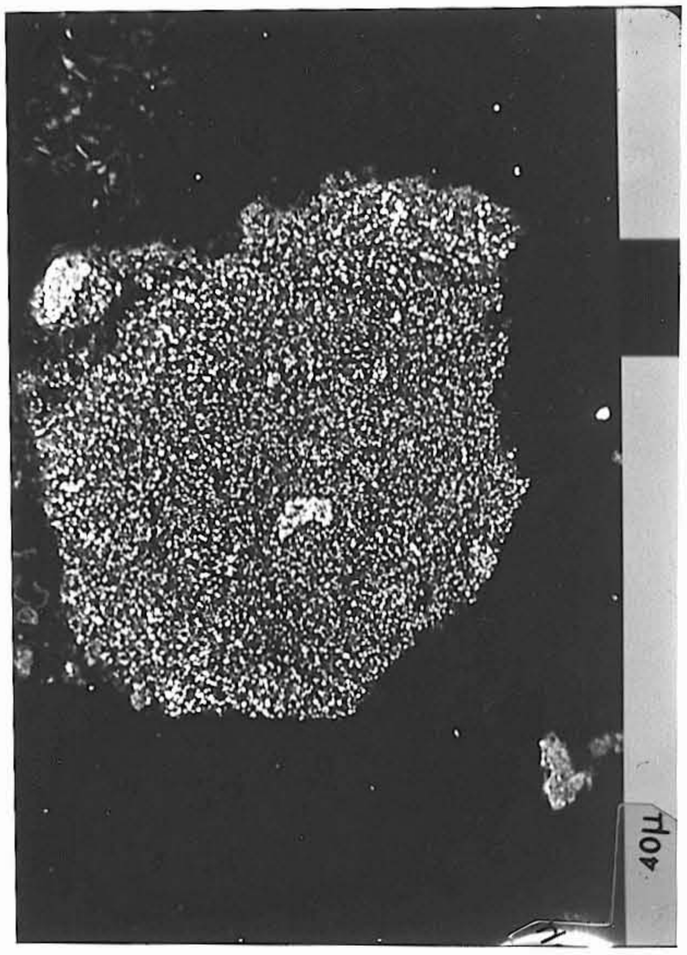

IXb

PLATE X:

Xa Electronmicrograph of red mud catalyst particle exhibiting heterogenous nature. High reflectivity grains are iron oxide (α-Fe_2O_3) (N_2 + red mud catalyst, 425°C) (25Kv, secondary electrons, X 250)

Xb Red mud catalyst particle containing grains of iron oxide (X 250)

Xc Distribution of $Fe_{K\alpha}$ in Figure Xb. Note concentration of iron in iron oxide grains (SEM/EDS)

Xd Distribution of $S_{K\alpha}$ in Figure Xb. Note very slight concentration of sulphur in area of iron oxide grains in the red mud particle (SEM/EDS)

PLATE X

Xc

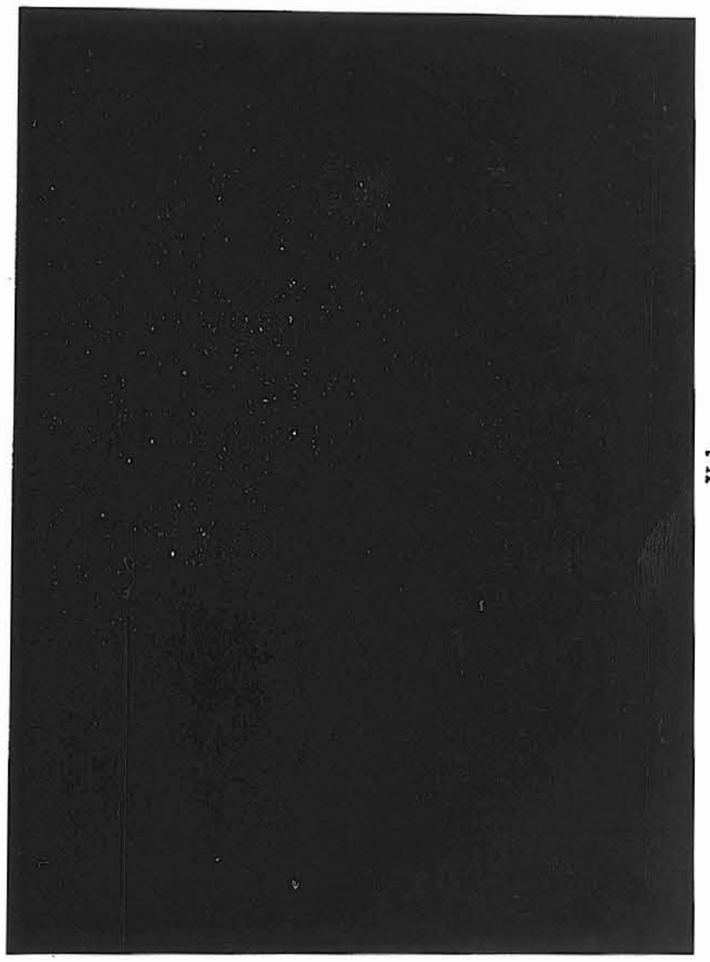

Xd

Xa

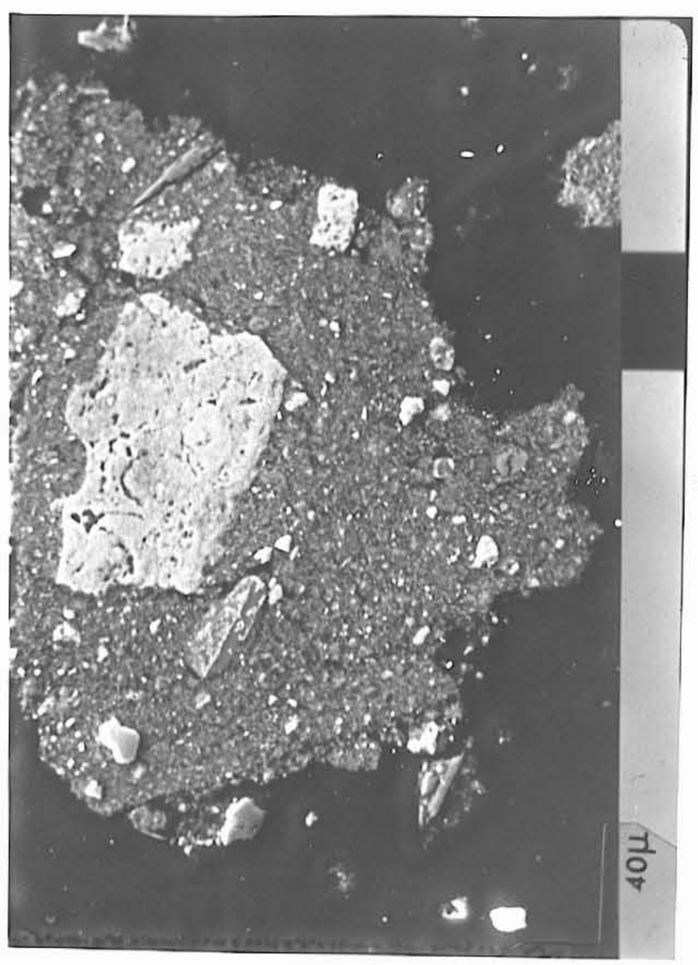

Xb